SOME DISCUSSIONS ON THE STABILITY OF STRUCTURAL AND MECHANICAL SYSTEMS

A THESIS

Presented to

The Faculty of the Division of Graduate Studies and Research

by

Milton Harold Bank II

In Partial Fulfillment

of the Requirements for the Degree

Doctor of Philosophy

in the School of Aerospace Engineering

Georgia Institute of Technology

August 1971

SOME DISCUSSIONS ON THE STABILITY OF STRUCTURAL AND MECHANICAL SYSTEMS

Approved: _____

_____

Chairman

_____

_____

Date approved by Chairman: 8-17-71

ACKNOWLEDGEMENTS

It is with pleasure and pride that I acknowledge the contributions of my advisor, Professor Wilfred H. Horton. Although burdened by physical illness and a multitude of other responsibilities, he was always available for consultation, and his guidance and encouragement were invaluable.

The contributions of Capt. Luis Ortiz, who manufactured the plexiglass specimen for this work, and Mr. Baynes W. Bank who assisted in its testing, are gratefully acknowledged.

This work was carried out with the support and sponsorship of the Veterans Administration, the National Aeronautics and Space Administration and the Department of the Navy under various contracts and programs. Their assistance was appreciated.

Finally, I must thank my wife, Linda, and my son Milton III, for their understanding and patience.

FOREWORD

This thesis, being concerned with some aspects of stability in structural and mechanical systems, naturally divides into two sections. The first of these, Chapters I through III, is concerned with the development of a non-destructive method for evaluating the stability of non-circular cylindrical shells. Chapter I describes an investigation made on the simplest non-circular body - a cylindrical shell of elliptical cross-section. This section is chosen because the usual circular cylinder is a natural limiting case. The study progressed to the stiffened body of circular cross-section. Such bodies in some respects may be regarded as a conglomeration of struts, interlocked by the thin skin which acts in unison with the more robust stringers. Thus, a consideration of partially restrained columns under axial compression became pertinent, and this issue is reviewed, studied, and clarified in Chapter II. Thus, in straight forward manner the questions of Chapter III were raised, and when these were resolved the foundations of a truly non-destructive test technique for stiffened shells were thoroughly laid.

In the final chapter of the thesis, the design of a device of importance to the survival of human beings exposed to adverse acceleration environments is considered. This device is the prime component of a facility for the investigation of human response to virtually instantaneous and very high "g" accelerations. Two feasible designs are outlined. The study indicates that the more promising of these is

one which depends upon the use of a mechanical system displaced from a position of unstable equilibrium.

TABLE OF CONTENTS

LIST OF TABLES

LIST OF ILLUSTRATIONS

GLOSSARY OF ABBREVIATIONS

A	semi-major axis of ellipse
B	semi-minor axis of ellipse
BN	buckle number, defined in Chapter I
$\overline{BN}$	mean buckle number, elliptical shell parameter defined in Chapter I
EI	flexural rigidity
g	acceleration due to gravity, 32.2 ft/sec^2
k	rotational spring constant
L	length
L*	distance between inflection points of buckled deflection curve
ℓ	distance between inflection points of lateral-load bending curve
LVDT	linear variable differential transformer
M, m	mass (Chapter IV)
m	mass per unit length (Chapter II)
P	axial load
R	radius of curvature at location of buckle center
$\overline{R}$	center of radius of curvature group
t	thickness of shell wall
V	velocity
W	lateral force
y	lateral deflection
α, β	rotational end restraint coefficients, $\alpha, \beta = \frac{kL}{EI}$
δ	maximum deflection due to unit load applied at point of maximum compliance

ϵ error function

θ angular location of buckle center, measured from end of semi-major axis

λ circumferential dimension (width) of buckle

λ first eigenvalue of characteristic buckling equation

$$\lambda^2 = PL/EI$$

μ first eigenvalue of characteristic frequency equation

$$\mu^4 = \frac{\omega^2 mL^4}{EI}$$

ξ lateral stiffness, W/y

ω natural frequency

Subscripts

cr critical value

α, β rotational restraint coefficients at ends of beam - when used with P implies critical value as well

SUMMARY

This thesis divides naturally into two sections. The first is concerned with non-destructive evaluation of the stability of shells, and the second with the use of an unstable mechanical device in the design of an ultra-high g crash simulator.

The investigation of the structural problem begins with an experimental study of elliptical shells under axial compressive load. It turns then to the non-destructive evaluation of rotationally restrained columns, and culminates in the development of a general method of non-destructive evaluation of shells.

The study of elliptical shells indicates that such bodies are imperfection sensitive for major-to-minor-axis ratios (B/A) as small as 0.5, and that significant postbuckling strength is present for B/A less than 0.7. As with circular shells it was found that the width of buckles is dependent upon the length and thickness of the shell as well as the radius of curvature. Detailed examination of the test data reveals that the local behavior of elliptical shells is comparable to that for equivalent (i.e. equal curvature) circular shells. In all, 21 steel specimens were tested and 424 data points generated.

The emphasis in the non-destructive column testing study is concentrated on a demonstration that various semi-empirical relationships previously known can be derived from the governing equations by a consistent approximation method. As a result of this study a new,

accurate, non-destructive technique for the investigation of the stability of shells is suggested, and its applicability to a stringer-stiffened plexiglass circular cylinder under axial compression is demonstrated.

In the final section the design of a prime mover for an instantaneous 200g crash simulator is discussed. Two feasible design approaches are outlined. The first is based on the use of momentum transfer, and the second on direct force generation. The study indicates that the latter has greater potential. It obtains its characteristics from the use of a mechanical system displaced from a position of unstable equilibrium.

CHAPTER I

AN EXPERIMENTAL INVESTIGATION OF THE BUCKLING OF ELLIPTICAL SHELLS

Introduction

The literature on the behavior of shell bodies under various types of loading is voluminous. Nash (1,2) listed some 1455 papers and books on the subject published prior to 1954, and 884 between 1954 and 1956. In the light of space and weapons system applications, it is logical to assume that this accelerating growth has continued. Still it is only recently that the subject of the instability of elliptical cylindrical shells under axial compression has received attention. A literature search disclosed less than a dozen papers published. Of these only three have included experimental results, a total of 59 non-circular shell bodies having been tested (3,4,5).

It is unfortunate that the study of the elliptical shell has been neglected. The behavior of such a body, especially under axial compression, is very interesting. Where the circular cylinder is extremely imperfection sensitive, the initial theoretical studies of Kempner and Chen (6,7) indicated that, for sufficient eccentricity of its section, the oval shell might be quite imperfection insensitive. Later, Hutchinson's (3) analysis of imperfection sensitivity showed that even for highly eccentric cross sections, the elliptical shell remained imperfection sensitive. Subsequent papers by Kempner and Chen

(8), Tennyson, Booton, and Caswell (4), and Feinstein, Erickson, and Kempner (5) have confirmed this result. In any case, it is agreed that although elliptical shells of low eccentricity collapse upon reaching their critical load, more eccentric shells have significant post-buckling strength. What is not known, however, is the value of B/A at which this affect becomes noticable. Here more experimental information would be helpful.

Some years ago Zahorski (9) discussed the segmental buckling of a cylinder, and drew attention to the possible relationship between the behavior of a compressed thin-walled shell and its behavior under a concentrated radial load. Starting from the work of Bijlaard (10), he computed the size of buckles due to normal loading. It is interesting to note that Zahorski's predictions bear a strong resemblance to the experimental results of Komp (11) for thin shells in axial compression. Figure (1) demonstrates this point.

There is excellent agreement between the two studies for R/t values less than 1000. Although the agreement for $R/t \geq 1000$ is not as good, we note that Zahorski's calculations were made for a constant length cylinder, and thus his L/R values varied from 7 to 16. The L/R's in Komp's studies were, in general, much less. Komp showed, however, that for L/R values above 10, the influences of this parameter are small. This may in some way begin to explain the discrepancies between the two studies.

There are other significant features of Komp's work which have not been mentioned thus far. To summarize briefly, Komp demonstrated that the size of the buckles produced on thin-walled circular cylin-

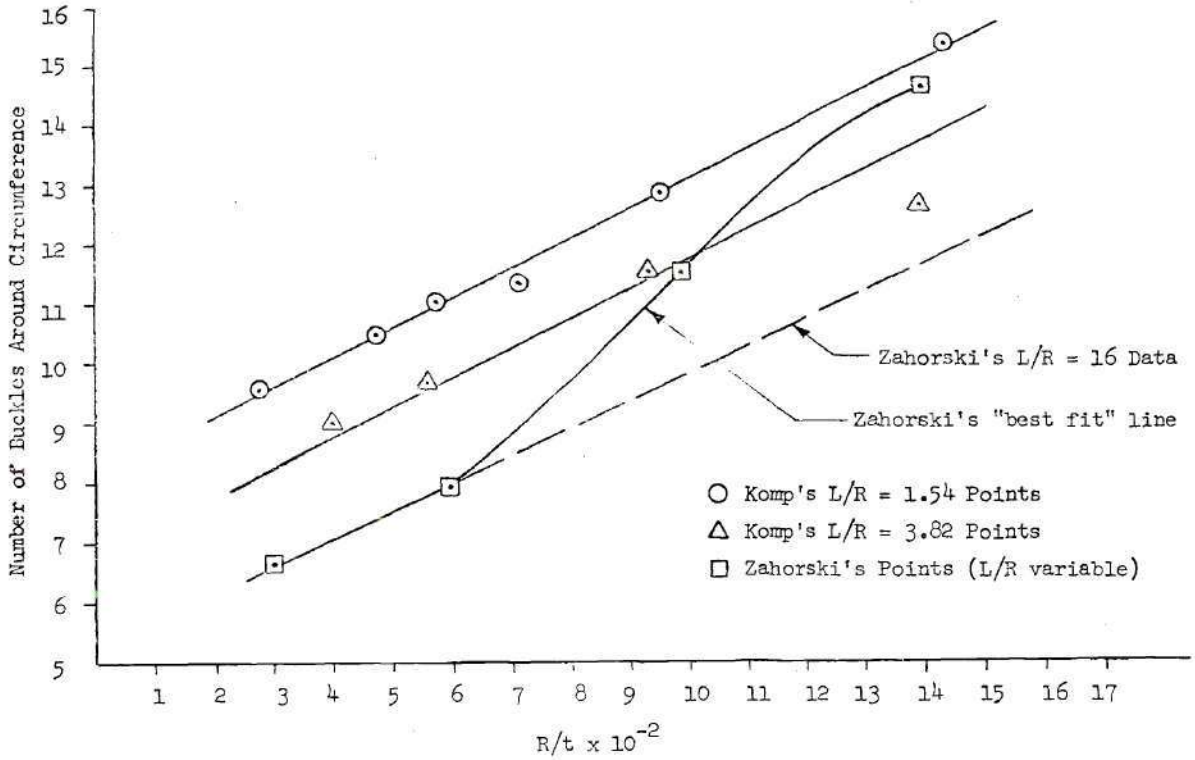

Figure 1. Comparison of Zahorski's and Komp's Results.
Number of Buckles around Circumference vs R/t.

drical shells by an axial compressive load does not depend upon the quality of the shell tested, the material from which it was made, or the force required to cause collapse. It is a function solely of the shell geometry. Furthermore, he showed that, for a constant R/t, the number of buckles required to fill the circumference decreases (buckle size increases) with increasing L/R until this quantity reaches a value of approximately 10, after which the effect of L/R is small. As R/t increases, the number of buckles increases (their normalized size decreases), the relationship being linear over the range studied. Test machine stiffness effects were also examined, and were found not to be an influential factor.

The question is, then, whether the observations of Zahorski and Komp are applicable only to the circular body, or whether they have a more general significance. To resolve this issue, at least partially, and to form a basis for later studies, a series of tests was made on elliptical shells. This program sought to ascertain the nature of the buckles produced when such a body is compressed to the point of instability.

Hoff's (12) suggestion that critical compressive stress could be computed from a consideration of buckle geometry led Komp (11) to use buckle size as a measure of the effect on the buckling process of changes in the dimensions of circular cylindrical shells. Komp's scheme offers a great advantage to the elliptical shell experimenter. Horton and Cox (13) showed that buckling is essentially a local phenomenon, occurring when the local stress reaches the critical level. In an elliptical shell the radius of curvature varies continuously

around the circumference. Thus, if we use buckle size as a measure of the effect on the buckling process of changes in shell geometry, each buckle on an elliptical shell is an individual data point. This means that it is not necessary to test a great many specimens, but only to measure a great many buckles. In the study reported here 21 specimens yielded 424 data points (buckles).

Outline of the Experimental Program

Komp (11) demonstrated that, for a large sample of nominally identical circular cylindrical shells buckled under axial compression, the circumferential dimension of the buckles is normally distributed. He then investigated the effect of variations in radius to thickness ratio (R/t), length to radius ratio (L/R), and Young's modulus on the "Buckle Number" (BN), which he defined as the ratio of the circumference of the shell to the mean buckle width.

The study reported in this chapter builds on that foundation. Accepting Komp's conclusion regarding normal distribution, experiments were conducted to determine the effect of variations in L/R, L/t, and R/t on the buckle number. For elliptical shells buckle number is redefined to be the ratio of the circumference of a circle with radius equal to the local radius of curvature, to the buckle width. That is,

$$BN = \frac{2\pi R}{\lambda}$$

where R = local radius of curvature at the center of the buckle, and

λ = circumferential dimension (width) of the buckle.

Three families of specimens were constructed, each having a characteristic L/t. Members of these families varied in eccentricity of cross section. One of the families consisted of two sub-families which had different length and thickness dimensions but the same L/t. A single specimen of higher L/t was tested in an effort to increase coverage of the L/T vs R/t plane.

Since the radius of curvature at the buckle varied with the buckle location, each buckle on a given specimen yielded data on the effect of changing L/R and R/t for a constant L/t.

Specimens

Test vehicles for this study were constructed from steel shimstock. Some dimensional limitations were imposed by the choice of this material: maximum unpotted specimen height was 12 inches (the width of commercially available stock), and minimum usable thickness was .003 inches. Thinner shimstock than this was damaged in packaging. Although these characteristics severely curtailed the program, they were accepted since the cost of any other construction method would have been prohibitive.

The specimens were constructed with a soldered lap joint parallel to the axis. The lap joint was located at or near the semi-minor axis of the finished cross section. This location was chosen to minimize the curvature at the joint, thus facilitating construction.

Manufacture was accomplished in five steps:

1. Three exterior templates of the desired elliptical cross section were cut from medium-weight illustration board. The circum-

ference of the ellipse was measured.

2. Shimstock of the desired thickness was squared and cut accurately to the required length and width, including a 1/8th inch allowance for seam overlap. Outer edge location for the overlap was measured and marked.

3. Soldering flux was applied to the inner seam overlap area and the seam was clamped between a steel U-section and an extruded aluminum angle. The seam was soldered.

4. The seamed cylinder was inserted into the elliptical templates, which were positioned near the L/8, L/2, and 7L/8 axial stations along the shell.

5. The shell was potted into aluminum endplates with an EPON 826/DTA epoxy system to hold the elliptical shape. Alignment of reference marks on the endplates and templates ensured that the axis of the shell passed through the centerline of the ball-joint seat in the upper endplate. The templates were removed after potting.

Angular orientation marks were made every 10° around the shell in three bands at L/4, L/2, and 3L/4.

To ensure that specimen dimensions used in calculations were actually those of the specimen tested, each specimen was measured accurately after removal from the end plates following testing. Length measurement was taken to be the free length between the epoxy end castings.

Test Procedure

Tests were conducted in a standard Instron Model TT-D Universal

Test Instrument. The specimen was mounted on the test machine cross-head, and a ball joint centered on the upper endplate to transmit purely axial load. Load measurement was accomplished using the internal strain-gage load cell and chart recorded of the TT-D Instrument.

Tests were conducted at a test machine end-shortening setting of 0.020 inches per minute between buckling events. The occurrance of a buckling event was readily apparent to the test operator: a characteristic and plainly audible noise was heard, accompanied by a sudden departure of the recorded load trace from its smoothly increasing path. At each buckling event the test machine and load recorder were stopped while new buckles were measured and marked. The test was continued until the cross-head of the test machine could no longer keep up with the end displacement; i.e. until load decreased with increasing end shortening.

The width of each buckle was measured to the nearest 0.005 inches with a steel rule. Circumferential location of the buckle center was estimated to the nearest five degrees using the ten-degree reference marks.

Results

Load Behavior

All specimens exhibited a marked change in buckling load behavior with a change in eccentricity of the elliptical cross section. Specimens of least eccentricity (B/A = 0.85) behaved much like circular cylinders: after initial buckling they were able to carry only a fraction of their initial buckling load; i.e. "critical" and "collapse"

loads coincided. An increase in eccentricity to B/A = 0.7 brought dramatic changes in the character of the buckling process. An average of two buckling events preceded collapse, and in some cases two or more buckling events took place at or very near the collapse load. A further increase in eccentricity to B/A = 0.55 increased the average number of pre-collapse buckling events to about 2.6, and again multiple buckling events at or near collapse load were noted.

Figures 2, 3, and 4 are typical load versus time traces (at constant end-shortening rate) from the Instron recorder. In general character they support the theoretical predictions contained in Hutchinson's paper. It is noted that although Hutchinson's experiments demonstrated no difference between critical and collapse loads until B/A was reduced to 0.333, the work reported here shows a marked difference in every test for B/A = 0.7 or less.

Buckle Geometry

Komp showed by testing 64 shells of identical material and geometry that the distribution of the circumferential buckle number is normal for a constant radius of curvature. Thus, the mean buckle number at a given radius of curvature has much more significance than do the individual buckle numbers from which it is computed. Some difficulty in elliptical shell testing is caused by the fact that buckles occur at different local radii of curvature over a given shell. However, there seems to be no reason why Komp's conclusions regarding buckle number distribution should not apply equally to elliptical shells. Thus, it seems logical to group the buckle number data on local radii of curvature and compute a "mean buckle number"

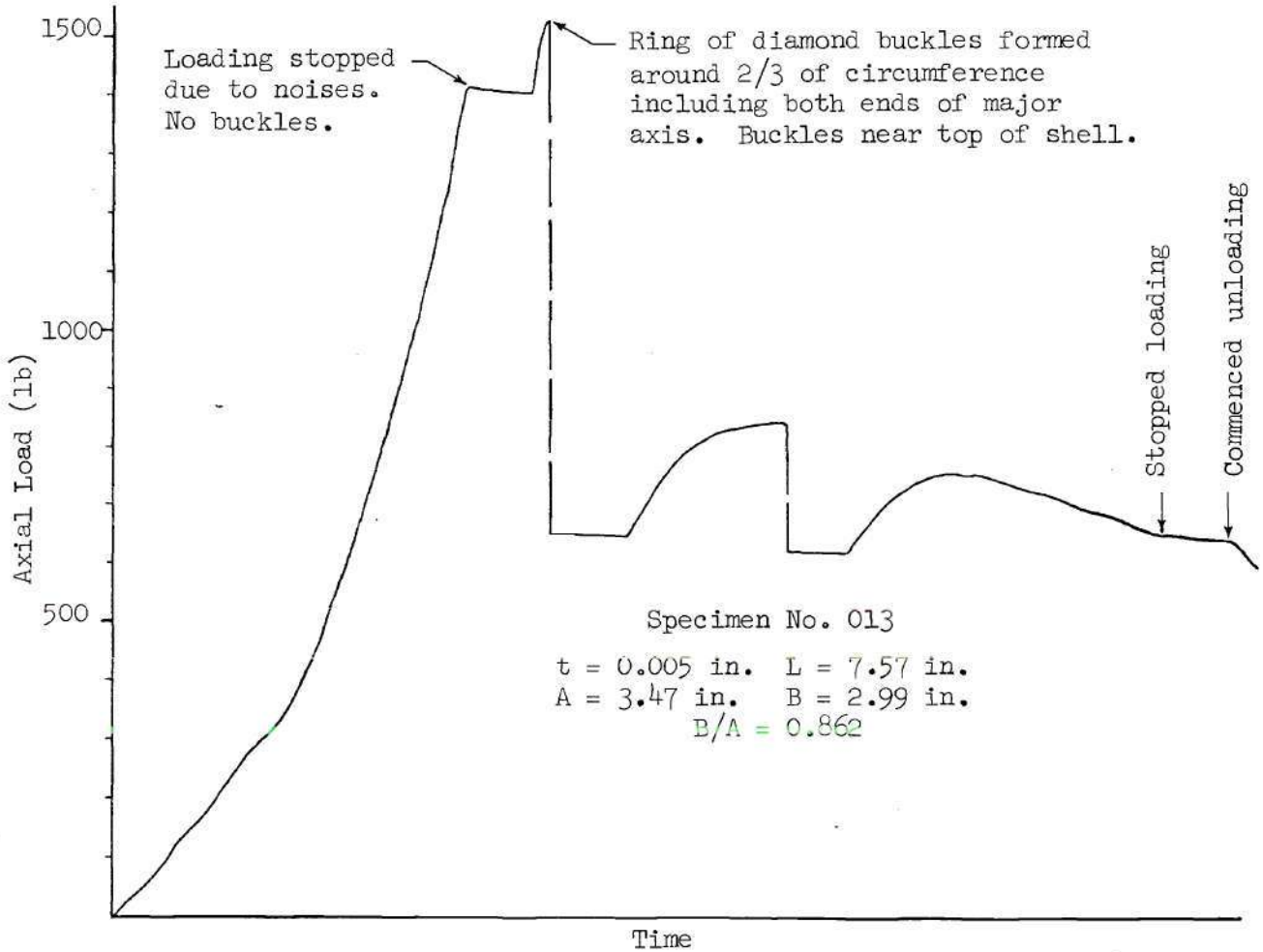

Figure 2. Load vs Time Elliptical Cylinder Tests - Specimen No. 013.

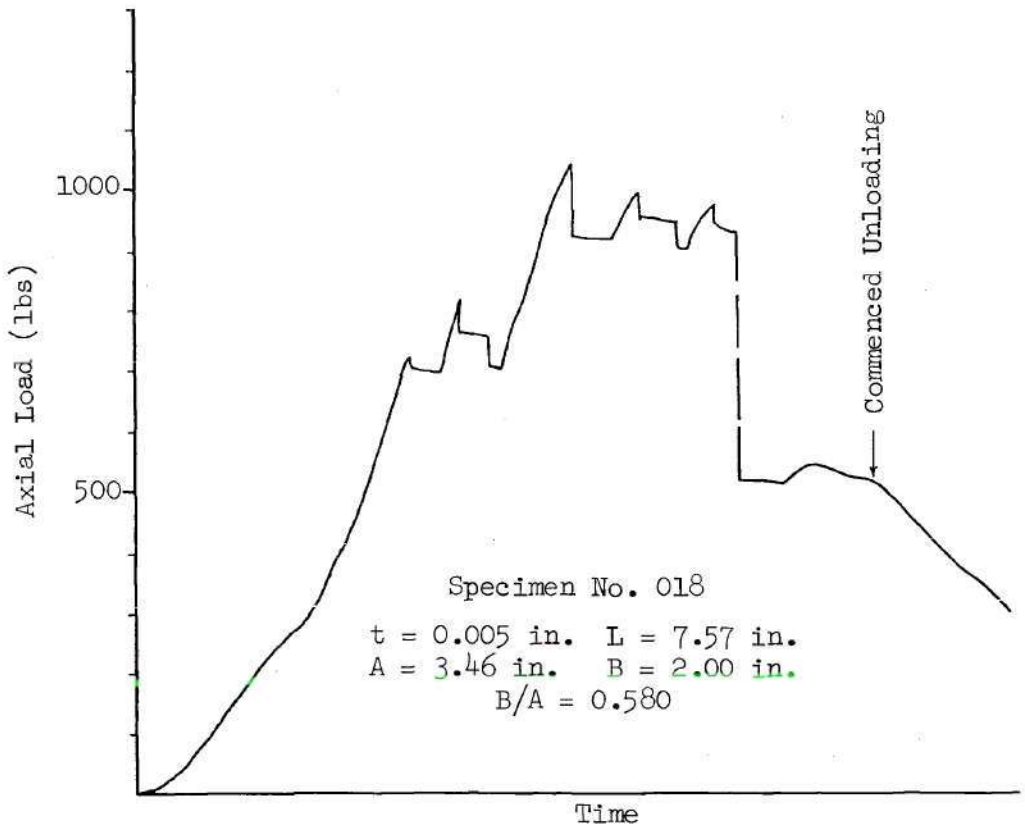

Figure 3. Load vs Time Elliptical Cylinder Tests - Specimen No. 018.

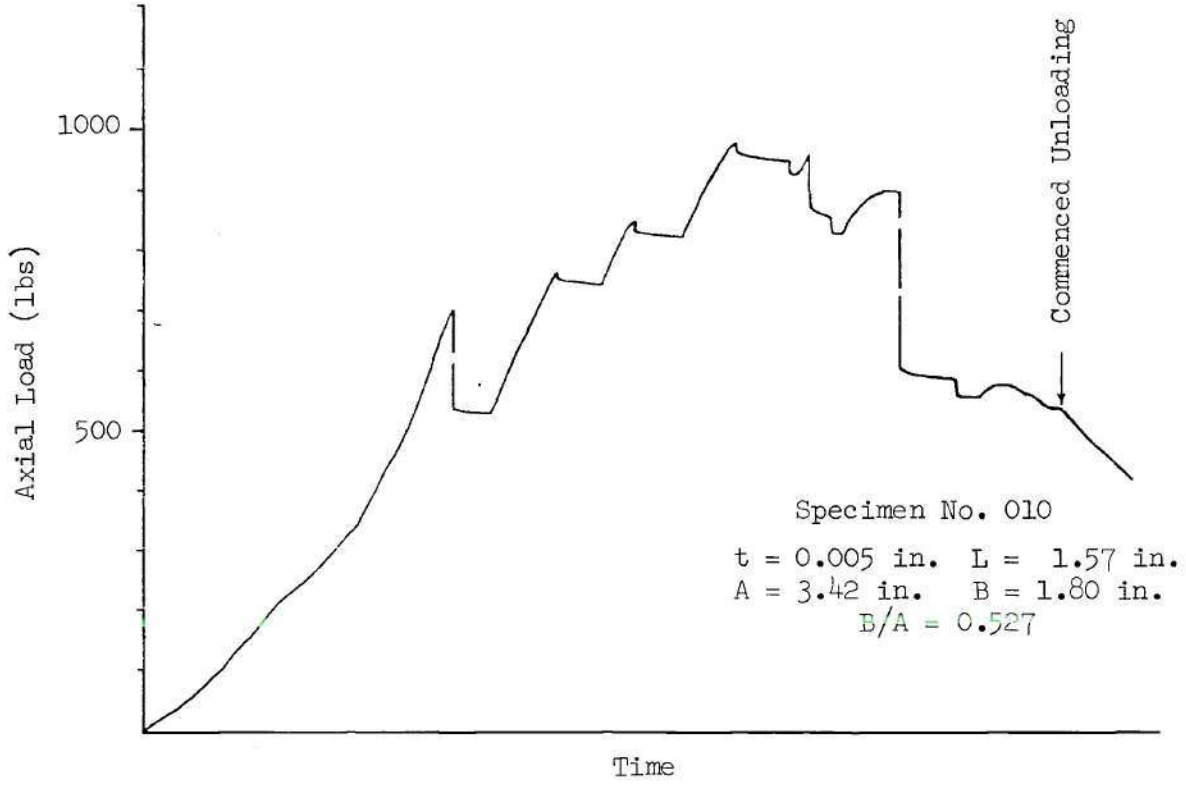

Figure 4. Load vs Time Elliptical Cylinder Tests - Specimen No. 010.

for each group. This was done.

Data recorded during elliptical cylinder testing, together with computed radii of curvature, are presented in Appendix B, Tables 23-43. Table 1 shows mean buckle width ($\bar{\lambda}$) and mean buckle number ($\overline{BN}$) computed from this data grouped on local radius of curvature.

Figures 5 through 9 are graphical representations of the data in Table 1, each figure depicting $\overline{BN}$ vs $\bar{R}/t$ for a given L/t family. In each case the data points are virtually colinear. (Data points "x-ed" out are those determined from only one or two buckles, and are thus lightly weighted).

Figure 10 shows the relationship between the $\overline{BN}$ vs $\bar{R}/t$ lines of the several families. An increase in L/t results in a decrease in slope. It is notable that the plots for the two L/t = 2315 sub-families are exactly parallel, but their magnitude differs. This would seem to indicate that L/t is not sufficient in itself to characterize the elliptical shell families.

Figure 11 shows the data from Table 1 in the three non-dimensional coordinates $L/\bar{R}$, $\bar{R}/t$, and $\overline{BN}$. Sections of constant $L/\bar{R}$ and $\bar{R}/t$ cut from this figure were compared with corresponding figures from Komp's paper. Figure 12 combined Komp's circular cylinder data and the elliptical shell data. Figure 13 includes Zahorski's theoretical predictions as well. For a constant R/t = 400 the two sets of information are consistent (Figure 12). Likewise for an $L/\bar{R}$ parameter of 3.82 there is good agreement between the elliptical and circular results (Figure 13). The double values of buckle number for L/t = 2315 are, of course, evident here also.

Table 1. Elliptical Cylinder Test Data Grouped on Radius of Curvature

	Local Radius of Curvature (in.)	0.5-1.0	1.0-1.5	1.5-2.0	2.0-2.5	2.5-3.0	3.0-3.5	3.5-4.0	4.0-4.5	4.5-5.0	5.0-5.5	5.5-6.0	6.0-6.5	6.5-7.0
L/t=1514 L=7.57; t=.005	No. of Data Pts	2	8	9	12	24	12	21	5	7	0	5	0	1
	L/ $\bar{R}$	10.1	6.05	4.32	3.36	2.75	2.32	2.02	1.78	1.59	1.44	1.32	1.21	1.12
	$\bar{R}$/t	150	250	350	450	550	650	750	850	950	1050	1150	1250	1350
	$\bar{\lambda}$	0.92	0.95	1.48	1.60	1.60	1.79	1.87	1.97	2.07		2.15		2.2
	Buckle No.	5.10	8.28	7.44	8.85	10.80	11.4	12.6	13.56	14.41		16.80		19.3
L/t=2315 L=11.57; t=.005	No. of Data Pts	2	7	15	11	17	14	7	10	13	1	2	1	0
	L/ $\bar{R}$	15.4	9.25	6.61	5.15	4.21	3.56	3.08	2.72	2.44	2.20	2.01	1.85	1.71
	$\bar{R}$/t	150	250	350	450	550	650	750	850	950	1050	1150	1250	1350
	$\bar{\lambda}$	0.65	1.04	1.36	1.71	1.66	1.96	1.96	2.14	1.96	2.65	2.3	3.25	
	Buckle No.		7.56	8.1	8.27	10.41	10.41	12.0	12.48	15.22	12.48	15.75	12.1	
L/t=2315 L=9.27; t=.004	No. of Data Pts	2	8	9	14	21	13	10	6	9	2	4	3	1
	L/ $\bar{R}$	12.37	7.42	5.30	4.12	3.37	2.86	2.47	2.18	1.95	1.77	1.61	1.48	1.37
	$\bar{R}$/t	187.5	312.5	437.5	562.5	687.5	812.5	937.5	1062.5	1187.5	1312.5	1437.5	1562.5	1687.5
	$\bar{\lambda}$	0.725	1.19	1.37	1.67	1.70	2.00	1.86	2.23	1.98	1.78	2.14	2.23	2.25
	Buckle No.	6.5	6.6	8.03	8.48	10.18	10.21	12.68	12.00	15.08	18.55	16.88	17.62	18.38
L/t=2892 L=11.57; t=.004	No. of Data Pts	0	10	12	10	17	10	9	6	8	9	3	1	2
	L/ $\bar{R}$	15.4	9.25	6.61	5.15	4.21	3.56	3.08	2.72	2.44	2.20	2.01	1.85	1.71
	$\bar{R}$/t	187.5	312.5	437.5	562.5	687.5	812.5	937.5	1062.5	1187.5	1312.5	1437.5	1562.5	1687.5
	$\bar{\lambda}$		1.03	1.275	1.5	1.66	1.85	1.85	1.99	1.77	2.12	1.97	1.5	2.25
	Buckle No.		7.64	8.63	9.43	10.42	11.06	12.75	13.43	16.9	15.6	18.37	26.2	18.9
L/t=3855 L=11.57; t=.003	No. of Data Pts					11	9	6	3					
	L/ $\bar{R}$					4.21	3.56	3.08	2.72					
	$\bar{R}$/t					916.7	1083.3	1250.0	1416.7					
	$\bar{\lambda}$					1.56	1.67	1.81	2.05					
	Buckle No.					11.1	12.23	13.0	13.05					

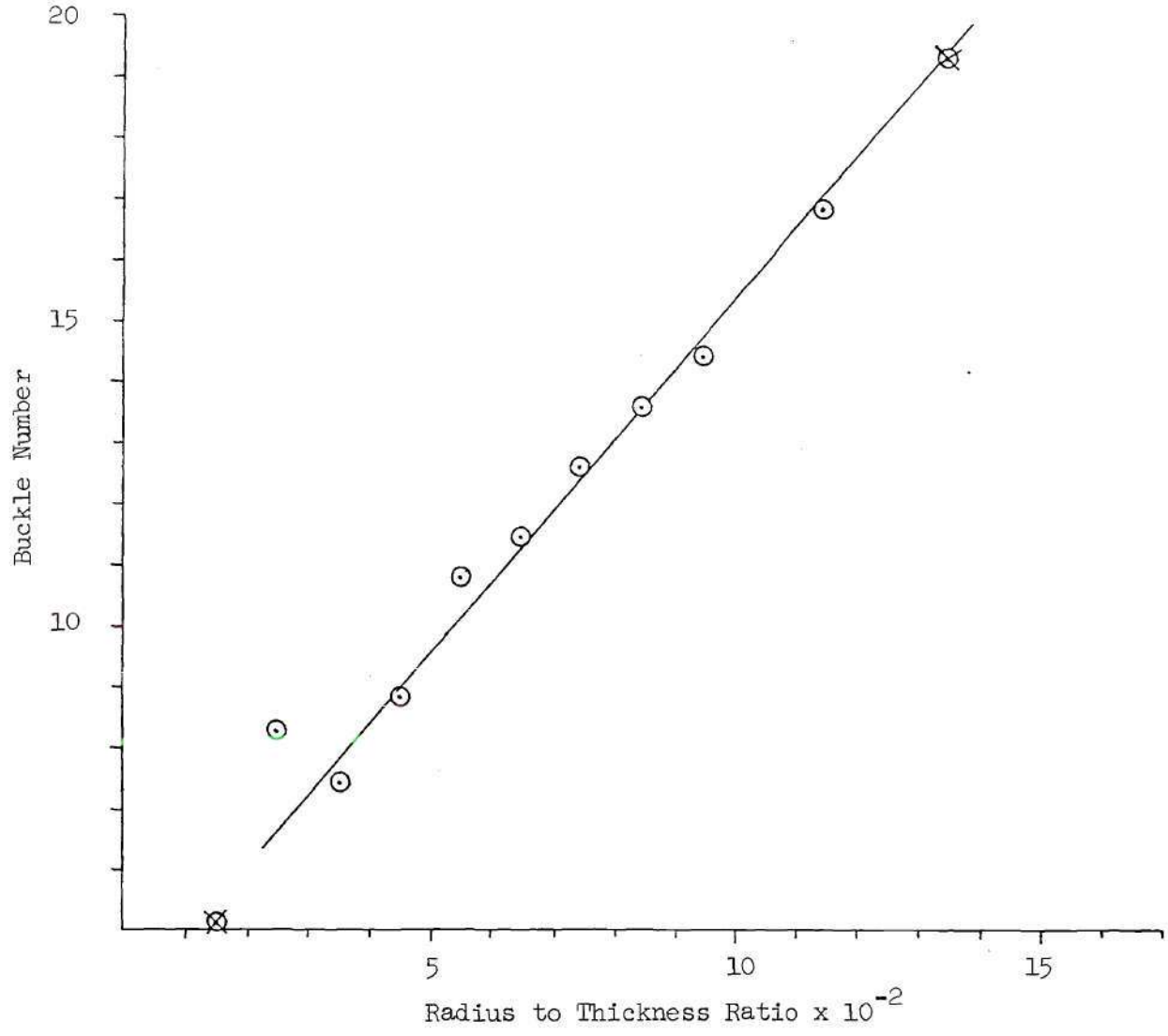

Figure 5. Buckle Number vs Radius to Thickness Ratio - Elliptical Cylinders with L/t = 1514.

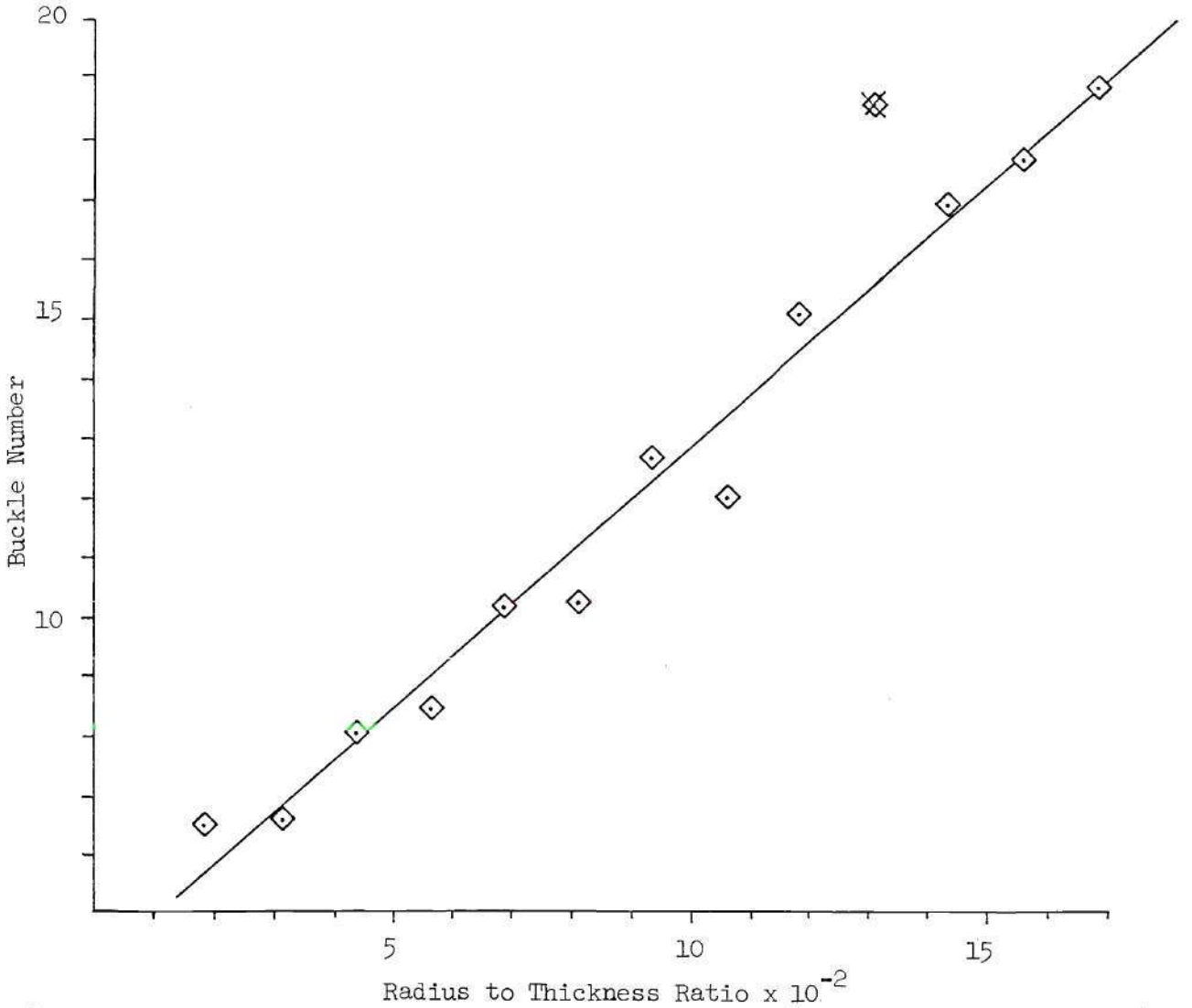

Figure 6. Buckle Number vs Radius to Thickness Ratio - Elliptical Cylinders with L/t = 2315, (L = 9.27 in., t = 0.004 in.).

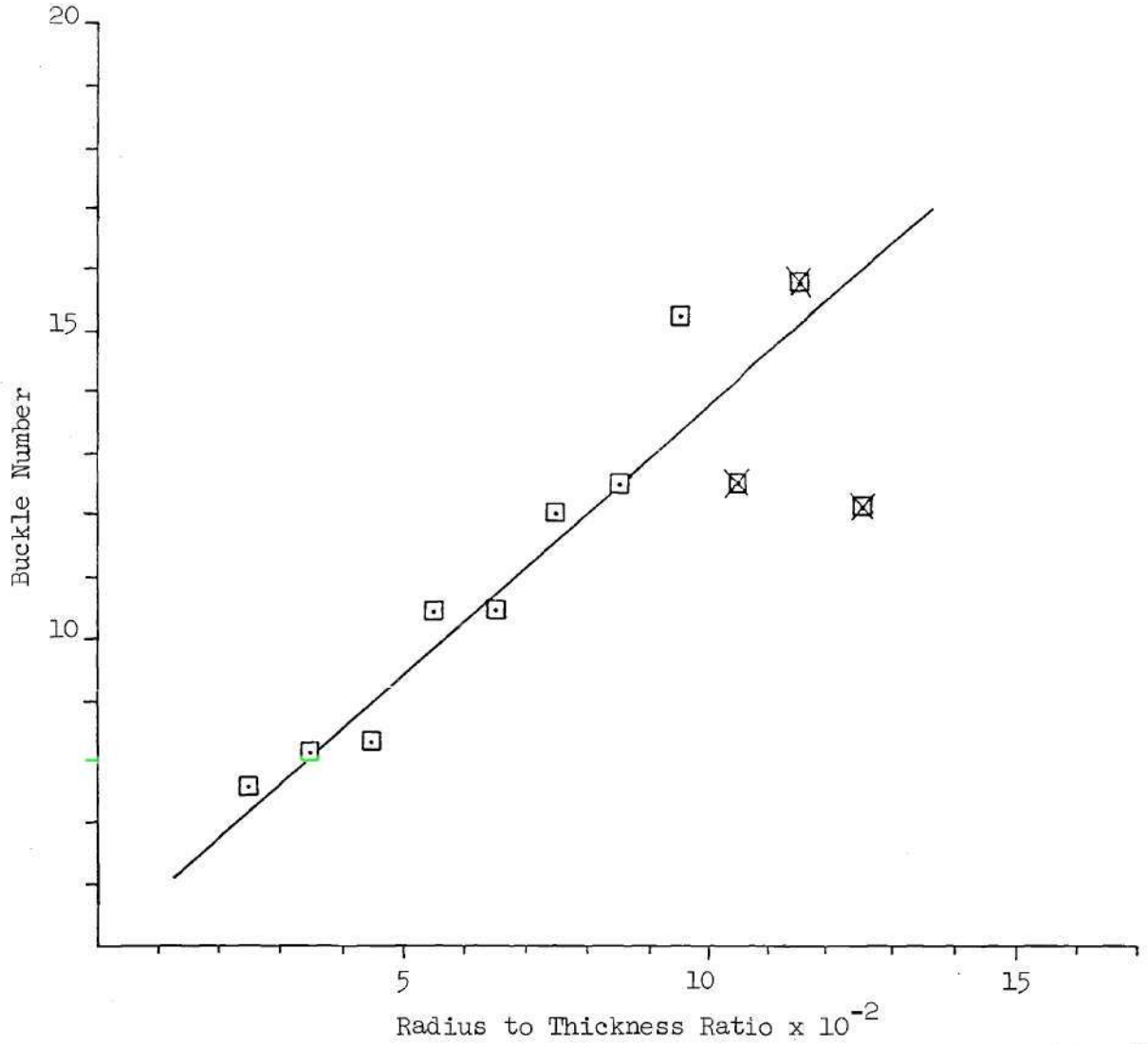

Figure 7. Buckle Number vs Radius to Thickness Ratio - Elliptical Cylinders with L/t = 2315, (L = 11.57 in., t = 0.005 in.).

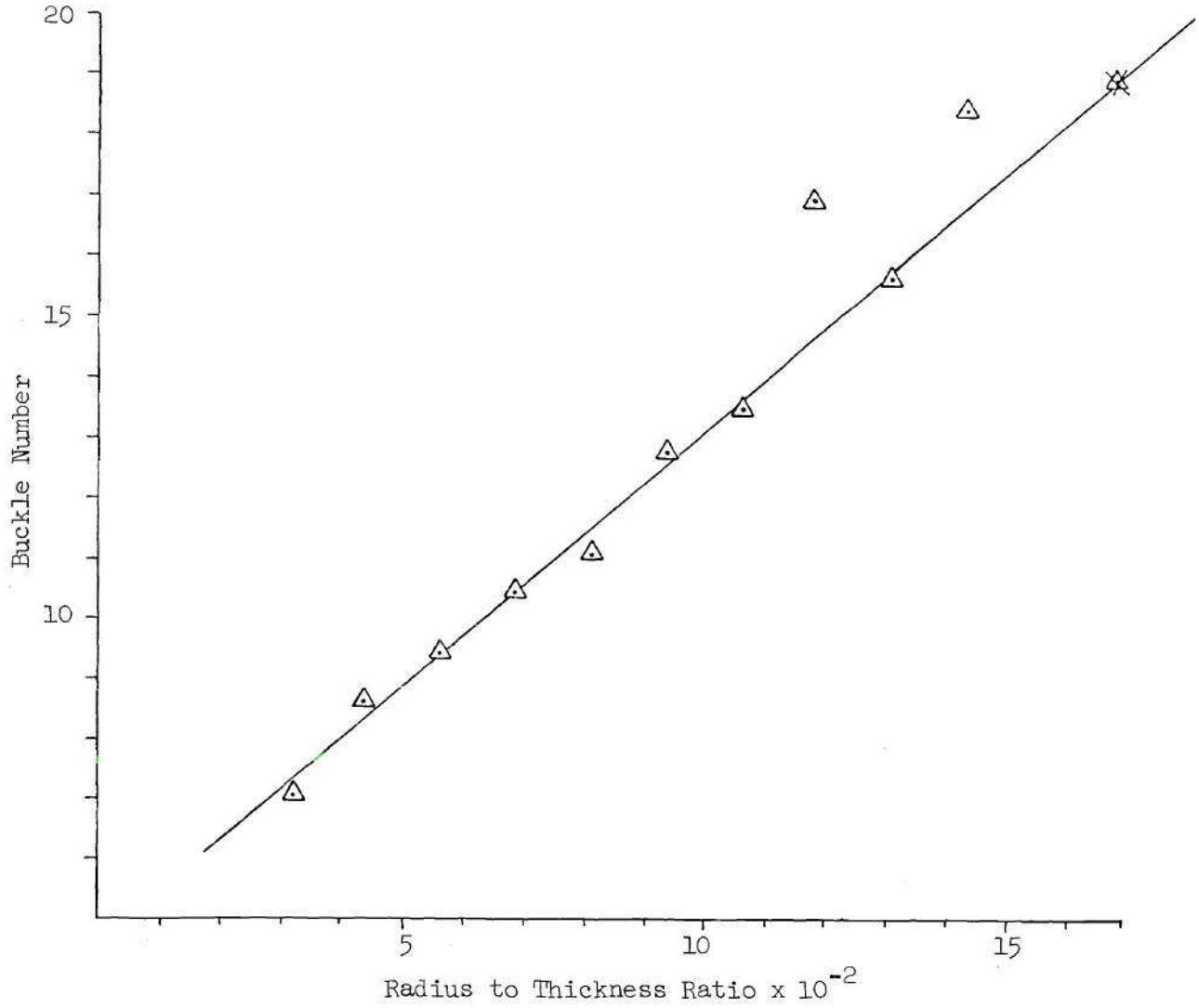

Figure 8. Buckle Number vs Radius to Thickness Ratio - Elliptical Cylinders with L/t = 2893.

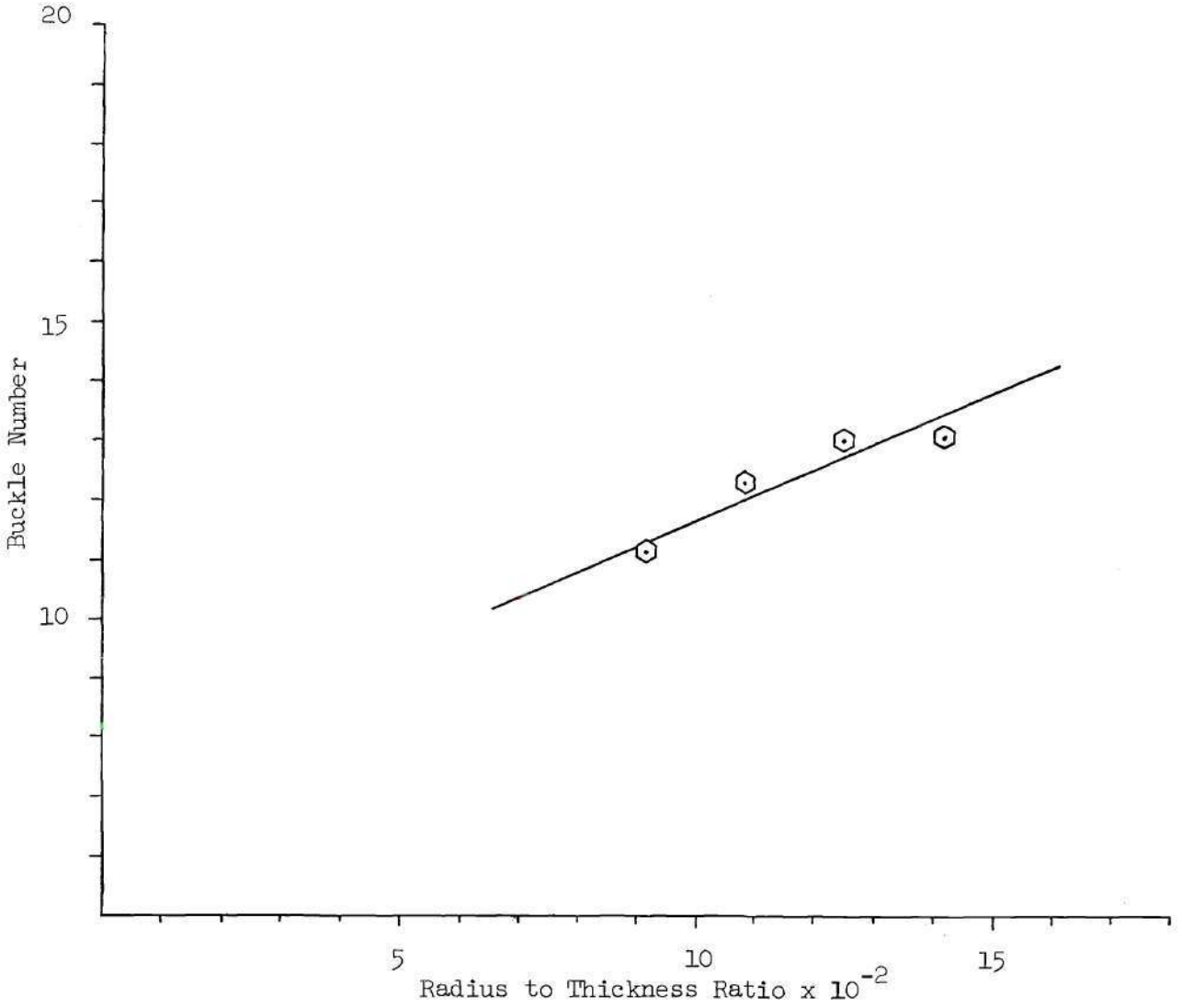

Figure 9. Buckle Number vs Radius to Thickness Ratio - Elliptical Cylinders with L/t = 3855.

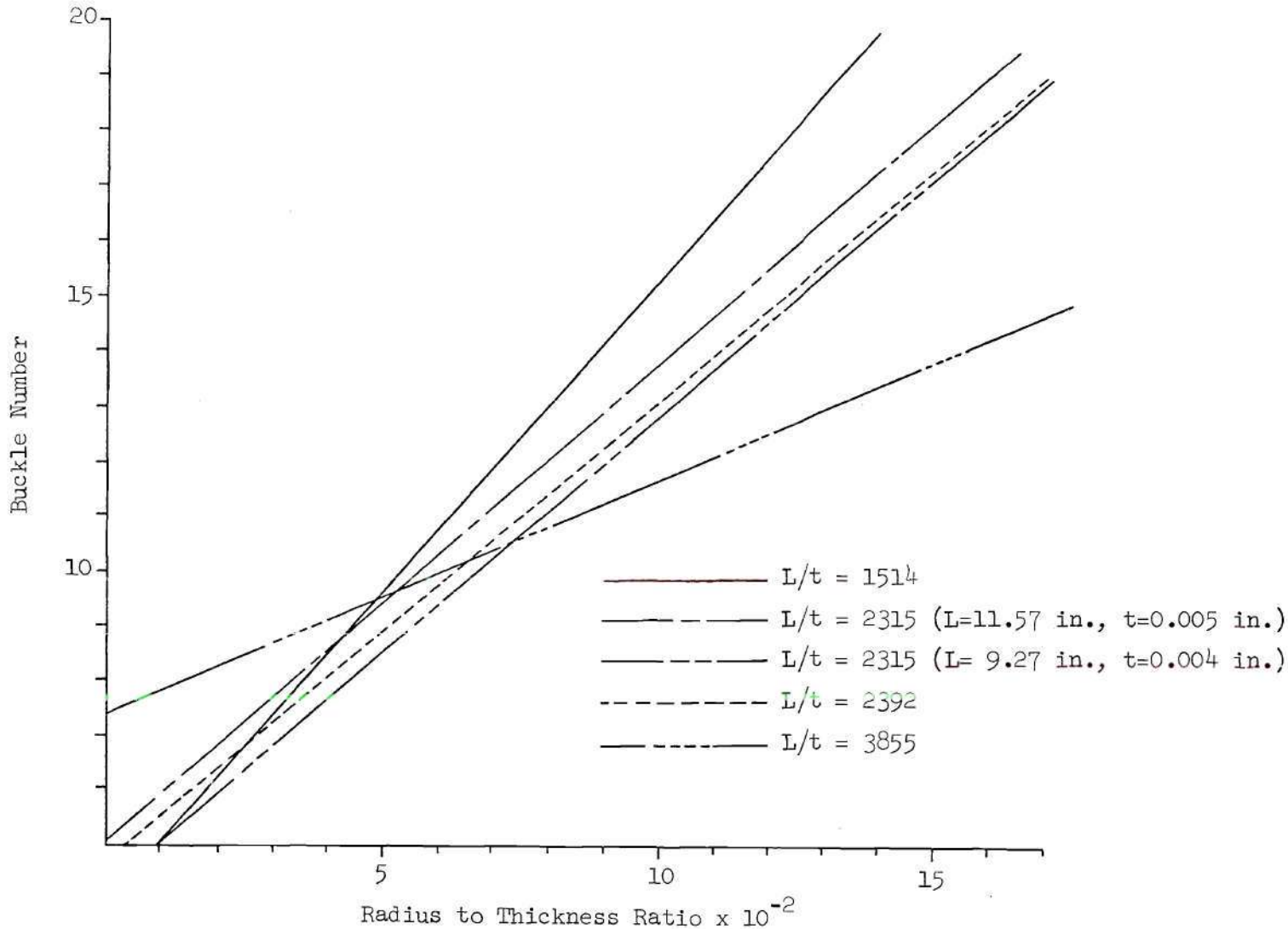

Figure 10. Comparison of BN vs R/t Curves for Different Values of L/t Elliptical Cylinder Tests.

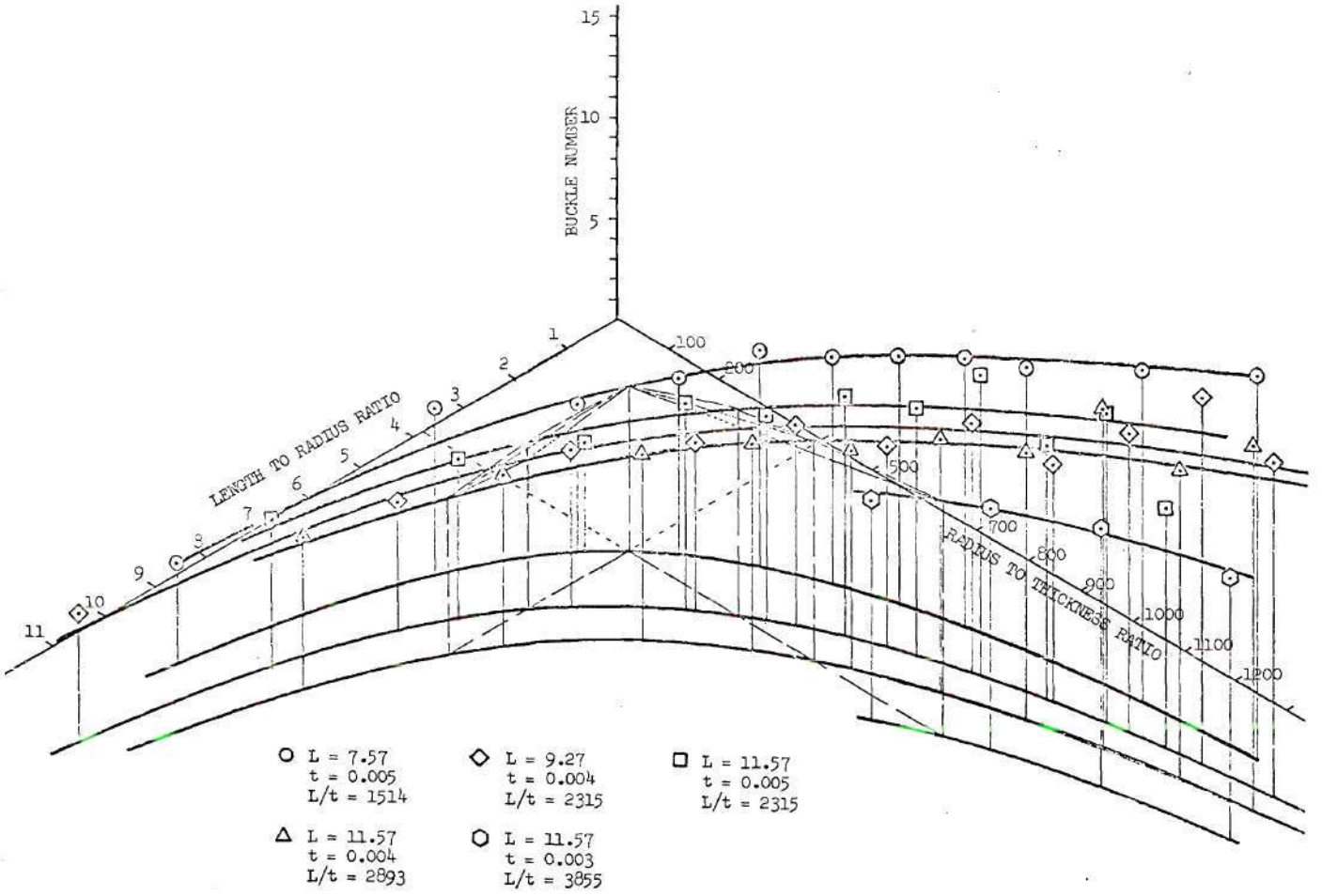

Figure 11. Elliptical Cylinder Test Data, Buckle Number vs Length, Radius, and Thickness.

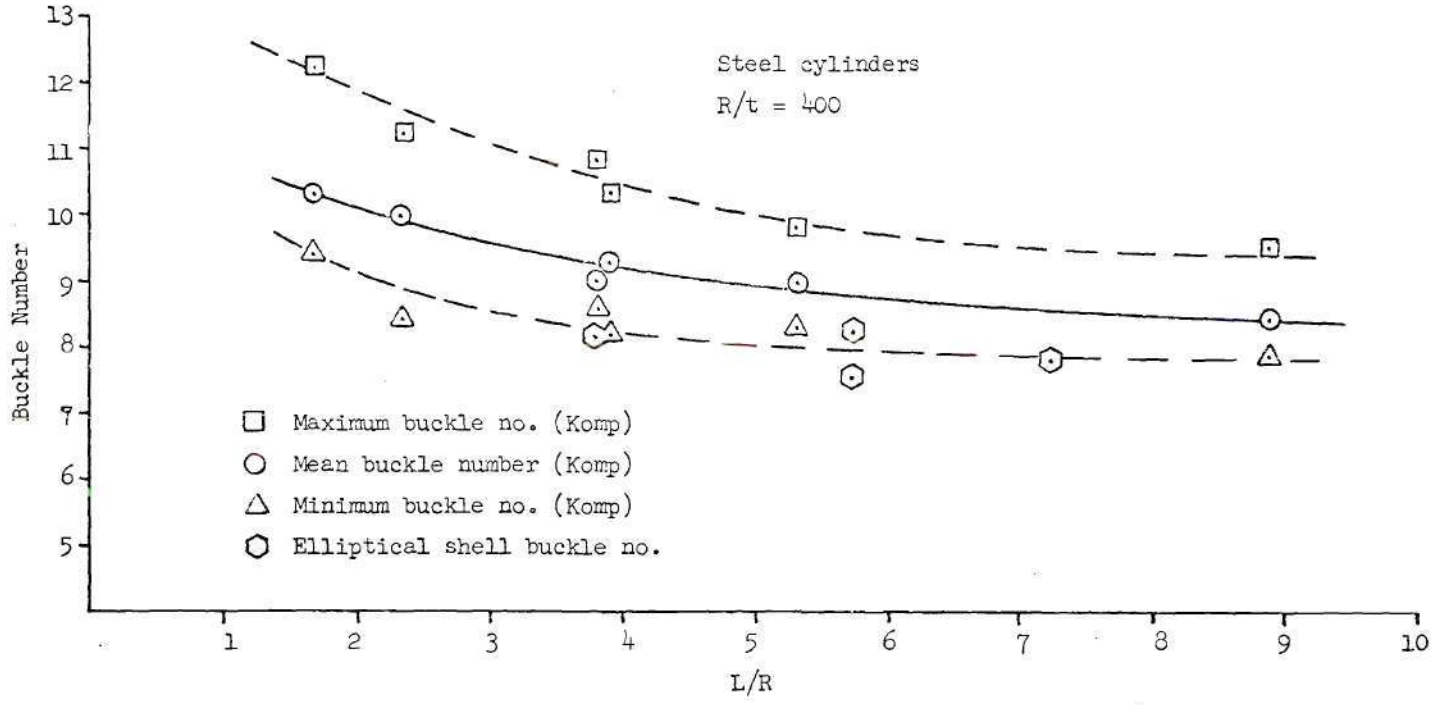

Figure 12. Comparison of Komp's and Elliptical Shell Results - Buckle Number vs L/R for Constant R/t.

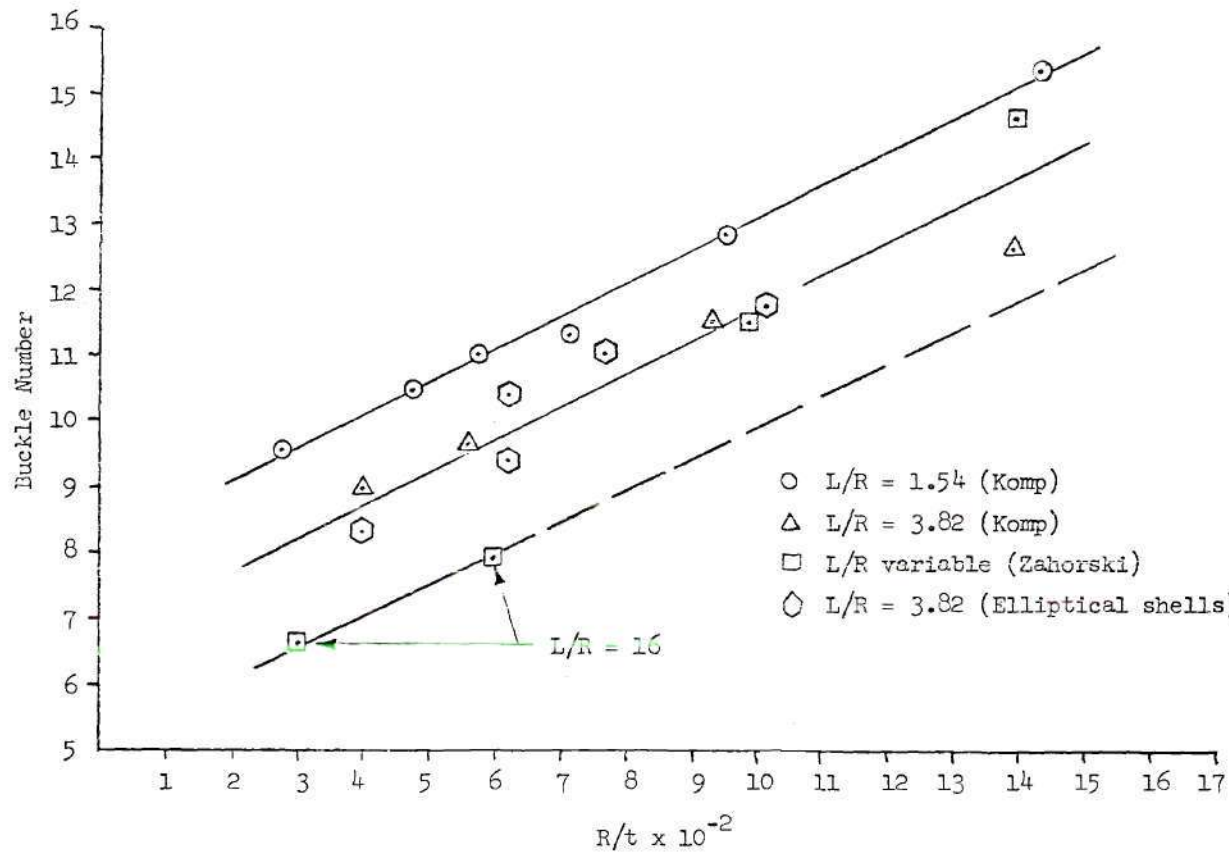

Figure 13. Comparison of Results - Buckle Number vs R/t for Three Values of L/R.

Conclusions

The results of this study of elliptical shells lead to the following conclusions:

1. Elliptical shell buckling differs from cylindrical shell buckling in that, for sufficient eccentricity of the cross section, initial buckling is not catastrophic, and that buckling events may take place subsequent to the initial at the same or higher loads. This effect becomes noticable somewhere between $B/A = 0.855$ and $B/A = 0.7$.

2. Mean buckle number is a function of the local radius of curvature, the thickness, and the length of the shell.

3. The non-dimensional parameter L/t seems to define a family of elliptical shells insofar as the rate of change of buckle number is concerned. However, L/t is not sufficient to completely characterize the buckle number behavior of the shell.

In addition, this research shows the conjectures of Zahorski and the studies of Komp, both based on the circular shell, to be entirely consistent with the observed behavior of a buckled elliptical shell. Thus, it is demonstrated that the local buckling characteristics of the elliptical shell under axial compression are the same as those of an equivalent (i.e. equal curvature) circular cylinder. This being the case, non-destructive testing techniques applicable to circular shells should be applicable to elliptical shells, if they are such as to focus primarily on local rather than general behavior.

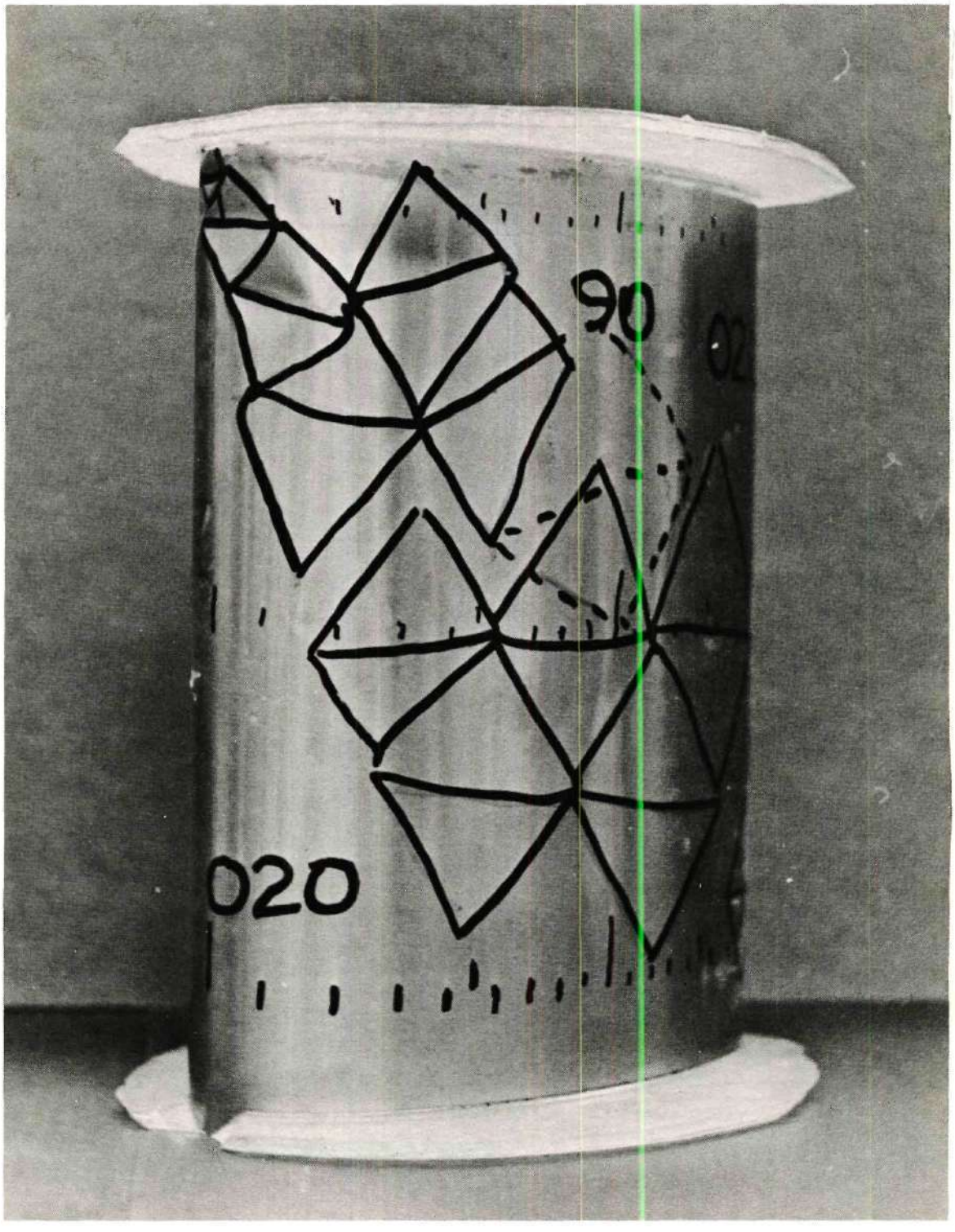

Figure 14. Buckle Patterns on Elliptical Shell 020 - B/A = 0.510, L/t = 2315.

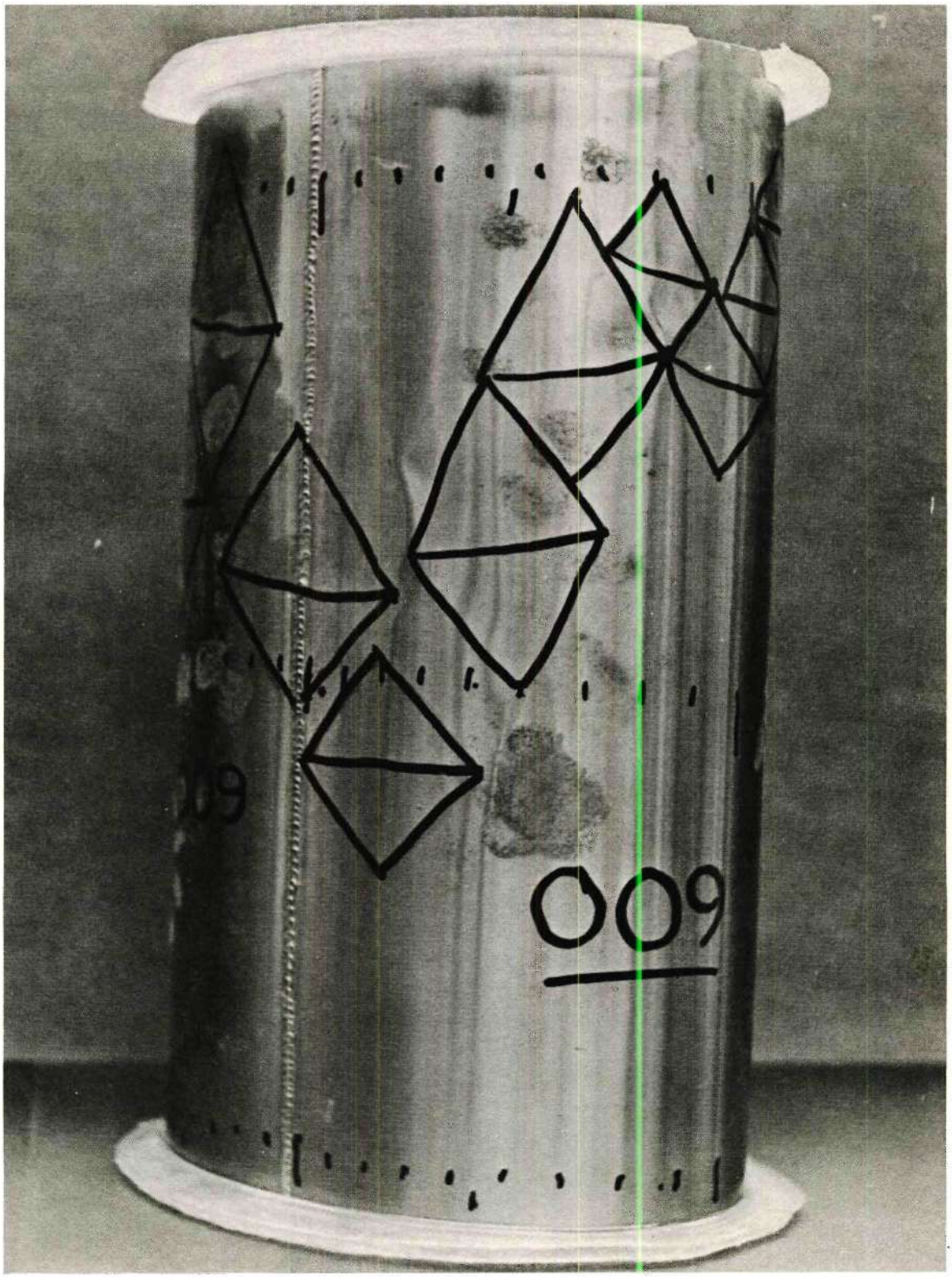

Figure 15. Buckle Patterns on Elliptical Shell 009 - B/A = 0.704, L/t = 2315.

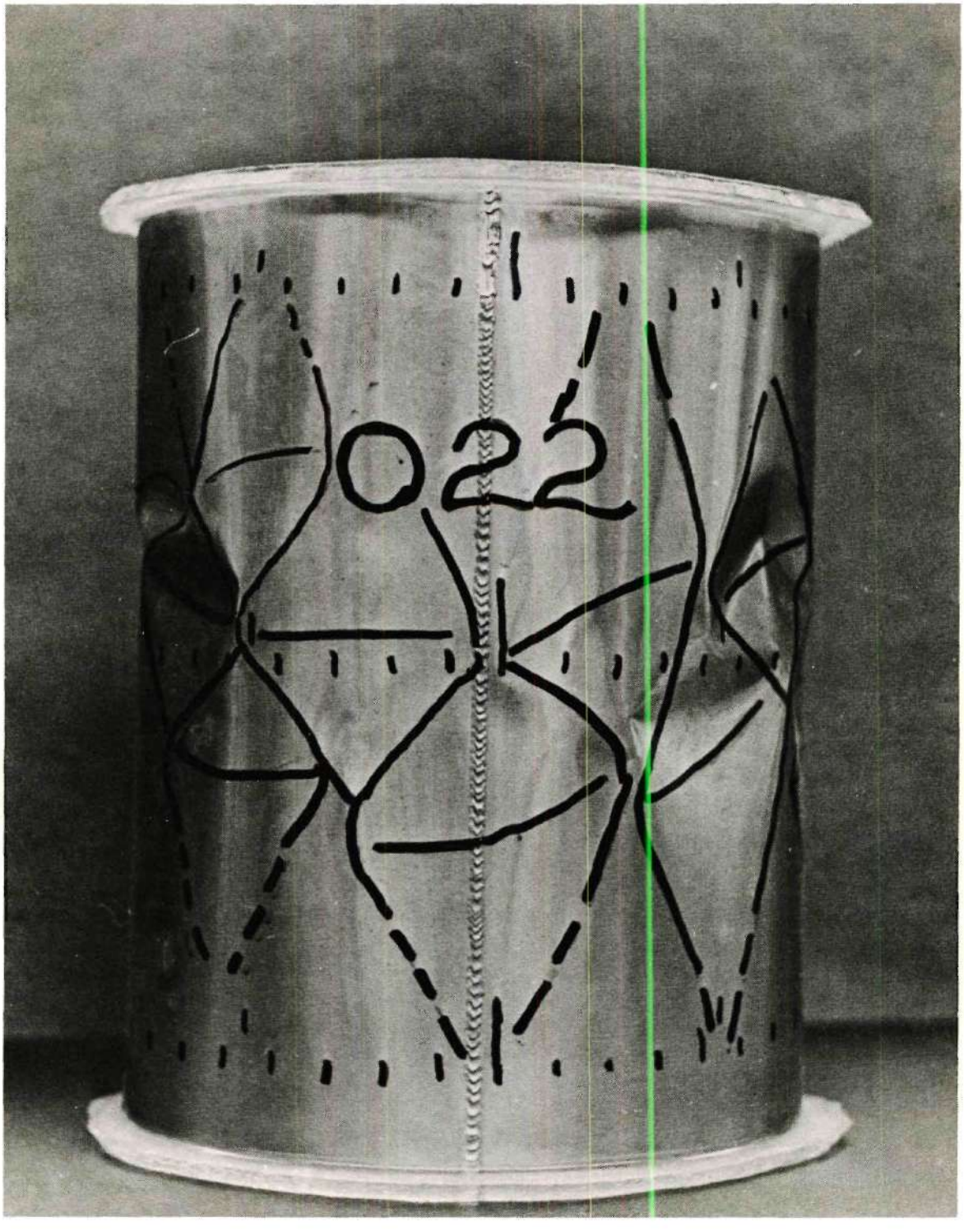

Figure 16. Buckle Patterns on Elliptical Shell 022 - B/A = 0.855, L/t = 2315.

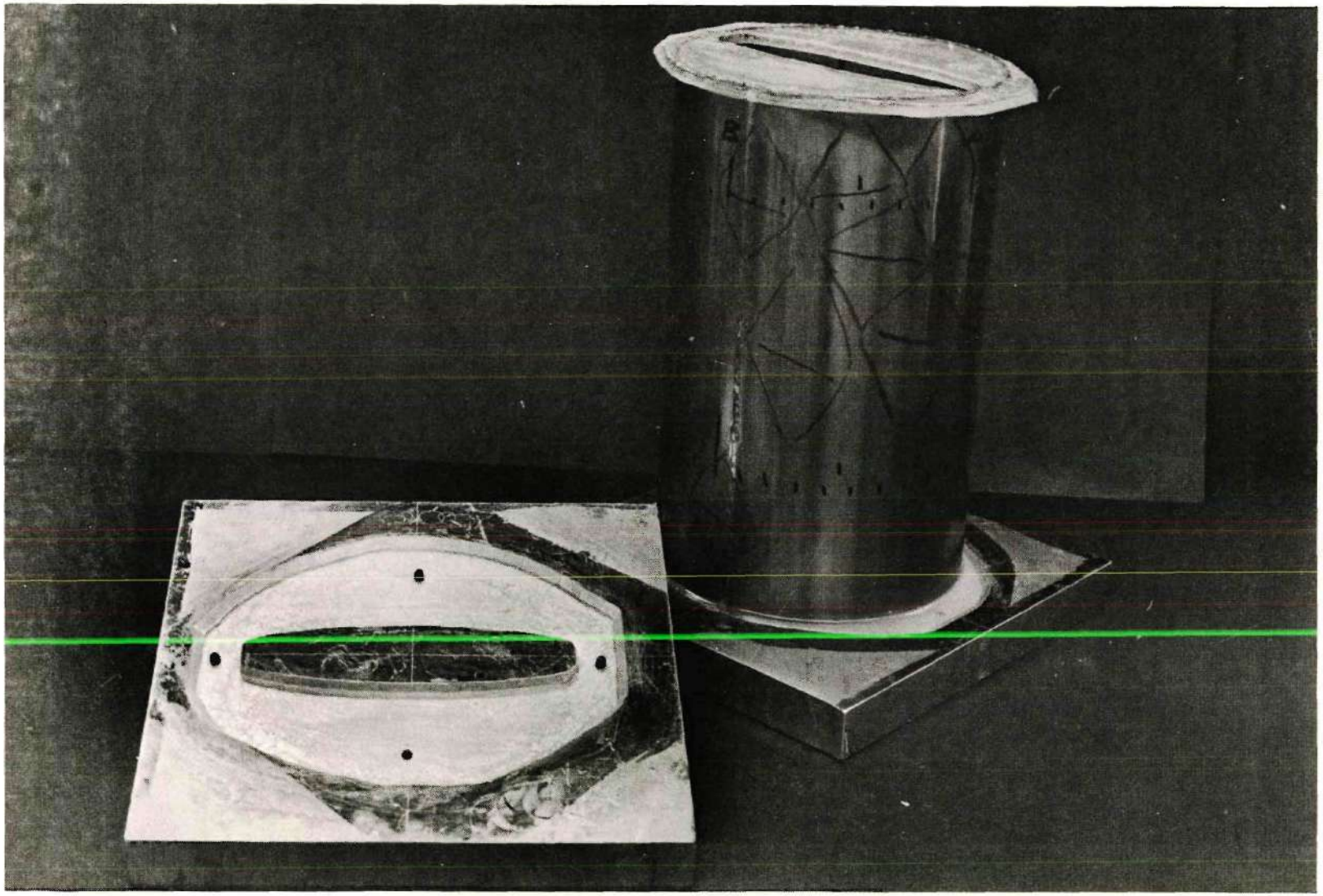

Figure 17. Elliptical Shell and End Plates.

CHAPTER II

RELATIONSHIPS BETWEEN BEHAVIORAL CHARACTERISTICS OF A BEAM WITH ROTATIONAL END RESTRAINT

Introduction

In Chapter I it was demonstrated that the buckling behavior of a non-circular cylindrical shell is the same, in a given locality, as that of a circular cylinder with equal radius of curvature. Thus, it was suggested that an experimental technique which produces information on the buckling of a circular shell under axial compression could be used to investigate the behavior of a non-circular shell under the same loading, if the technique used gave local rather than general information.

Unfortunately, there are few techniques for non-destructive evaluation of structures in which stability is an issue of concern. This is especially true of shell bodies, in which almost any applied loading may be destabilizing. However, for design purposes at least, the stiffened cylinder under axial compression may be regarded as an array of columns (14), each stringer with an "effective width" of skin being considered as a member of this array. When circumferential frames are added as is usual in aircraft construction, the stringer length between frames becomes, in effect, a rotationally restrained column. Thus, it was deemed advantageous to consider methods pertinent to the rotationally restrained strut.

Historical Note

The problems which result from boundary restraint in struts have long been recognized (15). Nevertheless the mathematical treatments of the subject have been concerned, more often than not, with the extreme cases, i.e. pinned or fixed boundaries, and the experiments which have been made frequently have striven to accomplish a restraint corresponding to these extremes. A review of the numerous devices developed in such attempts over the years is given in reference (16). Some 50 years ago, Salmon (17), in his classic treatment of columns, stated the need quite clearly when he wrote,

> The most pressing point for future research on the subject of columns is undoubtedly the degree of imperfection common in practical fixed ends; in short, what value of K(c) should be assumed for such ends? A complete answer to this question is difficult, but at present the designer has no real data whatsoever regarding practical end conditions.

Nevertheless, in the years which followed this remark no concerted effort was made systematically and thoroughly to resolve this question. Admittedly, Newmark (18) gave, on the basis of numerical analysis, a simple formula connecting the rotational restraints at the ends of a column with the critical load for the perfect body. However, this work does not appear to have received much attention. Hoff (19,20) derived critical loads as functions of end restraint using a Rayleigh-Ritz procedure, and presented his results in graphical form. Stephens (21) presented an approach which tied the natural frequency of the column to the instability load, and Masonnet (22) wrote a treatise on vibrations and buckling loads. However, it is only recently that a serious effort has been made to interrelate

critical loads, natural frequencies, and deformations under lateral load, and to use the laws so established as the basis of a non-destructive method of column evaluation. This work has been done primarily by Horton and his collaborators (23,24,25,26). They have chosen to relate instability under axial load with deformations and with displacements under lateral loads using numerical correlation procedures. At the same time, Baruch (27) wrote an analytical paper on the same topic, and Pierce (28) presented a correlation between critical load and natural frequency.

The recent development by Horton (29) of a scheme for the approximate representation of solutions to complicated equations permits a synthesis of the results given by these various authors. In doing so a systematic procedure will be developed which might be extendable to allied problems.

Summary of Previous Results

The simple formula given by Newmark (18) for the critical load of a uniform column with rotational restraints at its ends is

$$P_{cr} \cong \left[\frac{\pi^2 + 4\alpha}{\pi^2 + 2\alpha}\right]\left[\frac{\pi^2 + 4\beta}{\pi^2 + 2\beta}\right] \frac{\pi^2 EI}{L^2} \qquad (1)$$

where α and β are non-dimensional stiffness coefficients for the rotational end restraints, and E, I, and L have their usual significance. This is a remarkably good approximation; the maximum error is 4 per cent when the lateral supports at the ends of the column are rigid.

This formula has recently been derived analytically by Hanagud, Chaudhari, and Horton (30), and a similar form, viz.

$$P_{cr} = \left[\frac{3\pi + 4\alpha}{3\pi + 2\alpha}\right]\left[\frac{3\pi + 4\beta}{3\pi + 2\beta}\right]\frac{\pi^2 EI}{L^2} \qquad (2)$$

has been developed by Horton and Singhal (31). This result is slightly more accurate than Newmark's earlier expression.

The empirical formula given by Horton, Struble, and Craig (23) and further developed by Struble (24), which relates the instability load for a column with rigid lateral end constraints and partial rotational end restraints is

$$P_{cr}\,\delta = \text{constant} = \frac{\pi^2 L}{48} \qquad (3)$$

where P_{cr} is the critical load for the uniform column assumed perfectly straight and centrally loaded, and δ is the maximum transverse deflection produced by a concentrated lateral load applied at the point of maximum compliance.

Horton, Iwamoto, and Rehfield (25) gave a formula, later expanded and amplified by Iwamoto (26), relating critical load and inflection point separation:

$$\frac{P_{cr}}{EI}\left[\frac{2\ell^3}{L + \ell}\right] \cong \pi^2 \qquad (4)$$

where P_{cr} is the critical load as defined above, and ℓ is the distance between the inflection points of the same member when subjected to a uniformly distributed lateral load. This formula is, in essence, a relationship between maximum slopes under uniform lateral load and critical load, as is shown fully in reference (26).

Pierce (28) suggested a relationship between the critical load for a uniform column and its first natural frequency:

$$\frac{P_{cr}L^2}{EI} \cong 0.2\ \mu^{3.4} \tag{5}$$

where P_{cr} is the critical load as previously defined, and μ is the natural frequency parameter defined by

$$\mu^4 = \frac{\omega^2 mL^4}{EI}$$

Method of Attack

It is accepted that the conditions of restraint at the boundaries of a given structure determine its flexural, buckling, and vibrational characteristics. Hence, it would seem possible to interrelate these characteristics through their mutual dependence on end restraint. This approach will be taken.

First it will be necessary to establish approximate formulae as functions of the rotational end restraint stiffness coefficients

for the several parameters involved; i.e. to write

$$P_{cr} = P_{cr}(\alpha,\beta) = P_{\alpha\beta} \tag{6}$$

$$\delta = \delta(\alpha,\beta) = \delta_{\alpha\beta} \tag{7}$$

$$\omega = \omega(\alpha,\beta) = \omega_{\alpha\beta} \tag{8}$$

where P_{cr} is critical load, δ is deflection due to a unit concentrated load at the point of maximum compliance, and ω is the natural frequency of vibration, and α and β are rotational end-restraint coefficients, all for the uniform column and with the restrictions previously mentioned. Having found such formulae, the manner in which these functions of α and β are related will be established.

Relation Between Buckling and Deflection Parameters

According to Horton and Singhal (31), the critical load for the column with unequal rotational end-restraint coefficients, α and β, may be approximated as

$$P_{\alpha\beta} \cong \left[\frac{3\pi + 4\alpha}{3\pi + 2\alpha}\right]\left[\frac{3\pi + 4\beta}{3\pi + 2\beta}\right] \frac{\pi^2 EI}{L^2} \tag{9}$$

It is immediately apparent from this expression that

$$(P_{\alpha\beta})^2 \cong P_{\alpha\alpha} P_{\beta\beta} \tag{10}$$

Table 2. Accuracy of $(P_{\alpha\beta})^2 = P_{\alpha\alpha}P_{\beta\beta}$

Errors in Percent

α \ β	0	0.2	0.5	1.0	2.0	5.0	10	20	50	100	200	500	1000
0	0	.07	.35	1.0	2.3	4.1	4.7	4.6	4.5	4.4	4.4	4.4	4.4
0.2		0	.11	.54	1.5	3.1	3.4	3.2	2.9	2.8	2.8	2.8	2.8
0.5			0	.17	.83	1.9	2.0	1.6	1.2	1.1	1.0	.96	.95
1.0				0	.25	.86	.68	.08	-.52	-.74	-.85	-.92	-.94
2.0					0	.11	-.30	-1.0	-1.9	-2.2	-2.3	-2.4	-2.4
5.0						0	-.24	-.88	-1.6	-1.9	-2.1	-2.2	-2.3
10							0	-.21	-.67	-.90	-1.0	-1.1	-1.1
20								0	-.13	-.24	-.32	-.37	-.38
50			Symmetric						0	-.02	-.04	-.06	-.07
100										0	-.005	-.01	-.02
200											0	-.002	-.003
500												0	-.0003
1000													0

i.e. that the critical compressive load for the column with non-symmetric rotational restraints, α and β, is the geometric mean of the critical loads for the two related symmetric cases. The accuracy of this result is excellent, as is shown in Table 2.

Next, let us consider the deflection, δ, which results from a unit concentrated load applied at the point of maximum compliance. When $\alpha = \beta = A$, it is obvious that the maximum-compliance load location is the center of the beam, and it can be demonstrated from Euler-Bernoulli theory that the deflection under a unit central load is

$$\delta_{AA} = \left[\frac{A + 8}{A + 2}\right]\left(\frac{1}{192}\right)\frac{L^3}{EI} \tag{11}$$

Using the method of approximate solution developed in reference (29), it is assumed that, regardless of the relative magnitudes of the rotational end-restraints, the greatest deflection due to a unit concentrated load applied at the point of maximum compliance can be given by an equation of the form

$$\delta^2_{\alpha\beta} = \frac{a\alpha\beta + b(\alpha + \beta) + c}{d\alpha\beta + e(\alpha + \beta) + f}\left(\frac{1}{192}\right)^2\left[\frac{L^3}{EI}\right]^2 + \epsilon \tag{12}$$

where ϵ is the error involved in the approximation. Equating this expression to the exact form, equation (11), yields after appropriate algebraic manipulation,

$$(\delta_{\alpha\beta})^2 = \frac{\alpha\beta + 8(\alpha+\beta) + 64}{\alpha\beta + 2(\alpha+\beta) + 4}\left(\frac{1}{192}\right)^2\left[\frac{L^3}{EI}\right]^2 + \epsilon \tag{13}$$

or

$$(\delta_{\alpha\beta})^2 = \frac{(\alpha+8)(\beta+8)}{(\alpha+2)(\beta+2)}\left(\frac{1}{192}\right)^2\left[\frac{L^3}{EI}\right]^2 + \epsilon$$

A comparison of this result with equation (11) leads to the conclusion that

$$(\delta_{\alpha\beta})^2 = \delta_{\alpha\alpha}\delta_{\beta\beta} + \epsilon \tag{14}$$

and it remains only to establish the magnitude of ϵ. The results of a numerical determination of ϵ are shown in Table 3. The error in $(\delta_{\alpha\beta})^2$ is some 12.7 per cent for the fixed-pinned case ($\alpha = 0$, $\beta = \infty$), but, of course, this means an error of 6.15 per cent in $\delta_{\alpha\beta}$. This is within normal engineering tolerance. Moreover, in any practical structure there is a certain amount of rotational restraint at any realizable joint. As seen from Table 3, the addition of a small amount of restraint at the pinned end makes the relationship virtually exact. Hence, the approximate relationship

$$(\delta_{\alpha\beta}) \simeq \sqrt{\delta_{\alpha\alpha}\delta_{\beta\beta}} \tag{15}$$

is accepted without reservation. Thus, the greatest deflection resulting from a concentrated load applied at the point of maximum compliance of a beam with rotational end restraint coefficients α and β is the geometric mean of the similarily obtained deflections for the two

Table 3. Accuracy of $(\delta_{\alpha\beta})^2 = \delta_{\alpha\alpha}\delta_{\beta\beta}$

Errors in Percent

α \ β	0	0.2	0.5	1.0	2.0	5.0	10	20	50	100	200	500	1000
0	0	-.08	-.41	-1.2	-3.1	-7.1	-9.9	-11.6	-12.4	-12.6	-12.7	-12.7	-12.7
0.2		0	-.13	-.69	-2.2	-5.6	-8.1	-9.5	-10.2	-10.3	-10.3	-10.3	-10.3
0.5			0	-.22	-1.2	-3.9	-6.0	-7.2	-7.7	-7.7	-7.7	-7.7	-7.7
1.0				0	-.40	-2.2	-3.8	-4.6	-4.9	-4.9	-4.8	-4.8	-4.8
2.0					0	-.72	-1.6	-2.0	-2.1	-2.0	-1.9	-1.8	-1.8
5.0						0	-.14	-.20	-.008	.16	.28	.36	.39
10							0	.03	.21	.36	.46	.54	.56
20								0	.07	.17	.23	.28	.30
50			Symmetric						0	.02	.04	.06	.07
100										0	.005	.02	.02
200											0	.002	.004
500												0	.0003
1000													0

related symmetric cases. It is evident from equations (10) and (15) that

$$(P_{\alpha\beta}\delta_{\alpha\beta}) \cong \sqrt{(P_{\alpha\alpha}\delta_{\alpha\alpha})(P_{\beta\beta}\delta_{\beta\beta})} \tag{16}$$

The individual terms of this expression are now examined. It is clear from equations (9) and (11) that

$$P_{\alpha\alpha}\delta_{\alpha\alpha} \cong \left[\frac{(3\pi + 4\alpha)^2}{(3\pi + 2\alpha)^2}\frac{\pi^2 EI}{L^2}\right]\left[\frac{\alpha + 8}{\alpha + 2}\right]\left(\frac{1}{192}\right)\frac{L^3}{EI} \tag{17}$$

$$P_{\alpha\alpha}\delta_{\alpha\alpha} = \frac{\pi^2 L}{192}\left\{4 + \frac{\alpha[(96-24\pi)\alpha + (96\pi-27\pi^2)]}{4\alpha^3 + (12\pi+8)\alpha^2 + (9\pi^2+24)\alpha + 18\pi^2}\right\}$$

$$P_{\alpha\alpha}\delta_{\alpha\alpha} = \frac{\pi^2 L}{192}\left\{4 + \epsilon\right\}$$

where ϵ is small, as is demonstrated in Table 4. Then by virtue of equation (16) the more general form may be written, viz.

$$P_{\alpha\beta}\ \delta_{\alpha\beta} \cong \text{constant} \cong \frac{\pi^2 L}{48} \tag{18}$$

Thus the result has been synthesized that the product $P\delta$ is approximately constant, as was stated in references (9) and (10).

Relation Between Buckling and Inflection Point Parameters

Using the same procedure, the relationship between the critical

Table 4. Accuracy of $P_{\alpha\alpha}\delta_{\alpha\alpha} = \frac{\pi^2 L}{48}$

α	$P_{\alpha\alpha}$	$\delta_{\alpha\alpha}$	$P_{\alpha\alpha}\delta_{\alpha\alpha}$	Error %
0	9.870	0.021	0.206	0
.2	10.654	0.019	0.207	-.584
.5	11.772	0.018	0.208	-1.38
1.0	13.492	0.015	0.211	-2.53
2.0	16.463	0.013	0.214	-4.26
5.0	22.670	0.0097	0.219	-6.64
10	28.168	0.0078	0.220	-7.02
20	32.782	0.0066	0.217	-5.68
50	36.514	0.0058	0.212	-3.16
100	37.947	0.0055	0.209	-1.78
200	38.701	0.0054	0.207	-0.94
500	39.164	0.0053	0.206	-0.39
1000	39.321	0.0052	0.206	-0.20

$$\frac{\pi^2}{48}L = 0.2056\ L$$

load, $P_{\alpha\beta}$, and the distance between inflection points under uniformly distributed lateral load will now be investigated. It is well known that the critical load is inversely proportional to the square of the effective length, i.e. that

$$P_{\alpha\beta} = \frac{\pi^2 EI}{(L^*_{\alpha\beta})^2} \quad \text{or} \quad \frac{1}{(L^*_{\alpha\beta})^2} = \frac{P_{\alpha\beta}}{\pi^2 EI} \tag{19}$$

where $L^*_{\alpha\beta}$ is the distance between inflection points on the buckled deflection curve when rotational end-restraint coefficients are α and β. By virtue of equation (9), for the equal end-restraint case,

$$\frac{1}{(L^*_{\alpha\alpha})^2} \cong \left[\frac{3\pi + 4\alpha}{3\pi + 2\alpha}\right]^2 \frac{1}{L^2} \tag{20}$$

Using elementary beam theory it has been demonstrated (26) that, for the case of symmetric rotational restraints, the "exact" distance between inflection points on the beam under uniformly distributed lateral load is

$$\ell^2_{\alpha\alpha} = \left[\frac{\alpha + 6}{3(\alpha + 2)}\right] L^2 \tag{21}$$

It follows then, from equations (20) and (21) that

$$\left[\frac{\ell_{\alpha\alpha}}{L^*_{\alpha\alpha}}\right]^2 \cong \frac{1}{(3\pi + 2\alpha)}\left[\frac{54\pi^2 + (144\pi + 9\pi^2)\alpha + (96 + 24\pi)\alpha^2 + 16\alpha^3}{18\pi + (12 + 9\pi)\alpha + 6\alpha^2}\right] \tag{22}$$

To achieve the simplest form possible, the numerator of this expression is taken in the form of a linear function of α multiplied by the denominator, plus some error term ϵ, viz.

$$54\pi^2 + (144\pi + 9\pi^2)\alpha + (96 + 24\pi)\alpha^2 + 16\alpha^3 = \tag{23}$$

$$= (n\alpha + m)[18\pi + (12 + 9\pi)\alpha + 6\alpha^2] + \epsilon$$

Values of m and n must be chosen which will cause this expression to be of acceptable accuracy. To do so the coefficients of like powers of α are equated indicating suitable ranges of the constants, and then m and n are adjusted appropriately. Equality of the α^0 terms (constants) leads to the result that

$$m = \frac{54\pi^2}{18\pi} = 3\pi \tag{24}$$

If m is chosen thus, the α^1, α^2, and α^3 terms show that n must lie between 2.67 and 2.86. A single value of n is required, so for convenience a value near the midpoint of the range is chosen:

$$n = 2.73 = 1 + \sqrt{3} \tag{25}$$

Substituting equations (24) and (25) into equation (23), the representation for the numerator of the approximate form becomes

$$[(1 + \sqrt{3})\alpha + 3\pi][18\pi + (12 + 9\pi)\alpha + 6\alpha^2] + \epsilon \tag{26}$$

Numerical comparison of this expression to that of equation (22) shows that the maximum value of ϵ is less than 2.5 per cent of the product term (see Table 5); thus, it is neglected. Then equation (22) becomes

$$\left[\frac{\ell_{\alpha\alpha}}{L^*_{\alpha\alpha}}\right]^2 \cong \frac{(1 + \sqrt{3})\alpha + 3\pi}{2\alpha + 3\pi} \tag{27}$$

At this stage the formula of reference (26) is recapitulated, viz.

$$\frac{P_{\alpha\beta}}{EI}\left[\frac{2\ell^3_{\alpha\beta}}{L + \ell_{\alpha\beta}}\right] \cong \pi^2 \tag{4}$$

and it is recalled that

$$P_{\alpha\beta} = \frac{\pi^2 EI}{(L^*_{\alpha\beta})^2} \tag{19}$$

It becomes apparent that to progress further in the verification of this rule, $\ell_{\alpha\alpha}$ must be evaluated. Following what by now is usual procedure, it is assumed that $\ell_{\alpha\alpha}$ may be written in the form

$$\ell_{\alpha\alpha} = \left[\frac{a\alpha + b}{c\alpha + d}\right] L + \epsilon \tag{28}$$

where ϵ is an error term. Evaluating this equation for the limiting cases when $\alpha = 0$ and $\alpha = \infty$, and taking ϵ to be zero, the following

Table 5. Error in Numerator Approximation [Eqn (29)]

α	Error in Percent
	ϕ
.1	* .129469
.2	* .249739
.3	* .3609
.4	* .463272
.5	* .557291
.75	* .758476
1	* .917173
2	* 1.25255
3	* 1.31211
4	* 1.24626
5	* 1.12493
7.5	* .758232
10	* .411803
20	*-.513818
30	*-1.0019
40	*-1.29601
50	*-1.49162
75	*-1.77773
100	*-1.93269
200	*-2.18152
300	*-2.26915
400	*-2.31388
500	*-2.34104
750	*-2.37758
1000	*-2.396
2000	*-2.42384
3000	*-2.43314
4000	*-2.43783
5000	*-2.44065
7500	*-2.44443
10000	*-2.44628

MAX ABS VALUE OF ERROR 2.44628 %, WHEN A= 10000

relationships between constants are found:

$$c = \sqrt{3}\, a \tag{29}$$

$$b = d \tag{30}$$

If, in addition, equation (28) is evaluated at $\alpha = 60$, with ϵ zero, it is found that

$$b = 4.712\, a \tag{31}$$

Substituting these values into equation (28),

$$\ell_{\alpha\alpha} = \left[\frac{\alpha + 4.712}{\sqrt{3}\alpha + 4.712}\right] L + \epsilon = \left[\frac{2\alpha + 9.424}{2\sqrt{3}\alpha + 9.424}\right] L + \epsilon \tag{32}$$

$$= \left[\frac{2\alpha + 3\pi}{2\sqrt{3}\alpha + 3\pi}\right] L + \epsilon$$

Numerical evaluation shows that ϵ is negligible for all values of α (see Table 6).

Returning to equation (27), it is seen that both numerator and denominator of the right side may be multiplied by 2, and terms re-grouped such that

$$\left(\frac{\ell_{\alpha\alpha}}{L^*_{\alpha\alpha}}\right)^2 \cong \frac{(2\alpha + 3\pi) + (2\sqrt{3}\alpha + 3\pi)}{2(2\alpha + 3\pi)} \tag{33}$$

Table 6. Accuracy of $\ell_{\alpha\alpha} = \left[\frac{2\alpha + 3\pi}{2\sqrt{3\alpha} + 3\pi}\right]L$

Alpha	Exact $\ell_{\alpha\alpha}$	Approx $\ell_{\alpha\alpha}$	% Error
0	1.0	1.0	0
.2	0.969	0.971	-.189
.5	0.931	0.934	-.369
1.0	0.882	0.886	-.509
2.0	0.816	0.821	-.544
5.0	0.724	0.726	-.351
10	0.667	0.668	-.162
20	0.6276	0.6279	-.050
50	0.59914	0.59916	-.003
100	0.58856	0.58854	+.003
200	0.58304	0.58302	+.003
500	0.57965	0.57964	+.001
1000	0.57850	0.57850	+.0008

$$\left(\frac{\ell_{\alpha\alpha}}{L^*_{\alpha\alpha}}\right)^2 = \frac{1}{2}\left[1 + \frac{2\sqrt{3}\alpha + 3\pi}{2\alpha + 3\pi}\right]$$

$$= \frac{1}{2}\left[\frac{\ell_{\alpha\alpha} + L}{\ell^3_{\alpha\alpha}}\right]$$

Hence,

$$\frac{1}{(L^*_{\alpha\alpha})^2} \cong \frac{1}{2}\left[\frac{L + \ell_{\alpha\alpha}}{\ell^3_{\alpha\alpha}}\right] \tag{34}$$

Thus, since

$$P_{\alpha\alpha} = \frac{\pi^2 EI}{(L^*_{\alpha\alpha})^2}$$

or

$$\frac{P_{\alpha\alpha}}{EI}(L^*_{\alpha\alpha})^2 = \pi^2$$

it follows that

$$\frac{P_{\alpha\alpha}}{EI}\left[\frac{2\ell^3_{\alpha\alpha}}{L + \ell_{\alpha\alpha}}\right] = \pi^2 \tag{35}$$

Thus, for equal rotational restraints the original semi-empirical result has been synthesized. To generalize this particular

result to the case of unequal rotational restraint, it is recalled that $P_{\alpha\beta}$ is, at least approximately, the geometric mean of $P_{\alpha\alpha}$ and $P_{\beta\beta}$. If $\ell_{\alpha\beta}$ and $(L + \ell_{\alpha\beta})$ also follow geometric mean laws, the relation can be generalized. A numerical evaluation shows that both parameters do in fact follow such laws to a close approximation (see Tables 7 and 8), i.e.

$$\ell_{\alpha\beta} \cong \sqrt{\ell_{\alpha\alpha}\ell_{\beta\beta}} \tag{36}$$

and

$$L + \ell_{\alpha\beta} \cong \sqrt{(L + \ell_{\alpha\alpha})(L + \ell_{\beta\beta})} \tag{37}$$

Since all three behavioral parameters obey geometric mean laws, equation (35) may be written in the more general form

$$\frac{P_{\alpha\beta}}{EI}\left[\frac{2\ell^3_{\alpha\beta}}{L + \ell_{\alpha\beta}}\right] \cong \pi^2 \tag{38}$$

This expression is identical to the empirical law previously referenced.

Relation Between Critical Load and Natural Frequency

The basic approximation technique used in the previous portions of this chapter is equally pertinent to the problems of vibration. The natural frequencies of vibration are found from the characteristic

Table 7. Accuracy of $\ell_{\alpha\beta}^{\ 2} = \ell_{\alpha\alpha}\ell_{\beta\beta}$

Errors in Percent

α \ β	0	0.2	0.5	1.0	2.0	5.0	10	20	50	100	200	500	1000
0	0	-.08	-.19	-.33	-.54	-.84	-1.0	-1.2	-1.3	-1.3	-1.4	-1.4	-1.4
0.2		-.15	-.23	-.33	-.48	-.71	-.86	-.97	-1.0	-1.1	-1.1	-1.1	-1.1
0.5			-.27	-.33	-.42	-.56	-.66	-.73	-.78	-.80	-.81	-.82	-.82
1.0				-.33	-.35	-.39	-.43	-.45	-.47	-.48	-.48	-.48	-.48
2.0					-.27	-.20	-.18	-.16	-.14	-.13	-.12	-.12	-.12
5.0						-.02	+.04	+.08	+.12	+.13	+.14	+.15	+.15
10							+.11	+.12	+.13	+.13	+.13	+.14	+.14
20								+.10	+.07	+.06	+.06	+.05	+.05
50			Symmetric						+.008	-.017	-.03	-.04	-.04
100										-.05	-.07	-.08	-.08
200											-.09	-.10	-.10
500												-.11	-.12
1000													-.12

Table 8. Accuracy of $(L + \ell_{\alpha\beta}) = (L + \ell_{\alpha\alpha})^{\frac{1}{2}}(L + \ell_{\beta\beta})^{\frac{1}{2}}$

Errors in Percent

α \ β	0	0.2	0.5	1.0	2.0	5.0	1.0	20	50	100	200	500	1000
0	+.008	-.039	-.11	-.21	-.39	-.72	-.97	-1.2	-1.3	-1.4	-1.4	-1.4	-1.4
0.2		-.069	-.11	-.19	-.33	-.60	-.82	-.99	-1.1	-1.2	-1.2	-1.2	-1.2
0.5			-.13	-.17	-.26	-.47	-.64	-.78	-.90	-.94	-.96	-.98	-.98
1.0				-.17	-.20	-.32	-.44	-.54	-.63	-.66	-.68	-.69	-.69
2.0					-.15	-.16	-.22	-.27	-.32	-.34	-.35	-.36	-.36
5.0						-.03	-.01	-.02	-.03	-.04	-.04	-.04	-.04
10							+.04	+.05	+.06	+.06	+.06	+.06	+.06
20								+.08	+.08	+.08	+.08	+.08	+.08
50			Symmetric						+.08	+.08	+.08	+.08	+.08
100										+.08	+.08	+.08	+.08
200											+.08	+.08	+.08
500												+.08	+.08
1000													+.08

equation

$$\frac{1}{L}\mu \left\{\sin \mu \left[\frac{\mu}{L} \sinh \mu + (\alpha + \beta)\cosh \mu\right] + \right. \tag{39}$$

$$\left. + \sinh \mu \left[\frac{\mu}{L} \sin \mu - (\alpha + \beta)\cos \mu\right]\right\} =$$

$$= \alpha\beta \left[\cos \mu \cosh \mu - 1\right]$$

where

$$\mu^4 = \frac{\omega^2 mL^4}{EI} ,$$

a frequency parameter proportional to the square root of the natural frequency.

Since the relation between critical load and μ found by Pierce has the form of a power law, approximate expressions for these parameters in the form of exponential functions will be most convenient. Thus, such expressions are sought.

As was done previously, the equal end-restraint problem is examined first. It is assumed that

$$\mu_{\alpha\alpha} = e^{\left[\frac{a\alpha + b}{c\alpha + d}\right]} + \epsilon \tag{40}$$

If the error is forced to zero at $\alpha = 0$, 5, and 50, the expression is found to be

$$\mu_{\alpha\alpha} = e^{\left[\frac{1.55\alpha + 5.05}{\alpha + 4.41}\right]} + \varepsilon \qquad (41)$$

and numerical evaluation shows that the error is negligible for all values of α (see Table 9).

It is now noted that the first eigenvalue of the buckling equation, $\lambda_{\alpha\alpha}$, can be expressed not only as the ratio of two polynomials in α, as is implied by equations (1) or (2), but also in the form of an exponential function similar to that used for $\mu_{\alpha\alpha}$. Since the two are to be interrelated the denominators of the exponents will be taken to be identical, if, of course, the resulting expression for $\lambda_{\alpha\alpha}$ has acceptable accuracy. Thus, it is assumed that $\lambda_{\alpha\alpha}$ may be written as

$$\lambda_{\alpha\alpha} = e^{\left[\frac{a\alpha + b}{\alpha + 4.41}\right]} + \varepsilon \qquad (42)$$

When this expression is matched to the exact values of $\lambda_{\alpha\alpha}$ at $\alpha = 0$ and $\alpha = \infty$ the result is

$$\lambda_{\alpha\alpha} = e^{\left[\frac{1.838\alpha + 5.05}{\alpha + 4.41}\right]} + \varepsilon \qquad (43)$$

As is shown in Table 10, ε is always less than 5 per cent.

Although the rational function exponents have no common factors in their respective numerators and denominators, some simplification

Table 9. Accuracy of $\mu_{\alpha\alpha} = e^{\left[\frac{1.55\alpha + 5.05}{\alpha + 4.41}\right]}$

Alpha	Exact $\mu_{\alpha\alpha}$	Error %
0	3.14159	.0008
.2	3.20229	.153
.5	3.28358	.288
1.0	3.39879	.368
2.0	3.57683	.315
5.0	3.89735	-.0002
10	4.15565	-.179
20	4.37370	-.151
50	4.56291	.044
100	4.64131	.173
200	4.68425	.255
500	4.71138	.312
1000	4.72066	.332

Table 10. Accuracy of $\lambda_{\alpha\alpha} = e^{\left[\frac{1.838\alpha + 5.05}{\alpha + 4.41}\right]}$

Alpha	Exact $\lambda_{\alpha\alpha}$	Approx $\lambda_{\alpha\alpha}$	Error %
0	3.14159	3.14283	.0395
0.2	3.26399	3.23874	.774
0.5	3.43101	3.37260	1.703
1.0	3.67319	3.57226	2.748
2.0	4.05752	3.9013	3.845
5.0	4.76129	4.54162	4.614
10	5.30733	5.08327	4.222
20	5.72555	5.54459	3.160
50	6.04265	5.94079	1.686
100	6.16014	6.10273	0.932
200	6.22099	6.19072	0.486
500	6.25815	6.24601	0.194
1000	6.27064	6.26487	0.092

can result from dividing the numerator by the denominator and expressing the result as a constant plus a rational function of the stiffness. In this case applying this technique to equations (41) and (43) gives

$$\lambda_{\alpha\alpha} \cong e^{\left[1.144 + \frac{0.693\alpha}{\alpha + 4.41}\right]} = \pi e^{\left[\frac{0.693\alpha}{\alpha + 4.41}\right]} \tag{44}$$

and

$$\mu_{\alpha\alpha} \cong e^{\left[1.144 + \frac{0.409\alpha}{\alpha + 4.41}\right]} = \pi e^{\left[\frac{0.409\alpha}{\alpha + 4.41}\right]} \tag{45}$$

If the factor π is taken to the left side of both equations, and the ratio of the logarithms of the resulting equations is formed, it is found that

$$\frac{\ell n \frac{\lambda_{\alpha\alpha}}{\pi}}{\ell n \frac{\mu_{\alpha\alpha}}{\pi}} \cong 1.694 \cong 1.7 \tag{46}$$

that is,

$$\frac{\lambda_{\alpha\alpha}}{\pi} \cong \left[\frac{\mu_{\alpha\alpha}}{\pi}\right]^{1.7} \tag{47}$$

Again generalization to the unequal end restraint case is possible if $\lambda_{\alpha\beta}$ and $\mu_{\alpha\beta}$ obey geometric mean laws. Since by definition

$$\lambda^2_{\alpha\beta} = \frac{P_{\alpha\beta} L}{EI} \tag{48}$$

it is obvious from equation (10) that an approximate geometric mean law holds for $\lambda_{\alpha\beta}$. A similar law is tested for $\mu_{\alpha\beta}$, and the errors found to be small (see Table 11). Thus, equation (47) may be written in the more general form

$$\lambda_{\alpha\beta} \cong \frac{\pi}{\pi^{1.7}} \left(\mu_{\alpha\beta}\right)^{1.7} = 0.45 \left(\mu_{\alpha\beta}\right)^{1.7} \tag{49}$$

or

$$(\lambda_{\alpha\beta})^2 = \frac{P_{\alpha\beta} L^2}{EI} \cong 0.2 \left(\mu_{\alpha\beta}\right)^{3.4} \tag{50}$$

The latter form is identical to Pierce's final statement of his empirical result. We see in Table 12 that the error in this expression is quite large. However, Pierce found the relationship based on consideration of the eigenvalues, which corresponds to equation (49). In this case the error is within normal tolerances, as is shown in Table 13.

Conclusions

It has been shown, then, that the several semi-empirical laws which have been promulgated to interrelate frequency, displacement under lateral loading, and critical axial load for the column with

Table 11. Accuracy of $(\mu_{\alpha\beta})^2 = \mu_{\alpha\alpha}\mu_{\beta\beta}$

Errors in Percent

α \ β	0	0.2	0.5	1.0	2.0	5.0	10	20	50	100	200	500	1000
0	0	.02	.11	.34	.86	1.97	2.79	3.29	3.55	3.60	3.62	3.62	3.62
0.2		0	.04	.19	.61	1.58	2.32	2.78	3.00	3.04	3.05	3.05	3.05
0.5			0	.06	.34	1.15	1.78	2.18	2.36	2.38	2.38	2.38	2.38
1.0				0	.12	.68	1.18	1.49	1.61	1.62	1.61	1.60	1.60
2.0					0	.23	.54	.74	.79	.77	.75	.73	.73
5.0						0	.06	.11	.08	.04	.01	-.01	-.02
10							0	.002	-.04	-.08	-.11	-.13	-.14
20								0	-.02	-.05	-.06	-.08	-.09
50			Symmetric						0	-.005	-.01	-.02	-.02
100										0	-.001	-.004	-.007
200											0	-.001	-.002
500												0	-.001
1000													0

Table 12. Accuracy of $P_{\alpha\beta} = 0.2\mu_{\alpha\beta}^{3.4}$

(Note: Maximum error is 10.2%, when $\alpha = \beta = 7.5$)

Errors in Percent

α \ β	0	0.2	0.5	1.0	2.0	5.0	10	20	50	100	200	500	1000
0	.68	1.24	1.94	2.81	3.82	4.24	3.09	1.11	-1.22	-2.32	-2.95	-3.35	-3.50
0.2		1.80	2.51	3.39	4.42	4.90	3.79	1.84	-0.48	-1.58	-2.21	-2.62	-2.76
0.5			3.22	4.13	5.19	5.75	4.70	2.79	0.50	-0.59	-1.22	-1.62	-1.76
1.0				5.06	6.19	6.89	5.96	4.12	1.86	0.78	0.16	-0.24	-0.38
2.0					7.44	8.42	7.70	5.99	3.82	2.77	2.16	1.76	1.62
5.0						10.01	9.76	8.38	6.40	5.41	4.82	4.44	4.31
10							9.91	8.81	7.00	6.05	5.49	5.12	4.99
20								7.89	6.18	5.26	4.70	4.33	4.21
50			Symmetric						4.50	3.57	3.01	2.64	2.51
100										2.63	2.06	1.68	1.55
200											1.48	1.11	0.98
500												0.72	0.59
1000													0.45

Table 13. Accuracy of $\lambda_{\alpha\beta} = 0.45\mu_{\alpha\beta}^{1.7}$

Errors in Percent

α \ β	0	0.2	0.5	1.0	2.0	5.0	10	20	50	100	200	500	1000
0	-.28	+.003	.36	.80	1.32	1.54	.94	.06	-1.23	-1.78	-2.09	-2.30	-2.37
0.2		.29	.65	1.10	1.63	1.87	1.30	.31	-.86	-1.41	-1.73	-1.93	-2.0
0.5			1.01	1.48	2.02	2.31	1.77	.79	-.37	-.92	-1.23	-1.44	-1.50
1.0				1.95	2.54	2.91	2.42	1.47	.32	-.23	-.54	-.74	-.81
2.0					3.19	3.71	3.33	2.44	1.32	.78	.47	.27	.20
5.0						4.54	4.41	3.68	2.65	2.14	1.83	1.64	1.57
10							4.50	3.91	2.96	2.47	2.18	1.99	1.92
20								3.43	2.54	2.06	1.77	1.58	1.52
50				Symmetric					1.66	1.19	.90	.71	.65
100	(Note: Maximum error 4.66% when $\alpha = \beta = 7.5$)									.71	.42	.23	.16
200											.13	-.06	-.13
500												-.26	-.32
1000													-.39

rotational end restraint may be developed by a systematic technique. As demonstrated, this technique depended on the fact that the parameters of interest may be expressed in a relatively simple form in terms of the rotational end restraint coefficients. These expressions were then interrelated algebraically. The success of the method in this case makes it reasonable to assume that an extension of the procedures followed here can lead to similar results in such other problems of this type as, for example, studies of other basic strucural elements.

CHAPTER III

AN EXPERIMENTAL APPLICATION OF THE LATERAL STIFFNESS CRITERION TO THE BUCKLING OF SHELLS

Introduction

To the analyst there are, as a survey of the literature readily shows, numerous ways in which a criterion for structural stability may be defined. These criteria have, of course, a common foundation: the state of deformation of the body and the stresses which produce it. To the experimentalist, however, the choice of criterion is, of necessity, restricted. He can deal directly with deformations and their measurement, stresses and their assessment, or stiffnesses and their determination. All other quantities are implicit rather than explicit, and at best his observations can only provide data from which they can be calculated. Thus, his working definitions of instability are threefold:

1. The deformation in some region increases disproportionately with an increase in load;

2. The stress at some point increases disproportionately with an increase in load; and

3. The stiffness in some region tends to zero with an increase in load.

In accepting these criteria there is a clear need to differentiate between structural and material instabilities, since the defin-

itions above are applicable to either. In any realistic situation both elements of behavior are present. In most structural problems buckling affects the totality of the structure, while material effects are local. Nevertheless, the separation of effects is difficult. The basic criteria however, are valid whether the material behavior is elastic or inelastic, linear or non-linear.

There are very few techniques for non-destructive evaluation of the stability of shell bodies. Admittedly, Horton and Durham (32) have demonstrated that a shell in which the depth of buckle is restricted by a close fitting mandrel can be buckled repeatedly without experiencing inelastic effects, and various investigators have used this method to advantage (33,34,35). However, when internally stiffened shells are to be tested, or when the scale is large, an interior mandrel becomes impractical.

The prime need in research, and the basic requirement of the practicing engineer, is for a method from which information about the instability of an actual test vehicle can be obtained without risking destruction of the specimen. "Without risk" is, of course, much easier to say than achieve, but "with minimum risk" may be practicable if the degree of risk involved is not precisely defined. This is, in essence, the philosophy which underlies the use of the Southwell process.

The technical basis for the Southwell method of data interpretation stretches back into history. It began, of course, with application to the column. A historic survey is found in reference (36). In more recent times it has been extended to the axially com-

pressed shell, both stiffened and unstiffened. In this regard the work of Flügge (37), Horton and Cundari (38), Singer (39), and Ford (40) should be mentioned. Bank (41) and Craig (42) have applied the technique to the shell in torsion, and Galletly and Reynolds (43) to the shell under external pressure.

The use of the Southwell process on a point by point basis is, however, precarious. There is great difficulty in choice of location. This is due without doubt to the fact that the deflection at a point is the local value of the sum of a series of periodic functions, which taken together form the distorted shape. Only rarely is the deflection due to a single harmonic. Thus, the greatest success has been achieved for the shell when methods have been adopted in which harmonic separation is possible. This later idea was first mentioned by Donnell (44), and discussed in greater detail by Tuckerman (45). Their discussions pertained to the column. Craig (42) and Ford (40) studied the question in relation to the tube in torsion and the reinforced cylinder in axial compression, respectively. The difficulty, however, with a method which depends upon separation of the distorted shape into its constituents is that it tends to be an averaging process. Thus, it does not necessarily give information which is representative of the local behavior. A more specifically localized method is desired.

It is to this end that the idea of loss of stiffness - stiffness approaching zero - is considered.

Analysis of the Lateral Stiffness of a Beam-Column

To obtain a feel for the issues involved, we examine the behavior

of a beam-column. First, let us consider a straight, uniform column with pinned ends, subjected to a compressive force, P, and a concentrated side load, W. According to the classical theory of beam-column analysis, the displacement, y, at the center of a column with a concentrated load at the mid-span is

$$y = \frac{W}{2\lambda P} \tan \frac{\lambda L}{2} - \frac{WL}{4P} \tag{51}$$

which can be rewritten as

$$y = \frac{WL}{4P} \left[\frac{\tan \frac{\pi}{2} \sqrt{\frac{P}{P_{cr}}}}{\frac{\pi}{2} \sqrt{\frac{P}{P_{cr}}}} - 1 \right] \tag{52}$$

This result is readily demonstrated to be approximately equivalent to

$$y = \frac{WL^3}{48EI} \left[\frac{1}{1 - \frac{P}{P_{cr}}} \right] \tag{53}$$

either by expanding the tangent and replacing an adjusted expansion by a geometric progression as did Salmon (46), or more simply, by the rational function method used in Chapter II. Defining lateral stiffness, ξ, as the ratio of the lateral load to the deflection it produces,

$$\xi = \frac{W}{y} \cong \frac{48EI}{L^3} \left[1 - \frac{P}{P_{cr}} \right] \tag{54}$$

It is apparent, then, that as the axial load approaches the critical value the stiffness approaches zero, and that the relationship is, at least approximately, linear.

If we turn our attention to the beam-column with encastré ends, we find that a similar condition obtains. Application of the classical theory results in the following formula for maximum displacement under a central concentrated lateral load:

$$y = \frac{W}{\lambda P} \tan \frac{\lambda L}{4} - \frac{WL}{4P} \tag{55}$$

This equation may be rewritten in exactly the form of equation (52), considering the difference in the critical load, and the procedure which generated equation (54) will lead in this case to the result

$$y = \frac{WL^3}{192EI} \left[\frac{1}{1 - \frac{P}{P_{cr}}} \right] \tag{56}$$

Thus, for the beam column with encastré ends,

$$\xi = \frac{W}{y} \cong \frac{192EI}{L^3} \left[1 - \frac{P}{P_{cr}} \right] \tag{57}$$

As before, the lateral stiffness, ξ, is seen to decrease linearly with increasing P, from its initial value of $192EI/L^3$ to zero as P is increased to P_{cr}. These are, of course, particular examples of the

Southwell relationship, and, thus, we may see the generality of the result.

Experimental Program

Having established that the lateral stiffness of a column can be regarded as approaching zero as and when the axial load approaches its critical value, and that a linear law of stiffness is apparent, we proceed to the study of the shell with some degree of confidence. Analytically, of course, the shell presents considerable complexity, whether the structure behaves in a linear fashion or not. In view of this fact, and the uncertainty which is consistently voiced concerning the matter, we proceed directly to the experiment. For the basic property of lateral stiffness approaching zero is true, in whatever manner the body behaves.

A number of tests were made to determine the change in lateral stiffness of a circular cylindrical shell reinforced with stringers as the shell was compressed. Details of the test vehicle, instrumentation and procedure are given in the following sections.

Equipment and Instrumentation

Specimen

The test vehicle chosen for this study was a stringer-reinforced plexiglass cylinder, the basic characteristics of which are as depicted in Figure 18. The shell was manufactured by the method described by Ford (40), and a series of 3/32 inch holes was drilled around the circumference through the midline of each stringer. The ends of the shell were potted into aluminum end rings, which were then attached

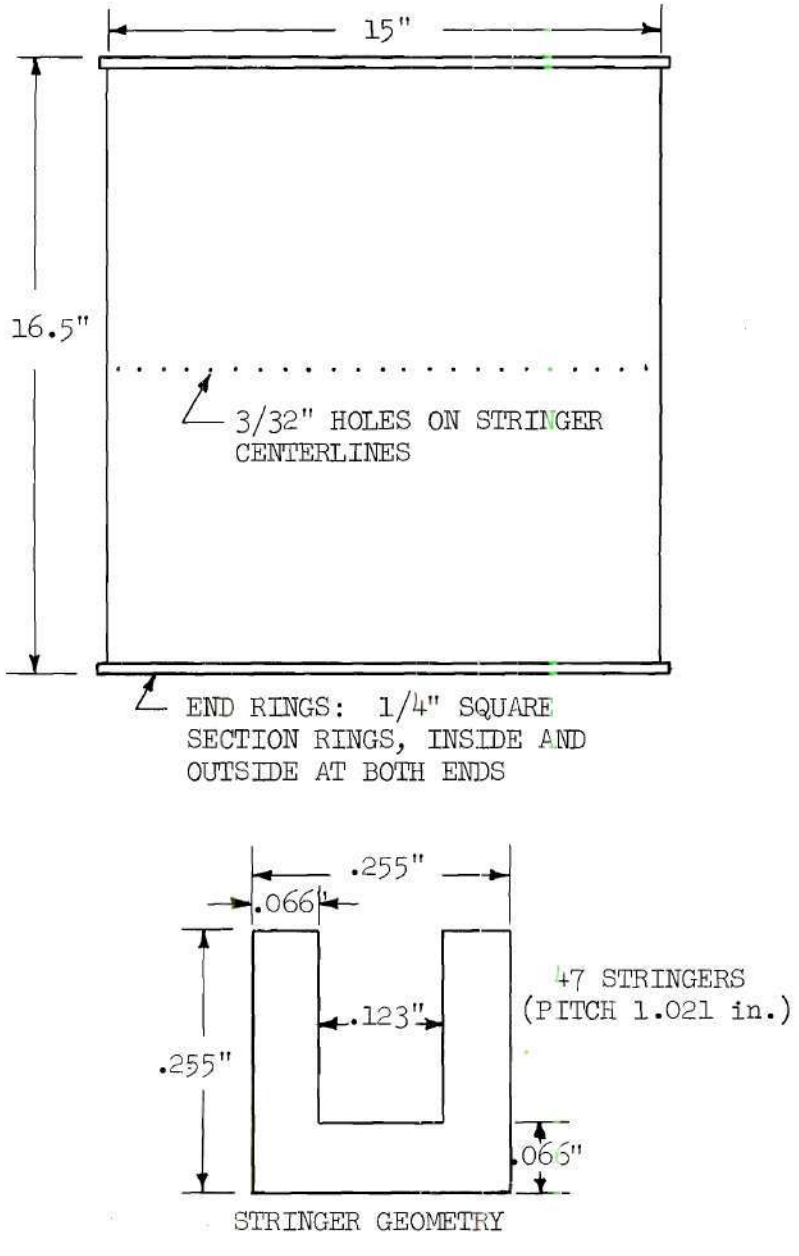

Figure 18. Test Specimen Dimensions.

to one-inch thick aluminum plates for mounting in the test machine.

Test Fixture Arrangement

Tests were conducted in a 120,000 pound capacity Baldwin screw-jack universal test machine. The arrangement of the specimen in the machine is shown in Figures 19 through 21.

The specimen base plate was clamped to the test machine table. A one-inch thick ground steel plate was added atop the upper aluminum plate to provide the necessary rigidity. A spherical bearing between this steel plate and the loading head completed the load path. Safety wires (not shown) attached the top fixtures to the loading head to minimize damage in the event of catastrophic failure of the specimen.

Nylon lines were attached to the shell wall through the mid-length hole of each stringer. They were led radially inward, over a teflon boss, and down a steel tube located on the axis of the shell. They passed through the test machine table to a loading station below. The multiplicity of cables enabled any section of the shell mid-plane to be investigated. At the end of each loading line there was a swivel-hook to which a loading weight could readily be attached.

Instrumentation

Axial load measurement was made by the strain-gage load cell of the Baldwin test machine. A voltage divider network driven by the test machine indicator system supplied an electrical load signal to the data acquisition system.

Wall motions were measured using linear variable differential transformers (LVDT's). Thin shim-steel leaf springs were used to support the LVDT cores, and were adjusted so that their spring constant

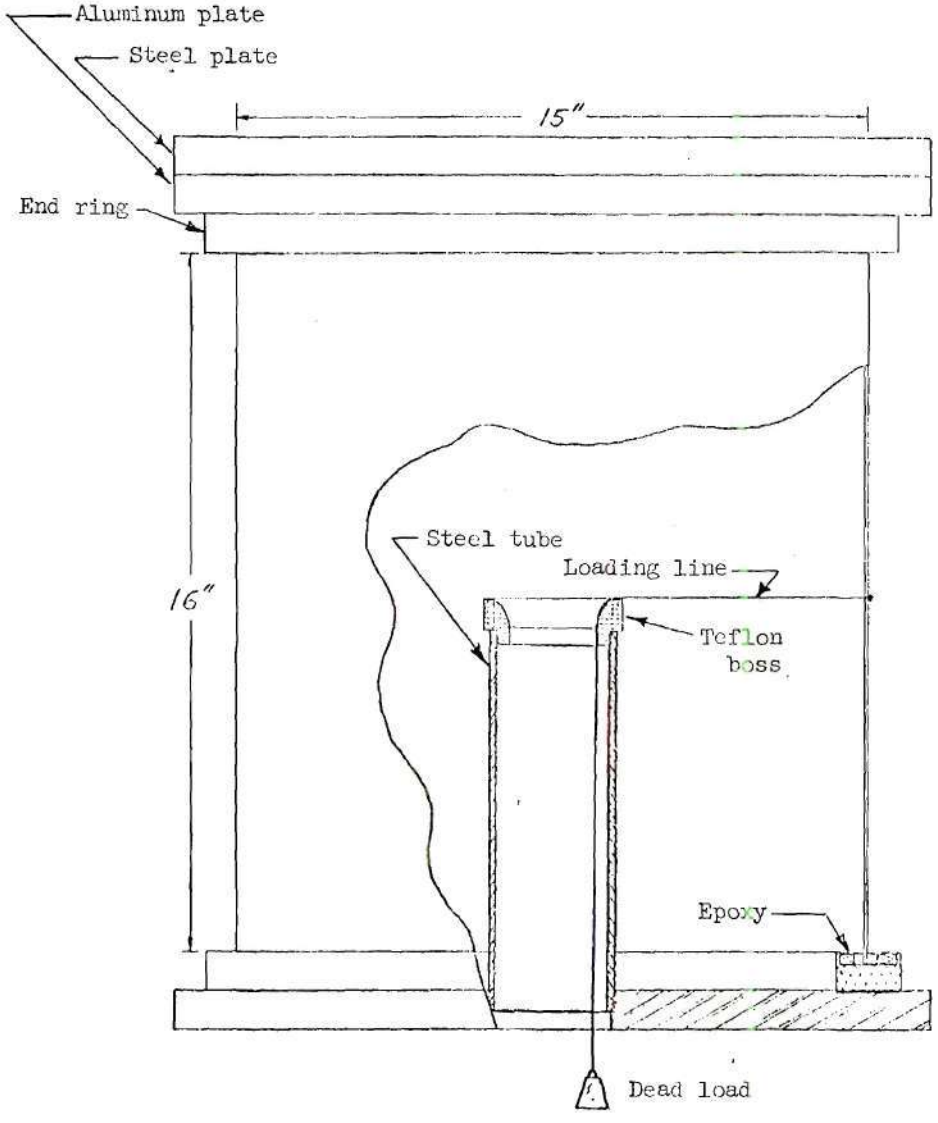

Figure 19. Arrangement of Specimen in Test Machine.

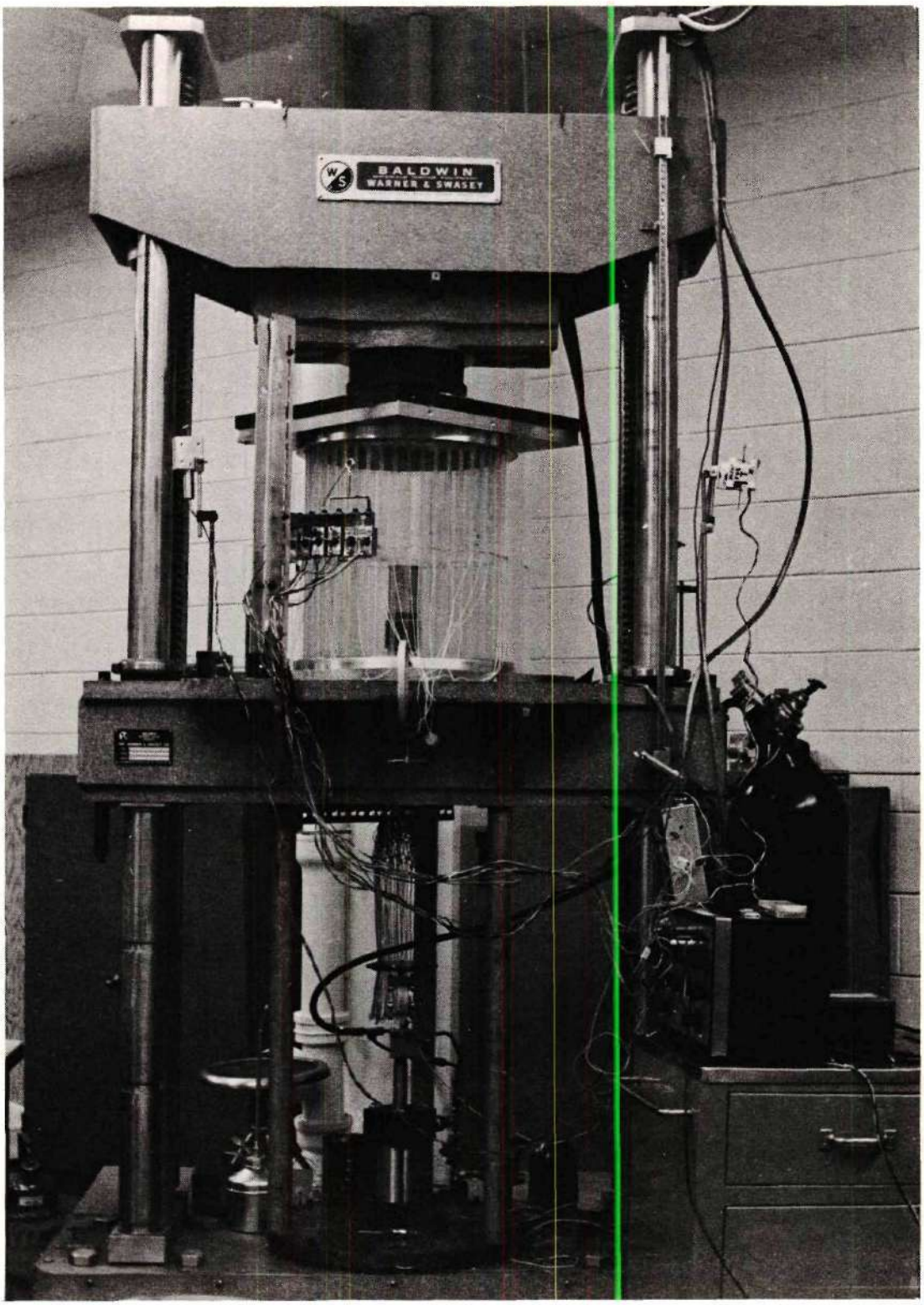

Figure 20. Plexiglass Specimen in Test Machine.

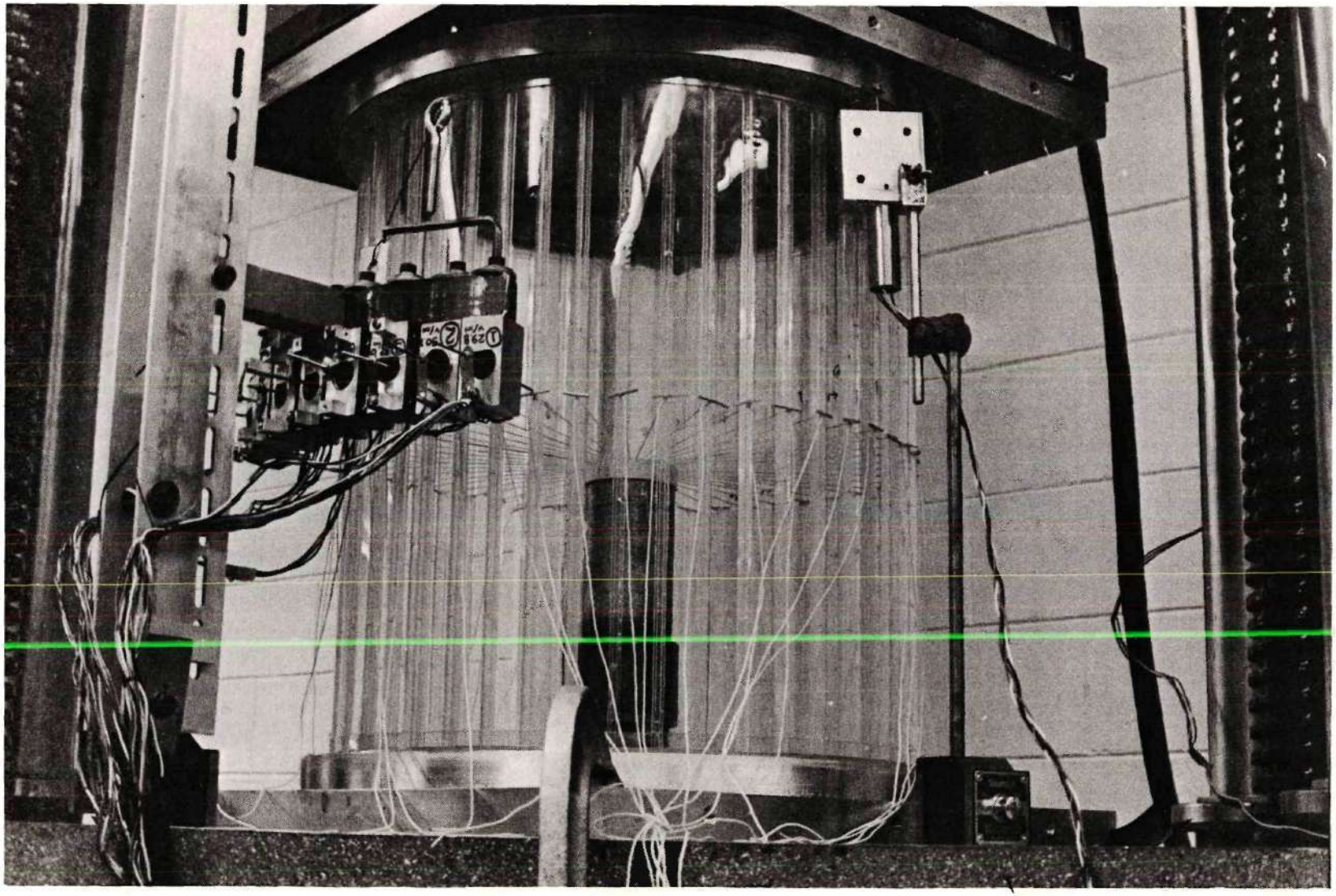

Figure 21. Loading Strings and Transducers.

was less than one gram per .010 inches displacement. Eight of these transducers were adjustably mounted on a magnetic stand (see Figure 21); this permitted a deflection scan of the immediate area of interest to be taken, as well as reading the deflection at the loaded point. Voltage outputs from the LVDT's were supplied to the data acquisition system.

End shortening measurements used in initial centering of the shell were made using vertically mounted LVDT's, one of which may be seen in Figure 21.

Data Acquisition System

The data acquisition system consisted of a Hewlett-Packard Model 2115 digital computer, interfacing with a cross-bar scanner and digital voltmeter, a magnetic tape unit, a high-speed paper tape punch, a high-speed paper tape reader, and a teletype unit. Computer operations were controlled by means of the teletype unit, the computer switch register, and a remote switch located at the test machine console. Data output was printed on the teletype. A flow diagram of the data acquisition system is shown in Figure 29, and the basic language data acquisition program is listed in Appendix A.

Procedure

The specimen was centered in the test machine and the load path was aligned with the shell axis. This was accomplished by arranging LVDT's to measure the end shortening under axial load at three stations, 120° apart, around the shell. Readings were taken and the location of the spherical bearing adjusted until the end shortenings

under a 2000 pound load were equal. The spherical bearing was then clamped in place.

The possibility of viscoelastic behavior of the plexiglass specimen was recognized, and a test procedure devised which minimized the effect of such behavior on the data. The time span of the test was kept short; loading was accomplished smoothly but rapidly. Immediately prior to each run the shell was "initialized" by loading to 2000 pounds. This was intended to mask any residuals from previous tests. Finally, a thirty minute interval between tests was rigidly maintained; this allowed ample time for recovery from the preceeding run. The justification for these steps is entirely experimental: as may be seen from the small scatter of the data and the repeatability of individual readings, they worked.

After the initializing run to 2000 pounds the load was returned to 100 pounds and zero deflection voltage readings of the LVDT's were taken. The axial load was then rapidly applied and stopped at the desired value. Deflection readings were taken, the lateral load weight was hung on the loading line, and deflections were read again. Readings were taken by the data acquisition system on command from the remote switch and stored on magnetic tape. The lateral load was removed and the axial load returned to 100 pounds. The entire test took from three to four minutes, depending on the magnitude of axial load to be applied.

Results

To determine the manner in which lateral stiffness varies with

a change in lateral load, forty-three tests were conducted at two locations on the midline of the shell. As a preliminary step to determine the form of the distorted shape of the shell, a complete circumferential deflection scan was made at several load levels. Since it was expected that an inward lateral load would have its minimum effect on the natural distortion wave form if it was located at the bottom of a "valley", i.e. an area of the shell which was displaced inward under axial load, two such points were selected for investigation.

The first tests were conducted at stringer number seven. Displacement readings at each axial load level were taken before and after the application of a one-pound inward radial load. The difference in these readings was used to compute the lateral stiffness. Data from these tests is listed in Table 14, and shown graphically in Figure 22. A straight line could readily be drawn through the points which resulted from tests at axial load levels between 2000 and 3200 pounds. At higher axial loads the data began to become non-linear, and at 3600 pounds the one-pound lateral load caused buckling. The extension of the linear portion of the curve intersected the zero stiffness axis at an axial load level of 4200 pounds.

A second series of tests was conducted at stringer number 15, again in a local valley. Data from this series of tests is listed in Table 15 and shown graphically in Figure 23. The first ten data points were taken with a lateral load of one pound. As in the initial test series, the loss of stiffness was linear from 2000 to 3200 pounds of axial load, and non-linear above that value. Buckling was caused by

Table 14. Lateral Stiffness at Stringer 7

Axial Load	Wall Displacements Free w/Lateral Load		Displacement Change	Stiffness
lbs.	m.in.	m.in.	m.in.	lb./in.
2000	1.0	14.4	13.4	74.63
2213	1.3	16.3	15.0	66.67
2300	1.3	15.7	14.4	69.44
2400	1.5	18.1	16.6	60.24
2402	2.5	17.7	15.2	65.79
2501	1.1	17.5	16.4	60.98
2598	2.0	19.5	17.5	57.14
2601	1.9	19.8	17.9	55.86
2701	2.0	20.0	18.0	55.56
2796	2.7	21.6	18.9	52.91
2900	2.4	23.3	20.9	47.85
2995	3.2	27.0	23.8	42.02
2997	2.8	28.8	26.0	38.46
3095	3.7	34.6	30.9	32.36
3112	3.5	29.3	25.8	38.76
3197	4.0	31.7	27.7	36.10
3203	3.4	28.4	25.0	40.00
3296	4.2	34.4	30.2	33.11
3298	5.3	41.9	36.6	27.35
3395	4.6	38.7	34.1	29.33
3401	5.3	44.2	38.9	25.71
3600	7.5	----------Buckled----------		

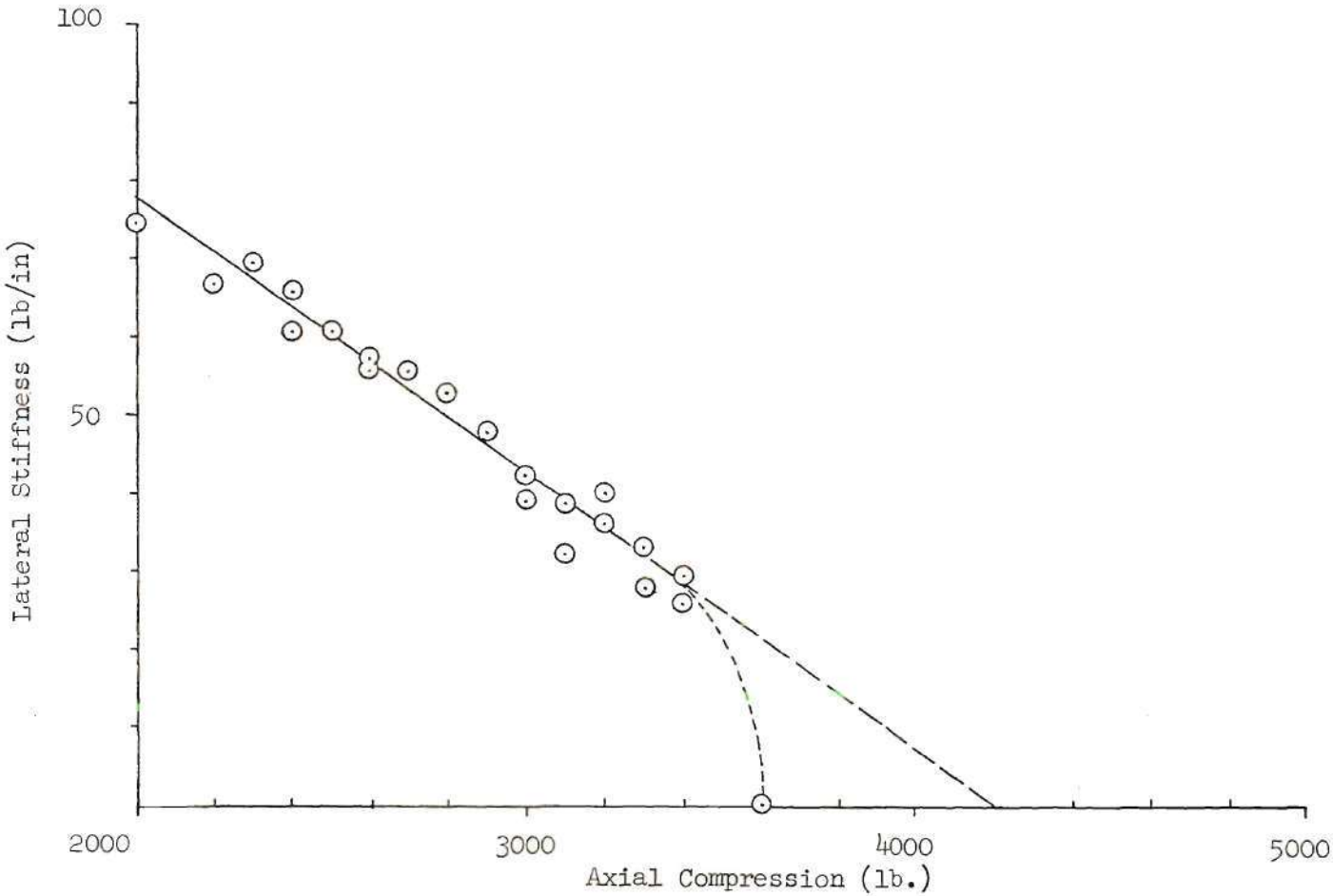

Figure 22. Change in Lateral Stiffness with Axial Compression, Stringer Stiffened Plexiglass Shell 1 lb. Lateral Load at Stringer No. 7.

Table 15. Lateral Stiffness at Stringer 15

Axial Load	Lateral Load	Displacements Free w/ Lateral Load		Displacement Change	Stiffness
lbs.	lbs.	m.in.	m.in.	m.in.	lb/in
2010	1.0	0.5	20.7	20.2	49.50
2206	1.0	1.0	23.5	22.5	44.40
2402	1.0	1.3	24.7	23.4	42.34
2612	1.0	2.7	30.9	28.2	35.46
2802	1.0	3.4	33.7	30.3	33.00
2995	1.0	5.3	43.2	37.9	26.39
3209	1.0	7.8	51.0	43.2	23.15
3299	1.0	9.4	51.2	41.8	23.92
3305	1.0	8.9	51.2	42.3	23.64
3417	1.0	12.0	----------Buckled----------		
2020	1.5	0.4	33.6	33.2	45.18
2200	1.5	1.0	37.7	36.7	40.87
2413	1.5	1.8	41.9	40.1	37.41
2812	1.5	3.8	50.9	47.1	31.85
3127	1.5	6.7	50.6	43.9	34.17
3380	1.5	12.1	----------Buckled----------		
2004	0.5	0.3	9.6	9.3	53.76
2797	0.5	3.5	17.0	16.5	30.30
3101	0.5	6.7	25.2	18.5	27.03
3216	0.5	8.6	31.1	22.5	22.22
3511	0.5	16.1	49.9	33.8	14.79

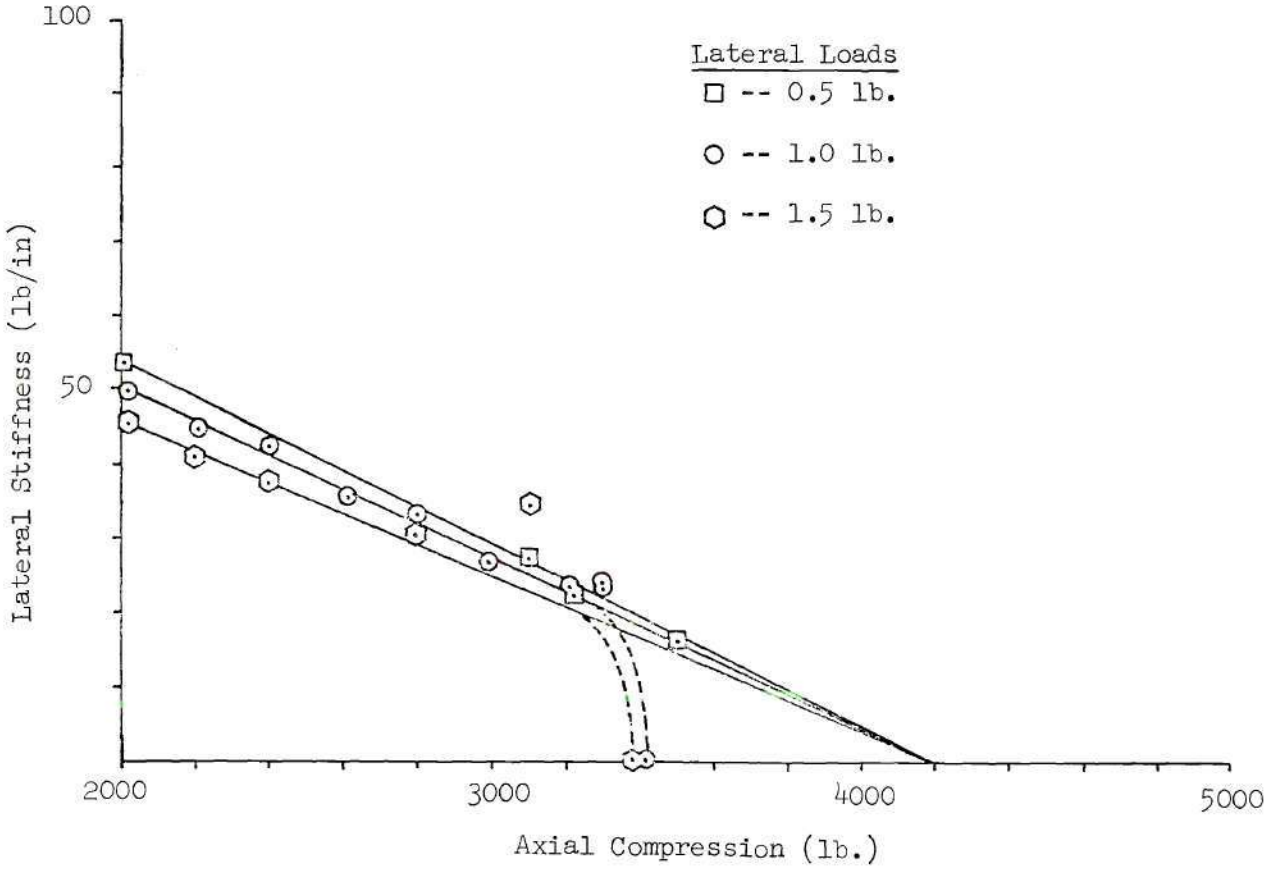

Figure 23. Change in Lateral Stiffness with Axial Compression, Stringer Stiffened Plexiglass Shell with Lateral Load at Stringer No. 15.

application of the one pound lateral load when the axial load was 3417 pounds. Again the extension of the linear portion of the curve intersected the zero stiffness line at an axial load of 4200 pounds.

The next eleven data points were obtained with different values of the lateral load. Six points were taken with one and one-half pounds lateral load, and five with one-half pound. It was apparent that while the stiffness lines which resulted were not colinear with the one pound line, they were very nearly so, and that extensions of the individual lines all intersected at the zero stiffness point, 4200 pounds. The stiffness difference was consistent, the one-half pound line lying above and the one and one-half pound line below the one pound stiffness line.

Following the stiffness tests the shell was loaded in pure axial compression until it buckled. The critical load was 4050 pounds.

Discussion

The importance of the result of this investigation is obvious. The extensions of the several stiffness lines have a common zero-stiffness intercept, which is within 3.71 per cent of the actual buckling load of the shell. Furthermore, the data defining the linear portion of the curve was obtained at compressive loads less than 70 per cent of the critical value. Thus, the method is seen to be both accurate and more nearly non-destructive than any previously known. It is easy to apply, in that only one point on the shell is loaded (in addition to the axial load), and one deflection measured. No involved analysis of data is required, and in fact it may readily be

plotted during the test to provide guidance as to axial load levels to be applied.

The precise reason for the slight difference in slope of the lateral stiffness lines for different side force magnitudes is not clear at this time. There is little doubt that a detailed extensive theoretical and experimental program will be necessary to completely resolve the issue. However, it may be that there is a valid analogy between the effect noted and the influence of non-linearities in the Southwell technique. Fisher (47) demonstrated that a local yielding caused a change in slope of the Southwell line, while Wang (48) and Braathen and Noton (49) demonstrated the validity of the process for inelastic buckling.

It is clear that regions of non-linearity, both geometric and material, existed in the structure tested, as in all practical structures of this type. However, in view of the very small side force applied it is most unlikely that there was any non-linear interaction until the system reached the bounds of stability. As this state was reached, of course, there was definite non-linearity, and a non-linear stiffness curve resulted.

Conclusions

These tests demonstrate that the wall of a stringer-reinforced shell under axial compression undergoes a progressive loss of lateral stiffness as the axial load is increased. Although the loss is apparently non-linear for some region of smaller axial loads, there is a usable region of linear loss for compressive loads considerably

lower than the critical load. Extending this linear portion of the stiffness curve to its zero-stiffness intercept permits prediction of the actual buckling load of the shell. The technique is accurate and more nearly non-destructive than any previous method of shell evaluation.

CHAPTER IV

THE USE OF AN UNSTABLE MECHANICAL SYSTEM IN THE DESIGN OF A VERY HIGH "G" CRASH SIMULATOR

Introduction

The histories of technology and of the quest for increased mobility are virtually synonymous. Man's success in moving himself and his goods, ever farther, ever faster, began with the dugout on the stream and lake. Inexorably it developed to the ship on the sea, the wheeled vehicle on the road and the locomotive on the rail. Then came the automobile and the airplane. These two devices have put within the grasp of the common man a facility and luxury of transportation denied to the kings and princes of but a hundred years ago.

The year 1903 was the beginning of the era. It was in that year that Henry M. Leland took three Cadillac automobiles to the Brooklands race track in England. He dismantled them, mixed the parts in a common pile, and added a new set. He then assembled three cars from the parts, and sent them round the track for 500 miles. Complete interchangability of parts was demonstrated, and mass production of the automobile inaugurated. And, on the 17th of December of the same year, at Kitty Hawk, North Carolina, Wilbur and Orville Wright made four flights of the biplane they had built and named simply "The Flyer."

This is not the place for a detailed account of man's progress

in transportation. It is sufficient to say that he has achieved a high degree of mobility, at a price. The price is pollution, noise, and damage to himself and his fellow-man. Today tens of thousands die in automobile accidents annually, and many more in aviation and maritime mishaps. The causes are many and varied. For the land and air vehicles, however, impact is a major factor: impact of the vehicles with one another, or with some immobile object, or impact of the occupants with some part of the vehicle due to a rapid change in the state of motion.

Impact, whether it be between man and machine or between machine and machine brings many serious problems. It is always accompanied by redistributions in momentum and energy - redistributions which frequently cause excessive g forces to be generated.

When people are subjected to a high g environment sometimes they survive, and sometimes they do not. Survival is a matter not only of the magnitude of the g, but also of the position and degree of protection and restraint provided the recipient. The very devices installed to protect are themselves often the cause of trouble: crash helmets can aggravate neck injuries, and ejection seats damage the spine. There is a vital need for more information on the subject, for a clearer understanding of both the steady state and dynamic response of the human body to high-level accelerations.

This has been fully appreciated only for the last quarter-century. Serious studies of the influence of high g on human beings began with the studies of Col. J. P. Stapp (50). This work aroused considerable interest not only in military aviation circles, but also

among public safety authorities. As a result today research on the effects of high g is being made in many parts of the world. The major portion of this work is still centered in the United States, and in this effort the Naval Aerospace Medical Research Unit in New Orleans plays a leading role.

The current interests differ, of course, from those of the early investigators. Where Stapp sought to establish maximum tolerance levels, today's researchers seek to understand dynamic responses. Where Stapp was interested in peak g and "time base" (time from initiation to end of the acceleration), aeromedical workers today are interested in time at peak g - the "flat top on the acceleration card." And where Stapp achieved his g pulse by decelerating a rapidly moving sled, leading authorities today believe that the surest way to acquire valid data on human response lies in its acquisition under acceleration rather than deceleration conditions (51).

Commercial equipment with the desired capabilities is not available. The absolute limit of standard equipment is on the order of 60g and the time base over which this level is experienced, less than 10 milliseconds. Research workers in the field feel a positive need for enhanced performance devices. They state that a system capable of generating a 200g acceleration (the equivalent of that experienced by an automobile travelling at 75 miles per hour impacting a bridge abutment, for example) would enable them to acquire information of extreme value in protecting the lives of motorists as well as military aviators. To this end the research described in this chapter was conducted.

The starting point for this study lay in a set of performance specifications compiled by the Naval Aerospace Medical Institute. These requirements are summarized in Table 16. It is readily apparent from this table that the need is not easily met.

Numerous acceleration producing devices have been developed over the years. Joyner and Horne (52) in a NACA design study list twelve types of catapult (see Table 17). Although none of these mechanisms in its state-of-the-art form could meet the present requirements, engineering is essentially an adaptive process. We shall investigate means whereby a catapult might be used indirectly. To do so we must use a momentum transfer process in which a mass moving at a suitable velocity is caused to strike a subject vehicle, accelerating it. A buffer between the two controls the g onset rate.

For convenience in our discussion we note at this point that whatever method we choose to utilize, the test subject will have to be placed in or on some type of vehicle. It will be necessary to equip this "subject car" with a certain amount of instrumentation, safety devices, deceleration systems, and various other appurtenances. Since the magnitudes of other quantities of interest depend directly on the mass of the subject car, we will fix its weight at 5000 pounds. This estimate is based on the prior experience of workers in the field.

Momentum Transfer Accelerator

The foundation of the momentum transfer system is the Principle of Conservation of Momentum, which for a non-rebounding collision with a stationary object may be written

Table 16. Crash Simulator Acceleration Performance Specifications
(supplied by Naval Aerospace Medical Institute)

	Profile	Max G	Duration at Peak T	Onset Rate	Time to Peak	Distance to Peak N	Velocity at Peak Z	ΔV at Constant a V	Δ Dist. at Constant a M	V_{max}	Distance S
		g	ms	g/s	ms	ft	ft/s	ft/s	ft	ft/s	ft
High Acceleration Requirement	A	200	15	40,000	5	.027	16.1	96.6	0.964	112.7	0.991
	B			10,000	20	.429	64.4		1.689	161.0	2.118
	C	150	30	10,000	15	.181	36.225	144.9	2.264	181.125	3.445
	D			5,000	30	.724	72.45		4.349	217.35	5.073
	E	100	50	5,000	20	.215	32.2	161.0	5.63	193.2	5.845
	F			1,000	100	5.367	161.0		12.07	322.0	17.437
	G	60	100	5,000	12	.046	11.592	193.2	10.819	204.792	10.865
	H			600	100	3.22	96.60		19.32	289.8	22.54
Low Acceleration Requirement	i	40	125	5,000	8	0.014	5.152	161.0	10.705	166.15	10.72
	j			200	200	8.587	128.80		26.16	289.80	34.75
	k	30	170	5,000	6	0.006	2.898	164.22	14.453	167.12	14.46
	l			200	150	3.622	72.45		26.27	236.67	29.89
	m	20	250	5,000	4	0.002	1.288	161.0	20.441	162.29	20.44
	n			200	100	1.073	32.20		28.17	193.20	29.24
	o	10	500	5,000	2	0.0002	0.322	161.0	40.411	161.32	40.41
	p			200	50	0.129	8.05		44.27	169.05	44.40

Table 17. Survey of Catapult Types (after Joyner and Horne, Reference 52)

No.	Type of Catapult	Motivation	Initial costs (development and construction)	Operating Costs
1	Dropping weight	Dropping weight (cable and sheave system)	Very high	Low
2	Flywheel	Flywheel (clutch, cable, and sheave system)	High	Low
3	Blowgun	Low-pressure, large-area piston (expansion of powder or compressed air)	High	High (with air) Low (with air)
4	Slotted tube	----------do----------	High	High (with powder) Low (with air)
5	Piston	High-pressure, small-area piston (hydraulic and compressed air, compressed air or powder actuated)	High	High (with powder) Low (with compressed air)
6	Rocket	Reaction type, solid fuel propellant (adds extra weight to carriage)	Low	Very high
7	Rocket	Reaction type, liquid fuel propellant (adds extra weight to carriage)	Low	Medium
8	Hydraulic (jet)	Reaction type, water and compressed air (added carriage weight prohibitive)	Medium	Low
9	Rocket	Impulse type, solid fuel propellant	Medium	Very high
10	Rocket	Impulse type, liquid fuel propellant	High	Medium
11	Hydraulic (jet)	Impulse type, water and compressed air	Low	Low
12	Electropult	Squirrel-cage electric motor laid out flat	Very high	Low

$$MV_1 = (m + M)V_2 \tag{58}$$

where M is the mass of the initially moving object, m the mass of the object accelerated, and V_1 and V_2 the initial and final velocities, respectively. The action is not unlike that of a golf shot, where the rapidly moving club strikes the ball, accelerates it, and then is slowed and diverted by the player's hands as the ball continues its flight. In the case of the momentum transfer accelerator we wish to have close control over the rate of rise of the acceleration, so we interpose a buffer-programmer between the impacter and the subject car.

As can be seen from equation (58), once the mass of the subject car is known and the final velocity, V_2, established by selection of an acceleration profile, the initial velocity, V_1, is a function of impacter mass. It must, of course, be greater than V_2. Selecting the most demanding performance profile from an energy standpoint, i.e. profile F, which requires maximum V_2, we compute V_1 and impacter kinetic energy prior to momentum transfer as a function of impacter weight. This information is plotted in Figure 24. It is evident that minimum impacter energy, and thus minimum facility energy capability, is required when impacter and subject car weights are equal. Energy input is not the only consideration, however. There is a loss of kinetic energy involved in the non-rebounding collision between impacter and subject car, and this energy must be absorbed by the buffer. The amount of energy input to the buffer will influence the

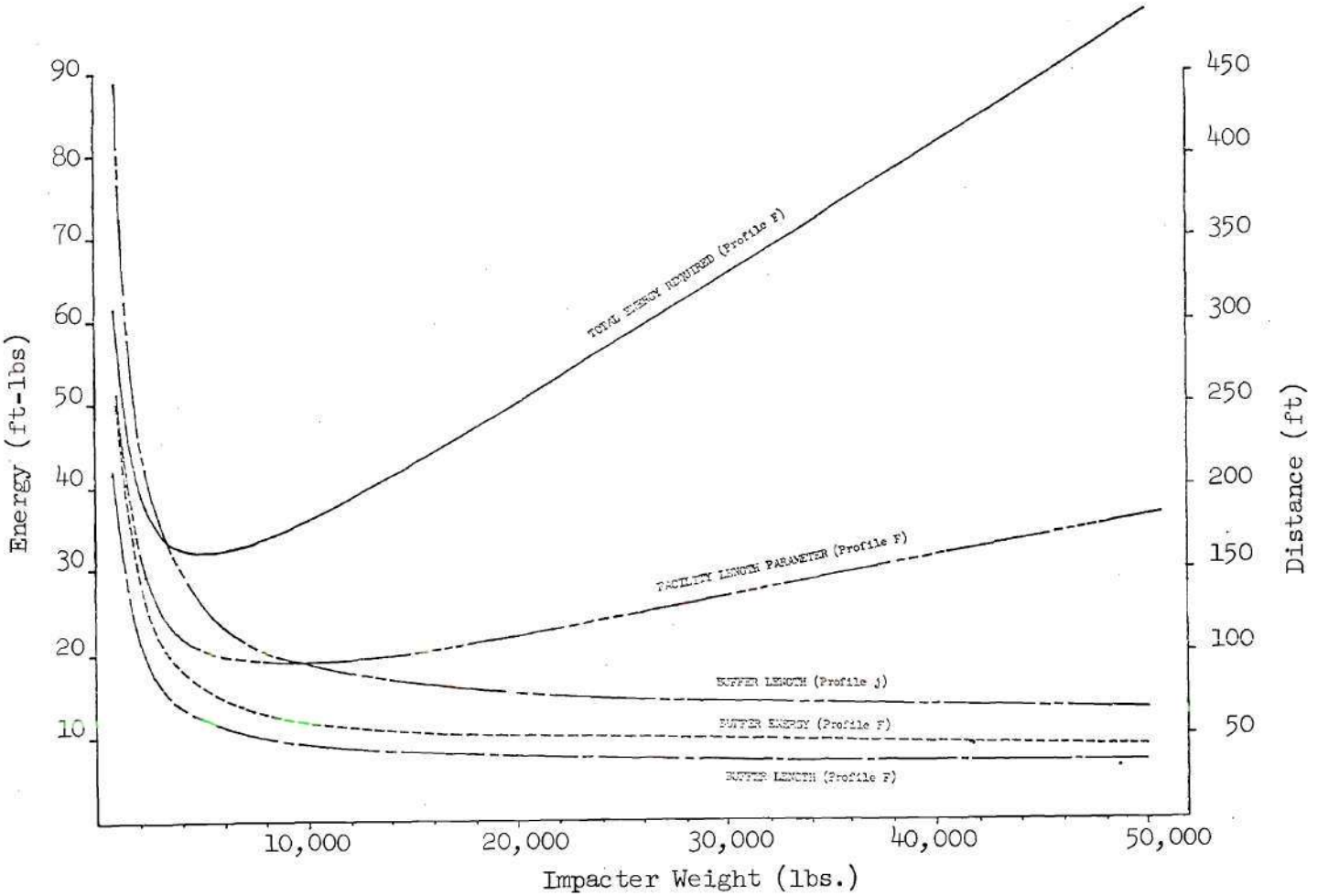

Figure 24. Impacter Weight Selection Curves.

difficulty in its design and construction, and thus it would be well to minimize this quantity. We compute and plot buffer energy as a function of impacter weight (Figure 24), and see that the greater the weight of the impacter the less demanding the buffer energy requirement.

Another factor determined by impacter weight is the buffer length. The distance travelled by the subject car during the acceleration phase of a given profile is a constant, but that travelled by the impacter depends on the entering velocity, V_1. The length of buffer required is, of course, the difference between these two distances. Buffer length was computed for profiles F and j as a function of impacter weight. This information is also plotted in Figure 24. The extreme lengths required for the lightweight impacters are clearly unacceptable. An estimate of the weight of a 45 foot buffer and impacter combination was made, and it was concluded that such a device would weight in excess of 40,000 pounds.

In the final design stage, of course, impacter weight for the various profiles will have to be determined in a trade-off process. Total energy input, overall facility length, buffer length and energy absorption, and minimum practical structural weight must be considered. It is likely that a variable weight impacter, or several different impacters, will prove most economic. For the purposes of this preliminary study an arbitrary conservative impacter weight of 50,000 pounds was chosen to size the facility required.

Having fixed the impacter mass, we may now consider the energy input requirements. For profile F, which demands the greatest V_2,

$$V_1 = \frac{M + m}{M} V_2 = 354 \text{ ft/sec} \qquad (59)$$

and

$$KE_1 = \frac{1}{2}MV_1^2 = 97.2 \times 10^6 \text{ ft lb} = 36.65 \text{ KW-hrs} \qquad (60)$$

It is obvious that a stored energy system will be necessary.

There are a number of ways in which such a quantity of energy can be stored and rapidly released:

Table 18. Stored Energy Force Generators

Type	Method of Storage	Method of Release
Rocket motor	Chemical, in fuel	combustion
Powder catapult	chemical, in gunpowder	combustion, piston, and cylinder
Steam catapult	superheated steam	expansion, piston, and cylinder
Linear induction motor	inertial, flywheel	generator and motor
Blowgun	compressed air	expansion, piston, and cylinder

Despite considerable research and development on the part of the military the first two remain so expensive and dangerous that they are usually disregarded even for military applications. On the other hand the steam catapult has become an everyday tool. Conversations with

the Navy's steam catapult experts indicate that present energy levels approach 70 x 10^6 ft lb, and that no great problem should be encountered in satisfying the 90 x 10^6 ft lb requirement. Unfortunately, however, the maximum repeatable velocity output is 290 ft/sec. To reach 350 ft/sec, they say, would require design of an "open-ended" catapult, a multi-million dollar project, and would bring a significant increase in maintenance and operation costs. A very large steam plant is required. All things considered, this is a costly approach.

The linear induction motor has received recent attention as a method of powering rapid transit trains. In a form called the "electropult" it was tested by the Navy as a take-off assist device for aircraft (53). Energy stored in a large flywheel was used to drive a generator, supplying about 10,000 KW during the 1000 ft take-off assist stroke. Maximum shuttle speed was 330 ft/sec. Although this speed is only slightly less than the maximum specified, we note that these tests were conducted at a much lower energy level, used a relatively long stroke to launch a light jet aircraft (F-80) operating at full thrust, and that even then the electropult was drawing a 7000 ampere current. Thus, to reach the energy levels we desire considerable expensive development is required. Current transfer could be a prohibitive factor.

We are left, then, with the blowgun. In this scheme the accelerated object itself is the piston, and is propelled through a suitable tube by air pressure behind it. The technology of compressing, storing, and controlling air is well understood. In the past problems have been encountered in construction of a large-diameter bore of sufficient

accuracy, and in guiding and sealing the piston. This design study was concerned with the elimination of these difficulties, and a scheme with potential to do so is now developed.

Pneumatic Driver System

To adapt the blowgun technique economically to high energy operations, we will need to:

(a) avoid the issue of a perfectly straight and circular launcher tube; thus, we must

(b) develop a workable seal that is virtually unaffected by irregularities in tube shape, and

(c) conceive an appropriately inexpensive track.

There are, of course, other systems which are vital to the facility, but their development is essentially secondary.

Low Pressure Seal

To solve our seal problems, we resort to an adaptation of the familiar oil-film shaft seal. As shown in Figure 25, a solid pressure bulkhead on the rear of the impacter fills the majority of the opening between the impacter and the cylinder wall. High pressure air supplied to the annular plenum exits at high velocity in a rearward direction, and acts as a barrier to the lower pressure air behind the impacter. Thus, an effective seal should be achieved without the necessity of close tolerances on wall straightness or tube circularity.

Launcher Tube

The question of optimum launcher tube length clearly will be decided by an interplay between the costs of real estate, construction and operation. For the purposes of this discussion, let us assume that

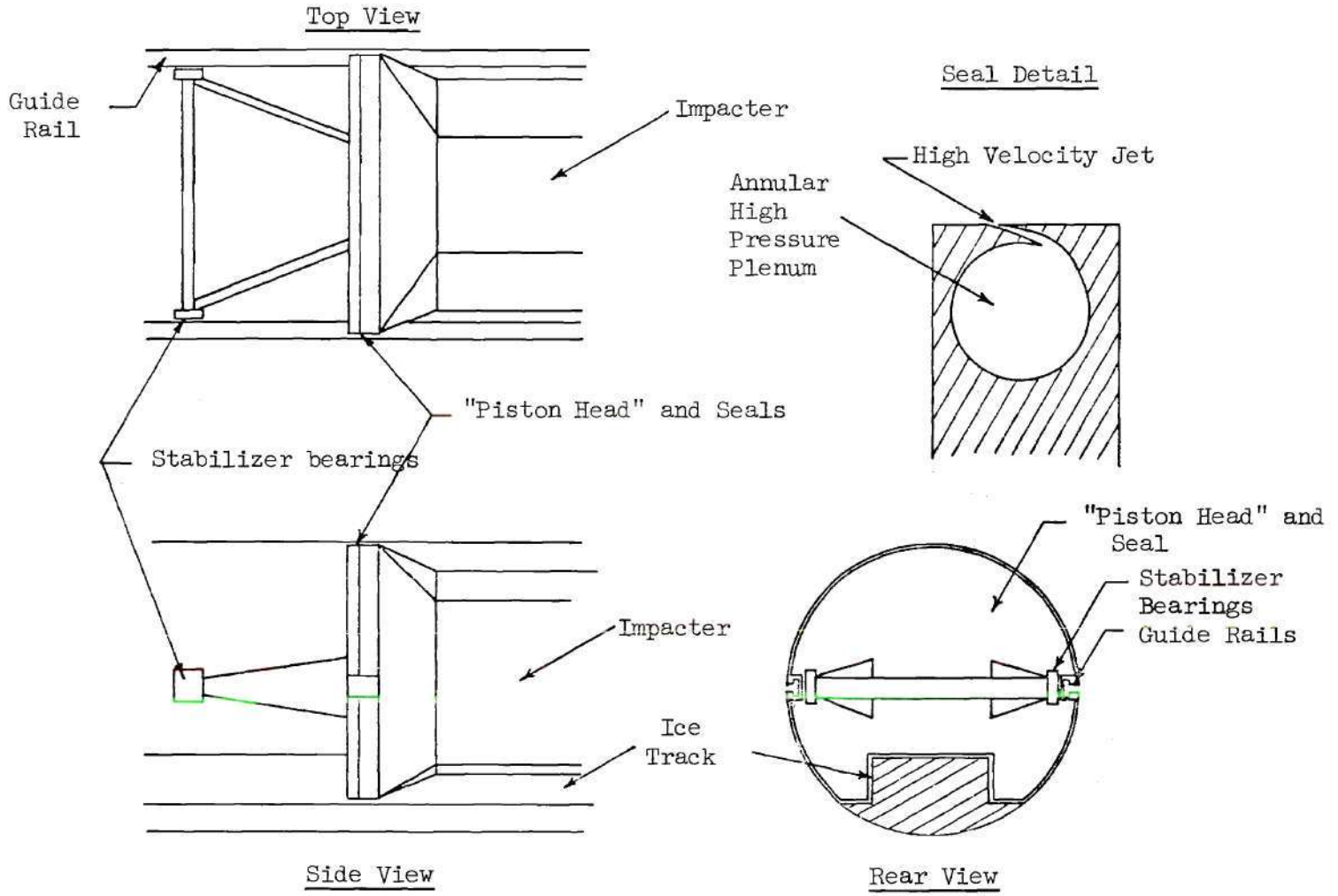

Figure 25. Blowgun Impacter Seal and Stabilization.

we will bring the impacter velocity to V_1 over a reasonable distance, say 100 feet. Then if we hold a constant acceleration, to achieve the velocity required for profile F would require over 805,000 pounds force. Assigning an average tube pressure value of 100 psi then implies 8050 square inches of area, or a tube diameter of approximately 100 inches. This size bore will easily accomodate the impacter, but to allow for floor and track we choose a diameter of 120 inches. We note that the largest commercially available concrete pipe has this diameter; since we can accept a certain lack of straightness in the tube and still maintain an acceptable seal, this method of construction would be relatively inexpensive. It will be necessary, of course, to add additional reinforced concrete around the tube to withstand the internal pressures.

It should be emphasized at this time that in practice, a uniform acceleration and pressure profile for the launcher would not be adopted. This point is clarified later.

Impacter Track

If the walls of the cylinder are not required to be perfectly straight, the motion of the impacter must be guided by some sort of track. While this presents no real problem, it is possible that there might be advantages in the use of a new technique here also. If the weight of the impacter is spread over a sizeable area considerable savings in impacter and track construction costs could be realized. This can be done by sliding the impacter with its lower surface resting on an ice track, like a great toboggan. The ice surface would be maintained by a refrigeration plant and cooling coils, much as is

an ice skating rink. The track would be kept straight and level by means of a mobile milling device riding on carefully aligned rails on the walls of the tube.

The lack of straightness of the tube sections certainly will result in small center of pressure movements on the back of the impacter. Compensation for the yaw inducing torques which would result from this movement is provided by high pressure air jets on arms extending behind the impacter; any rotation brings the jets in closer proximity to the straight rails and produces a restoring torque. Both research and development will be required here to insure that the sled-track-airjet combination has sufficient stability and damping.

Blowgun Pressure Profile

Although we have specified an average pressure behind the impacter of 100 psi as it is brought up to V_1, it is obvious that we do not wish to maintain a constant pressure during the 100 ft accelerating stroke. To do so would require movement of a very large volume of air, and would require a complex initiation and control system with complicated and expensive valves, multiple air inputs along the track, pressure sensors, and relief valves. In addition, as the impacter leaves the tube and enters the test section we would be venting a large supply (7850 ft^3) of 100 psi air into that area. Our interest, however, is only in achieving an average pressure of 100 psi, i.e. in having the area under the pressure-distance curve the same as that for a constant 100 psi profile. Thus, we choose a program such as that shown in Figure 26. No special valve opening characteristics are required for lower velocity profiles. For high velocity profiles it

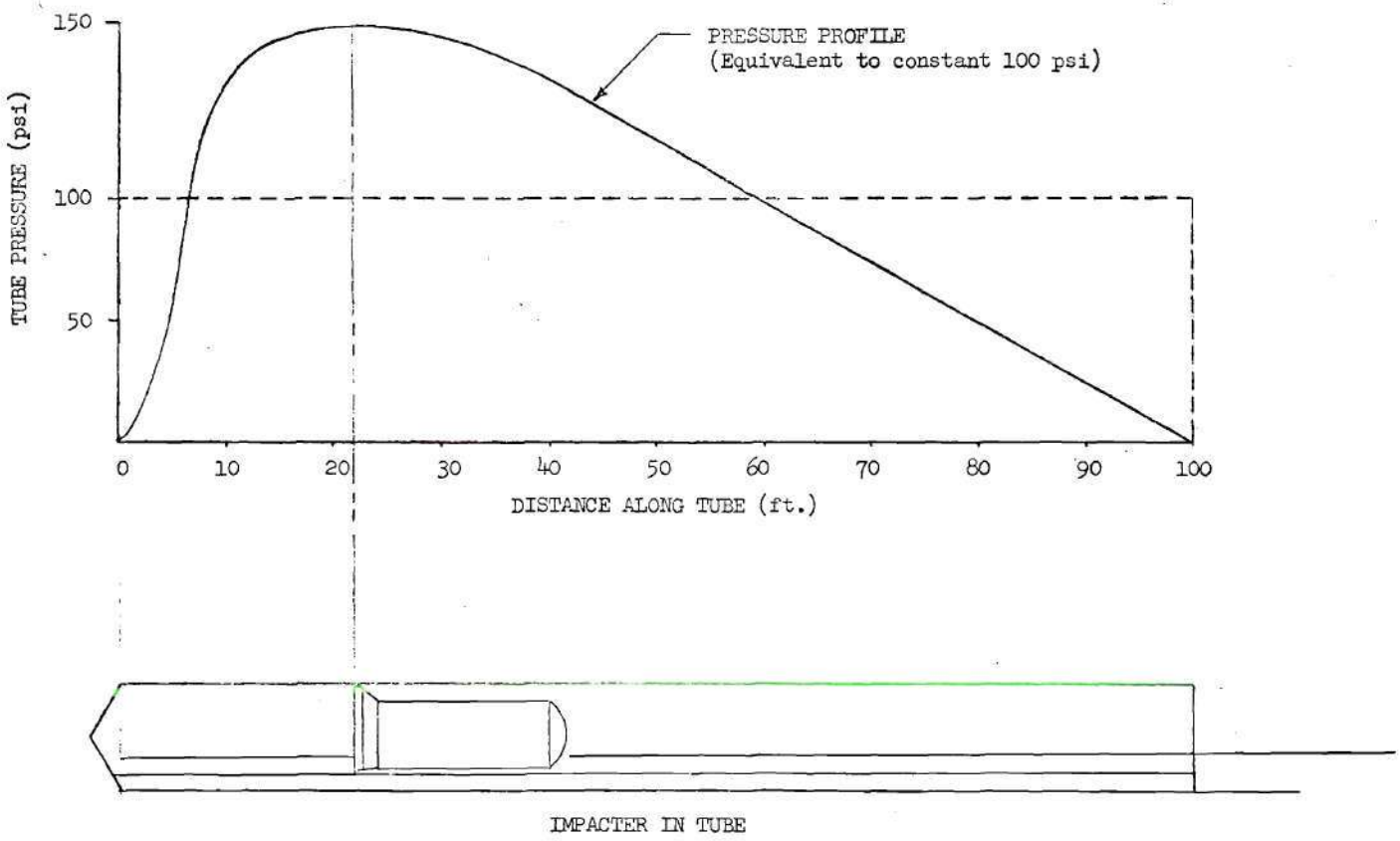

Figure 26. Sample Blowgun Pressure Profile, Equivalent to 100 psi Constant Pressure Throughout Travel

may be necessary to restrain the impacter while an initial pressure is built up in the tube, and to release it and burst a diaphragm to obtain a sufficiently rapid pressure rise. Considerable research and development may be required in this area.

Impacter and Buffer System

The impacter will have to be a large double car, containing as it must the high pressure air supply for the seals and guide jets, the buffer/programmer, and sufficient ballast to bring its total weight to that required for the desired profile. The "piston head" and seal and the guide jets together with the air tanks form the seal car, which is at the rear of the impacter. The buffer/programmer and ballast are contained in a second car, which is rigidly attached to the front of the seal car. This arrangement permits change of buffer/programmers to accomodate the different test profiles.

For ballast we use water - cheap and easy to handle - and to prevent sloshing the water is frozen by pre-launch connection of ballast cooling coils to the track refrigeration system. This gives an added advantage in that the ice serves as a heat sink for the buffer cylinders which it surrounds.

As may be seen in Table 19, the buffers vary widely in both stroke and maximum force capabilities. The longest stroke required with a 50,000 pound impacter is in excess of 65 feet, which implies that the forward end of the buffer will be near the three-quarter point of the launcher tube when the impacter is in the ready position. Shorter buffers are necessary for the high-g profiles. In such cases it might be advantageous to reduce impacter weights to reduce

Table 19. Buffer Requirements, 50,000 Pound Impacter

Profile	Maximum Force	Variable G Stroke	Constant G Stroke	Total Stroke
A	10^6	.60	.80	1.40
B	10^6	3.07	.80	3.87
C	750,000	2.79	2.37	5.16
D	750,000	6.38	2.37	8.75
E	500,000	4.01	4.37	8.38
F	500,000	29.49	4.37	33.86
G	300,000	2.65	10.74	13.39
H	300,000	28.36	10.74	39.10
i	200,000	1.45	11.04	12.49
j	200,000	54.25	11.04	65.29
k	150,000	1.09	15.35	16.44
l	150,000	35.07	15.35	50.42
m	100,000	7.15	22.17	29.32
n	100,000	22.14	22.17	44.31
o	50,000	.36	44.30	44.66
p	50,000	9.16	44.30	53.46

total energy input. For the higher onset rates it may be necessary to use a constant force buffer, and to use distortion of lead pellets to achieve the desired onset profile. Although it is an art rather than a science, this technique has been used with success at the Naval Air Engineering Laboratory in the past.

Evacuated Tube

The pressure rise in front of the impacter as it is accelerated down the tube will depend not only on the final velocity of the impacter, but also on the launcher pressure profile. The air in the tube, some 7850 ft^3 or 600 lbs is swept out by the power stroke, and must be removed from the system at some point. If a louver and fan system at the exit of the launcher tube will not suffice, doors in the tube wall may be required. It may be that the tube ahead of the impacter will have to be partially evacuated and quick opening doors provided to prevent choking of the flow out of the tube at higher velocities. This area will require both research and development.

Other Systems

Subject Car: The subject car must, of course, be designed to withstand the maximum g loading, to provide secure, all-attitude attachments for the test subjects and instrumentation, and to contain devices which will insure a smooth and safe stop. During the acceleration phase the subject car is supported by slippers on precision rails. For deceleration the vehicle will be picked up on rubber tires and stopped as wheeled vehicle.

Braking System: To stop the impacter a combination of devices is used. Initial braking is provided by a dual channel water brake

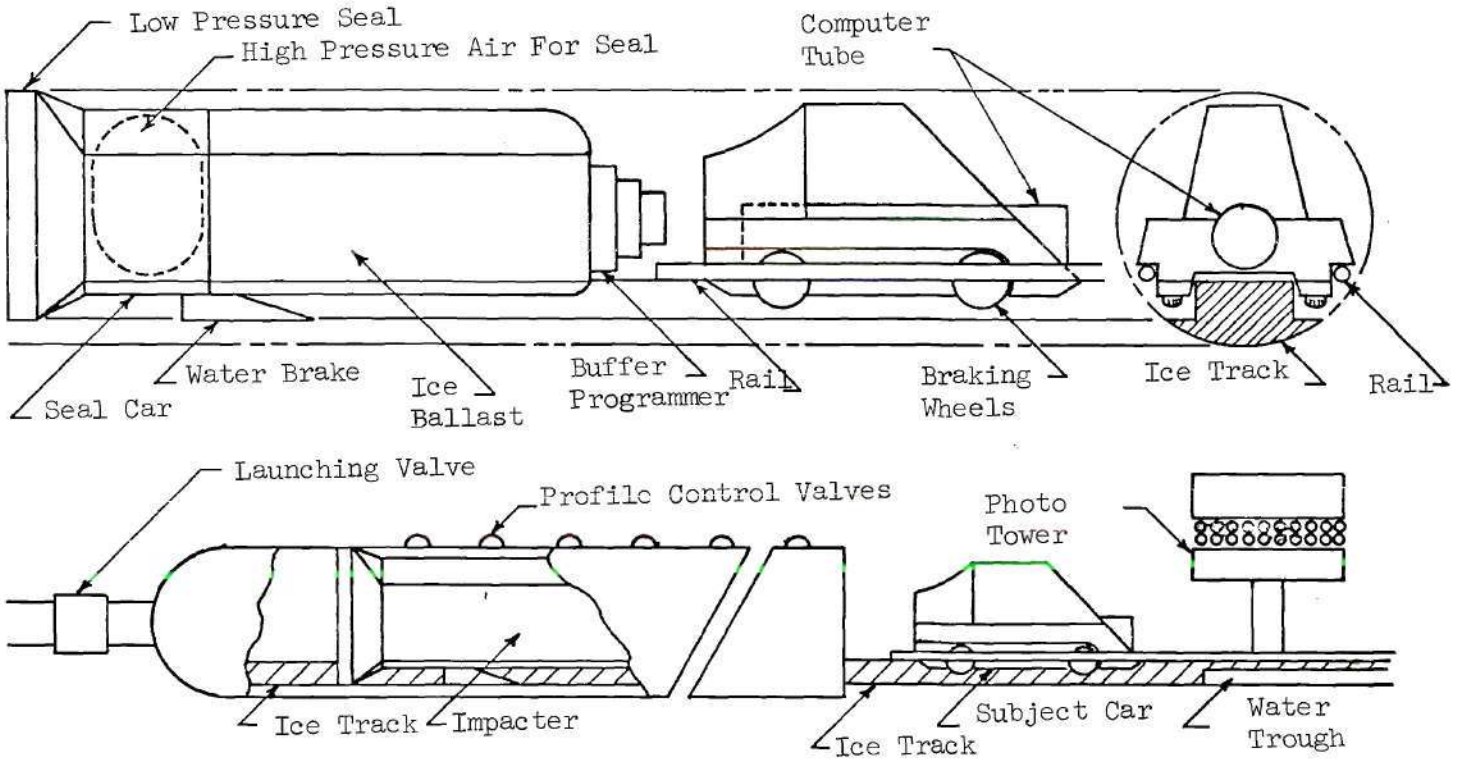

Figure 27. Momentum Exchange Accelerator.

on either side of the ice track (54). As velocity falls below 175 knots (292 ft/sec) most aircraft arresting gear motors become applicable to the problem. It is necessary, of course, to provide a positive stop beyond the normal stopping distance for protection of the subject car, especially in man-rated regime testing.

The subject car will be stopped by wheel brakes. Having cleared the impacter stopping area, the car slider track will terminate, and a guided wheel track will begin. An automatic braking system (such as that used on large aircraft) will set the wheel brakes and hold the desired deceleration program. Since it is imperative that this stop does not involve large g forces to avoid masking pertinent effects in certain tests, stopping distances will necessarily be long (see Table 20). Shipboard arresting gear and/or pneumatic bumpers will again be available in an overrun area to effect a stop in the event of brake failure.

Instrumentation: Two major instrumentation groups are involved, one on the subject car, and one fixed in the test section of the facility. Motion picture coverage will be provided in both groups. Presently available camers will not run in the higher g regimes (55,56), but all of these tests are completed within thirteen feet of travel. Satisfactory fixed camera coverage should be possible over this distance. Data from accelerometers and biomedical transducers will be stored on-car in a digital computer. Since present computer specifications guarantee performance in a 20 g environment (57), for higher accelerations it will be necessary to allow the computer package to be set aft by the acceleration, with a pneumo-hydraulic buffer main-

Table 20. Distance Required to Stop for Various Decelerations

V ft/sec	Stopping Distance for (n)G's (ft) 1	2	3	4	5	15
10	1.55	.78	.52	.39	.31	.10
20	6.21	3.10	2.07	1.55	1.24	.41
30	13.98	6.99	4.66	3.49	2.80	.93
40	24.84	12.42	8.28	6.21	4.97	1.66
50	38.82	19.41	12.94	9.70	7.76	2.59
60	55.90	27.95	18.63	13.98	11.18	3.73
70	76.09	38.04	25.36	19.02	15.22	5.07
80	99.38	49.69	33.13	24.84	19.88	6.62
90	125.78	62.89	41.92	31.44	25.16	8.38
100	155.28	77.64	51.76	38.82	31.06	10.35
110	187.89	93.94	62.63	46.97	37.58	12.53
120	223.60	112.8	74.53	55.90	44.72	14.91
130	262.42	131.2	87.47	65.61	52.48	17.50
140	304.35	152.2	101.4	76.09	60.87	20.29
150	349.4	174.7	116.5	87.34	69.88	23.29
160	397.5	198.8	132.5	99.38	79.50	26.50
170	448.8	224.4	149.6	112.2	89.75	29.92
180	503.1	251.6	167.7	125.8	100.62	33.54
190	560.6	280.3	186.9	140.1	112.1	37.37
200	621.1	310.6	207.0	155.3	124.2	41.41
210	684.8	342.4	228.3	171.2	136.9	45.65
220	751.6	375.8	250.5	187.9	150.3	50.10
230	821.5	410.7	273.8	205.4	164.3	54.76
240	894.4	447.2	298.1	223.6	178.9	59.63
250	970.5	485.2	323.5	242.6	194.1	64.70
260	1050	526	350	262	210	70
270	1132	566	377	283	226	75.5
280	1218	609	406	304	244	81.1
290	1307	653	435	327	266	87.0
300	1399	700	466	350	280	93.2
310	1492	746	497	373	299	99.5
320	1591	796	531	398	319	106

taining g levels below 20. Any control functions which prove necessary during the run can also be performed by the computer.

Air Compressors and Storage: Standard high-pressure compressors and storage tanks can be used in this facility. Overall capacity required is dependent on frequency of operation, of course, and division of this capacity between storage and compressors is an economic decision. A single-shot capability could be provided by 625 cubic feet of air at 3000 psi; this volume would have to be entirely replenished prior to a second firing.

Evaluation

We have projected a system which, if constructed, would be capable of meeting or exceeding the specifications. It is now necessary to evaluate the concept, both in relation to other conceivable related devices, and in an absolute sense. We trace our thinking in Table 21.

A stored energy system has been found necessary, and methods other than the blowgun have been rejected due to danger and expense. The blowgun requires both research and development, but appears to be practicable. However, we note a number of disadvantages inherent in the momentum transfer approach:

1. An impacter is required. It is heavy and awkward to handle. It must first be accelerated and then stopped. This demands systems which are expensive to build and maintain. They are not directly related to the acceleration of the subject. Over one quarter of the facility length is devoted to the impacter travel; thus, it adds to real estate costs.

Table 21. Evaluation of Blowgun Momentum Transfer Accelerator

200 g & 40,000 g/sec required
MOMENTUM TRANSFER POSSIBLE

97.2×10^6 ft-lb required
STORED ENERGY DEVICE NECESSARY

Type	ROCKET/POWDER CAT	STEAM CAT	LINEAR INDUCTION MOTOR	BLOWGUN
Energy storage	Chemical	Superheated steam	Inertial (flywheel)	Compressed air
Expense				
Initial	High	Very high	Very high	Moderate
Operation	High	Very high	Low	Low
Maintenance	Low	Very high	Low	High
R & D		Very high	Very high	High
Evaluation	Too dangerous	Too costly	R & D too costly	Possibly usable

BLOWGUN MOMENTUM TRANSFER ACCELERATOR

Components:

Peculiar to blowgun--
- Tube
- Impacter seal and stabilization
- Air supply

All momentum transfer--
- Impacter
- Impacter track
- Impacter braking
- Buffer/programmer

All crash simulators--
- Subject car
- Subject car track
- Subject car braking
- Instrumentation

Research and Development Areas--
- Pressure profile and control
- Impacter seal and stabilization
- Impacter track
- Choking of tube in front of impacter
- Instrumentation buffer

Disadvantages Inherent in Momentum Transfer

1. Impacter required.
   a. must be stopped -- requires extra system and maintenance
   b. wastes energy
   c. must be retracted -- slows cycle
2. Buffer/programmer required.
   a. requires maintenance
   b. wastes energy
   c. several buffers required -- adds to expense
3. Facility length great due to buffer and impacter distance requirements, adds to real estate costs.
4. Energy generation requirements high for rapid cycle -- low efficiency due to losses in (1) and (2) above.

2. A number of buffers are required. These devices require considerable maintenance, and absorb a great deal of energy. The total expense of the buffers would be considerable. And, since allowance must be made for the longest buffer, facility length is again increased.

3. Overall efficiency of the facility is low. In profile F, for example, 97.2×10^6 ft lb are supplied to the impacter; 8.05×10^6 ft lb, roughly 8.3 per cent of this energy reaches the subject car. The remainder, 91.15×10^6 ft lb is lost in the buffer and in impacter braking. This efficiency is a function of impacter weight, of course, but even in the best of circumstances a majority of the energy input is effectively lost. This increases the required size of the power plant, and slows our cycle time.

Since development is required in any case, it would seem that money might be better spent on a solution other than that afforded by momentum transfer. This assumes that there is another way to accelerate a 5000 pound object, one which requires neither impacter nor buffer. We shall see that this is the case.

Instantaneous Direct Force Generator

In the previous section the use of momentum transfer to generate accelerations was examined. It was concluded that although a satisfactory facility using this technique was feasible, the costs were excessive if any standard accelerating device were to be used to propel the impacter. The blowgun method appeared to have the greatest potential. Nevertheless, even if the blowgun method were adopted a considerable

R and D program would be necessary before a facility could be finally designed and constructed.

According to Newtonian mechanics, there is another, more direct approach. If a force of sufficient magnitude can be generated in a short enough interval, and maintained at a constant level for an appropriate duration, then this force applied directly to the subject car would perform the required task. The significant factor in this statement is the operator if.

To date, at least, no one has tried to develop a system of this magnitude because of the technological problems involved. The previously stated objections to pyrotechnic, steam, and linear induction motor devices remain applicable; a pneumatic device seems most promising. Unfortunately, following conventional practice in pneumatic engineering will lead us to a virtually insuperable problem of valving and control. We note, however, that the basic characteristic of the system we seek - a rapid change which generates, as a result, a large force - is in essence characteristic of an unstable system. Thus, the use of a pneumatic system displaced from a position of unstable equilibrium is the foundation of the design now to be described.

Pneumatic Thruster

The solution to our problem lies in the use of a mechanical system which can be placed in an unstable equilibrium configuration. When displaced from equilibrium, the device tends toward a stable configuration, with a large release of energy.

A diagram of such a device is shown in Figure 28. The basic components of the system are a high pressure plenum of large volume,

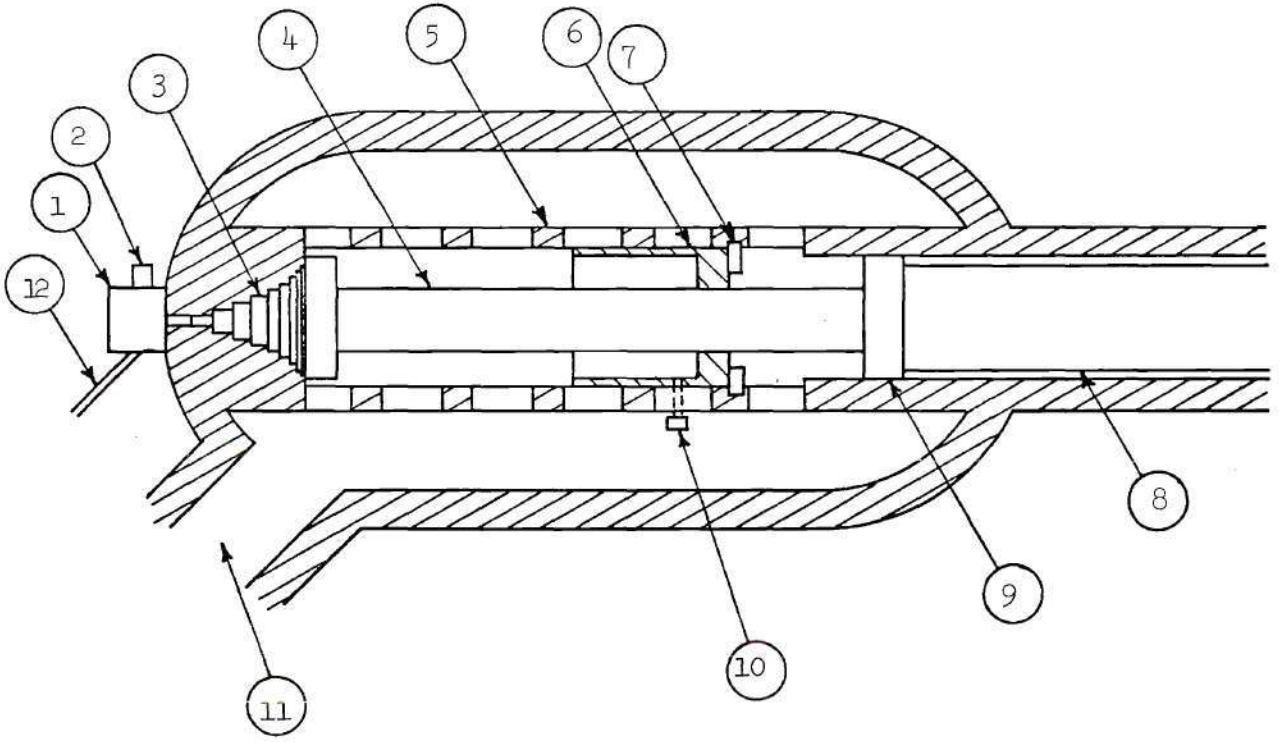

1. Launching Cavity
2. Launching Squib
3. G-Onset Programmer/Arresting Piston
4. Connecting Rod
5. Perforated Thruster Tube
6. Arresting Cylinder
7. Magnetic Locking Dog
8. Thruster
9. Sealing Piston
10. Pressure Release Valve
11. Line to High Pressure Plenum
12. Vacuum Line

Figure 28. Instantaneous Direct Force Generator.

connected to a pneumatic pressure cylinder and piston assembly. It should be noted that there are no valves between plenum and cylinder; operation of the system is not dependent on valve opening characteristics.

The thruster and its associated pistons are shown in the unstable equilibrium position in Figure 28. The g-onset programmer (3) is seated against the rear wall of the main thruster chamber. At this point the thruster is in equilibrium: forces on the sealing piston (9) are balanced by equal and opposite forces on the arresting piston face of the programmer (3). A partial vacuum in the launching cavity and mechanical locks on the thruster protect against inadvertent displacement of the thruster.

To operate the device the locks are released and the launching cavity vacuum vented. With the thruster in a state of unstable equilibrium a squib is fired in the launching cavity. The over pressure thus produced behind the g-onset programmer starts the thruster moving to the right, unseating the programmer and exposing its first segment. The force which results from pneumatic pressure on this segment is unbalanced, and thus accelerates the thruster down the tube. Additional segments are exposed in sequence, progressively increasing the effective piston area. Thus, the driving force is increased in a stepwise fashion, approximating the desired onset program. The thruster advances through the tube until the entire programmer is exposed, at which time the thruster force (and the concomittant subject car acceleration) has reached its maximum value.

At this point it is necessary to maintain a constant force for the duration of the prescribed "flat top" on the acceleration profile. To do so we ensure in our design that the maximum volume expansion during the thruster stroke is small in relation to the total of the thruster chamber and high pressure plenum volumes. The rapidity of the action precludes heat transfer; we assume an adiabatic expansion and size the plenum volume accordingly. The pressure may thus be maintained approximately constant.

On completion of the acceleration phase the thruster must be stopped. This is accomplished by using the forward side of the g-onset programmer (3) as a piston in the arresting cylinder (6). The onset programmer enters the cylinder compressing the air trapped in it, and thus brings the thruster to a stop. A pressure release valve vents the cylinder as the thruster stops, preventing rebound.

Return of the thruster to the "in battery" position is accomplished by means of hydraulic jacks which are connected to the thruster after completion of the power stroke. The energy thus added replaces that expended in accelerating the subject car; operating pressure recovery is virtually total.

While the programmer outlined above certainly could be made to work for the lower g onset rates, some doubt exists as to its success when the g onset must be accomplished in an extremely short distance (see, for example, profiles A, i, k, m, and o). In these cases programming may be accomplished by a very short stroke buffer, the force being applied instantaneously. A flat plate replaces the programmer's nested piston arrangement, and a cavity is provided behind the plate.

To initiate the thrust sequence a pyrotechnic device is fired into this cavity, raising the pressure to that of the thrust chamber. The acceleration stroke proceeds at essentially constant pressure and force. For the lower force levels it may be simpler to displace the equivalent low onset programmer from the wall and hold it with a magnetic clamp. Initiation of the sequence would then be accomplished by releasing the clamp.

Changes in stroke length can be accomplished by moving the arresting piston within the thruster chamber. A change in g-onset rate necessitates a change in the programming piston and its seat. Pressure must be vented and a new programmer assembly fitted. Since required periodic inspections could be made simultaneously this is not really a detriment to overall operating convenience.

As stated previously, the air storage capacity required depends on the maximum swept volume, and on the accuracy of the profile desired. Table 22 shows swept volumes for an operating pressure of 3000 psi. The maximum occurs in profile F. If it is desired to hold accelerations to within 5 per cent of this profile, a total volume of 543 ft^3 is required. It should be noted that the profile which results should be closely repeatable, and it is within 5 per cent of the specified profile. In addition, for most other profiles the error is less than 2 per cent.

More than one thruster could be connected to a single plenum. However, since added cutouts in a pressure sphere tend to drive costs up sharply, it may prove to be a much more flexible and only somewhat more expensive course to provide each thruster unit with its own plenum.

Table 22. Swept Volumes for 3000 psi Air Supply, and Accuracy for 675 ft^3 Volume

Profile	Force lb	Area Required in^2	Area $\underline{\underline{ft^2}}$	Stroke ft	Swept Volume	Error at 675 ft^3 %
A	10^6	333.3	2.32	0.991	2.30	0.6
B	10^6	333.3	2.32	2.118	5.06	1.1
C	750,000	250.0	1.74	3.445	6.00	1.5
D	750,000	250.0	1.74	5.073	8.83	1.9
E	500,000	166.7	1.16	5.845	6.78	1.7
F	500,000	166.7	1.16	17.437	20.25	5.0
G	300,000	100.0	0.695	10.865	7.55	1.8
H	300,000	100.0	0.695	22.54	15.63	3.6
I	200,000	66.7	0.463	10.72	4.97	1.0
J	200,000	66.7	0.463	34.75	15.96	3.7
K	150,000	50.0	0.348	14.46	5.03	1.3
L	150,000	50.0	0.348	28.89	10.05	2.5
M	100,000	33.3	0.232	20.44	4.74	1.0
N	100,000	33.3	0.232	29.24	6.78	1.4
O	50,000	16.7	0.116	40.41	4.68	1.0
P	50,000	16.7	0.116	44.40	5.15	1.3

Thus for 5% accuracy on profile F, V_{TOTAL} = 543 cubic feet

3% accuracy on profile F, V_{TOTAL} = 902 cubic feet

2% accuracy on profile F, V_{TOTAL} = 1383 cubic feet

Hydraulic and pneumatic pumping facilities could easily be shared, of course.

Subject car, track and instrumentation remain similar to those previously described. There is no requirement for impacter braking with its added track length and high-maintenance components. The buffer/programmer is eliminated from the system. Cycle frequency is limited only by the time needed to retract the thruster and reposition the subject car. In practice, test frequency will be limited by subject preparation time rather than acceleration mechanism delays.

Conclusions

The study outlined in this chapter demonstrated conclusively that a device which satisfies the most demanding requirements of the human-acceleration researchers is feasible. Two design approaches, either of which could lead to a device of appropriate capability, have been described. A new system of direct force application, based upon a deliberately designed unstable equilibrium configuration, appears to require the least expenditure of research and development funds, and to be less expensive in construction and operation. Moreover this system has potentially the shortest period between operations, and thus the greatest research capability.

APPENDICES

APPENDIX A

DATA ACQUISITION PROGRAM AND FLOW DIAGRAM

Lateral stiffness was computed from a knowlege of lateral load applied and displacement data gathered utilizing the below listed BASIC language program. Data and control flow was as is shown in Figure 29.

```
1   REM THIS IS DATA ACQUISITION TAPE DA-3/2 DTD
     6-22-71
2   REM THIS PGM USES DAC-1, HP MAG TAPE DRIVER(11-5-70)
     AND
3   REM RS-1.
4   REM "TEST SERIAL #" IS COMPOSED OF:
5   REM      SHELL NO.,DATE,TEST NO.,LOAD INCREMENT,
     FIRST LOAD.
6   REM "RUN DATA" IS COMPOSED OF:
7   REM      RUN#,LOCATION,FIRST WRITE RECORD,FILE,FIRST
     READ REC.
100   DIM U[20],K[30],G[9],S[12]
200   READ D,P,R,C0
210   FOR K=1 TO 12
220   READ U[K]
230   NEXT K
250   LET R=512*D+64*P+R+32
300   PRINT "TEST SERIAL #";
310   INPUT K[22],K[23],K[24],K[25],K[30],L1,L2
315   LET M=-1
316   LET M1=0
319   GOTO 329
320   PRINT "MORE?"
321   CALL (2,0,X0)
322   CALL (2,3,X3)
323   IF X3<0 THEN 9990
324   IF X0>0 THEN 321
329   PRINT "RUN DATA";
330   INPUT K[26],K[27],K[28],Z0,Z1
400   LET M=M+1
405   LET M1=0
```

```
410  LET K[28]=K[28]-1
500  CALL (10,0,S)
501  IF S#0 THEN 9900
505  FOR I=1 TO Z0
510  CALL (10,4,S)
511  IF S#0 THEN 9900
520  NEXT I
525  FOR I=1 TO K[28]
530  CALL (10,1,S)
531  IF S#0 THEN 9900
540  NEXT I
700  DATA 2,1,0,.881
721  DATA 29.8
722  DATA 30.1
723  DATA 32
724  DATA 36
725  DATA 26.7
726  DATA 41.8
727  DATA 35.4
728  DATA 24.4
729  DATA 40.3
730  DATA 6.697
731  DATA 24
732  DATA 6.467
1000  PRINT "SET OPTION"
1100  CALL (2,5,X5)
1105  CALL (2,6,X6)
1110  CALL (2,7,X7)
1120  CALL (2,8,X8)
1130  CALL (2,15,Y5)
1140  CALL (2,3,X3)
1150  CALL (2,0,X0)
1160  IF X0>0 THEN 1100
1170  IF X3<0 THEN 9990
1175  IF X5<0 THEN 320
1180  IF X6<0 THEN 2000
1190  IF X7<0 THEN 3000
1200  IF X8<0 THEN 4000
1210  GOTO 1000
2000  PRINT "NO CONTACT"
2010  CALL (2,0,X0)
2015  IF X0>0 THEN 2010
2020  CALL (1,G[1],80,R,9)
2025  PRINT "POSITION PROBE"
2030  CALL (2,0,X0)
2035  IF X0>0 THEN 2030
2040  CALL (1,S[1],80,R,9)
2045  FOR I=1 TO 9
2050  LET K[I]=(G[I]-S[I])/U[I]
2055  PRINT INT(K[I]*10000+.5)/10;
```

```
2065  NEXT I
2069  PRINT
2070  PRINT "OK #0, ELSE #1"
2075  CALL (2,0,X0)
2080  CALL (2,1,X1)
2085  IF X1<0 THEN 2025
2090  IF X0>0 THEN 2075
2100  PRINT "INITIALIZE"
2110  CALL (2,0,X0)
2115  IF X0>0 THEN 2110
2120  CALL (1,S[1],80,R,9)
2125  CALL (1,S[10],21,R,3)
2140  PRINT "READY"
2145  PRINT
2150  GOTO 1000
3000  CALL (4,Z)
3005  CALL (4,Z)
3010  CALL (2,2,X2)
3020  IF X2<0 THEN 3050
3030  IF Z>0 THEN 3005
3040  GOTO 3100
3050  PRINT "RUN TERM, REC";K[28]
3060  GOTO 1000
3100  CALL (1,K[1],80,R,9)
3110  CALL (1,K[29],20,R,1)
3115  CALL (1,K[10],21,R,3)
3120  FOR I=1 TO 12
3125  LET K[I]=10000*(K[I]-S[I])/U[I]
3130  LET K[I]=INT(K[I]+.5)/10
3135  NEXT I
3140  LET K[29]=1000*K[29]/C0
3145  IF Y5>0 THEN 3200
3150  LET D0=ABS(K[9])-M1
3155  FOR I=1 TO 9
3160  LET D1=SGN(K[I])
3165  LET K[I+12]=ABS(K[I])+D0
3170  LET K[I+12]=K[I+12]*D1
3175  NEXT I
3178  IF M>0 THEN 3200
3180  LET M1=ABS(K[13])
3200  LET K[28]=K[28]+1
3205  CALL (11,K[1],S,30)
3207  IF S#0 THEN 9900
3210  PRINT INT(K[29]);"LB/REC";K[28]
3220  PRINT
3225  GOTO 3000
4000  LET Z2=K[28]-Z1+1
4010  CALL (10,2,S)
4011  IF S#0 THEN 9900
4015  CALL (12,K[1],S,30)
```

```
4016  IF S#0 THEN 9900
4020  IF K[28] >= Z1 THEN 4045
4025  FOR K=1 TO (Z1-K[28]-1)
4030  CALL (10,1,S)
4031  IF S#0 THEN 9900
4035  NEXT K
4040  GOTO 4065
4045  FOR K=1 TO (K[28]-Z1+1)
4050  CALL (10,2,S)
4051  IF S#0 THEN 9900
4060  NEXT K
4065  FOR J=1 TO Z2
4075  CALL (12,K[1],S,30)
4076  IF S#0 THEN 9900
4080  PRINT
4100  PRINT K[22];"/";K[23];K[24];K[25];"/";K[30];"
    -- ";
4101  PRINT K[26];"/";K[27];"   //  ";K[28]
4105  PRINT
4110  PRINT "LAT DISP"
4115  PRINT "LVDT.STRINGER";TAB(40);"I"
4118  IF Y5>0 THEN 4126
4120  PRINT "MASSAGE OPTION REMOVED"
4126  FOR I=1 TO 8
4127  PRINT (I+(K[27]+1-I)/100);TAB(K[I]+40);"*";K[I]
4128  PRINT
4129  NEXT I
4130  PRINT TAB(40);"I"
4135  PRINT "END SHORT:",K[10],K[11],K[12]
4155  PRINT "LOAD: ";INT(K[29]);"LB"
4156  PRINT
4157  PRINT
4160  NEXT J
4165  PRINT
4170  GOTO 320
9900  PRINT "ERROR CODE IS S=";S
9901  GOTO 320
9990  PRINT "TEST TERMINATED.  FINAL RECORD WAS
    ";K[28]
9999  END
```

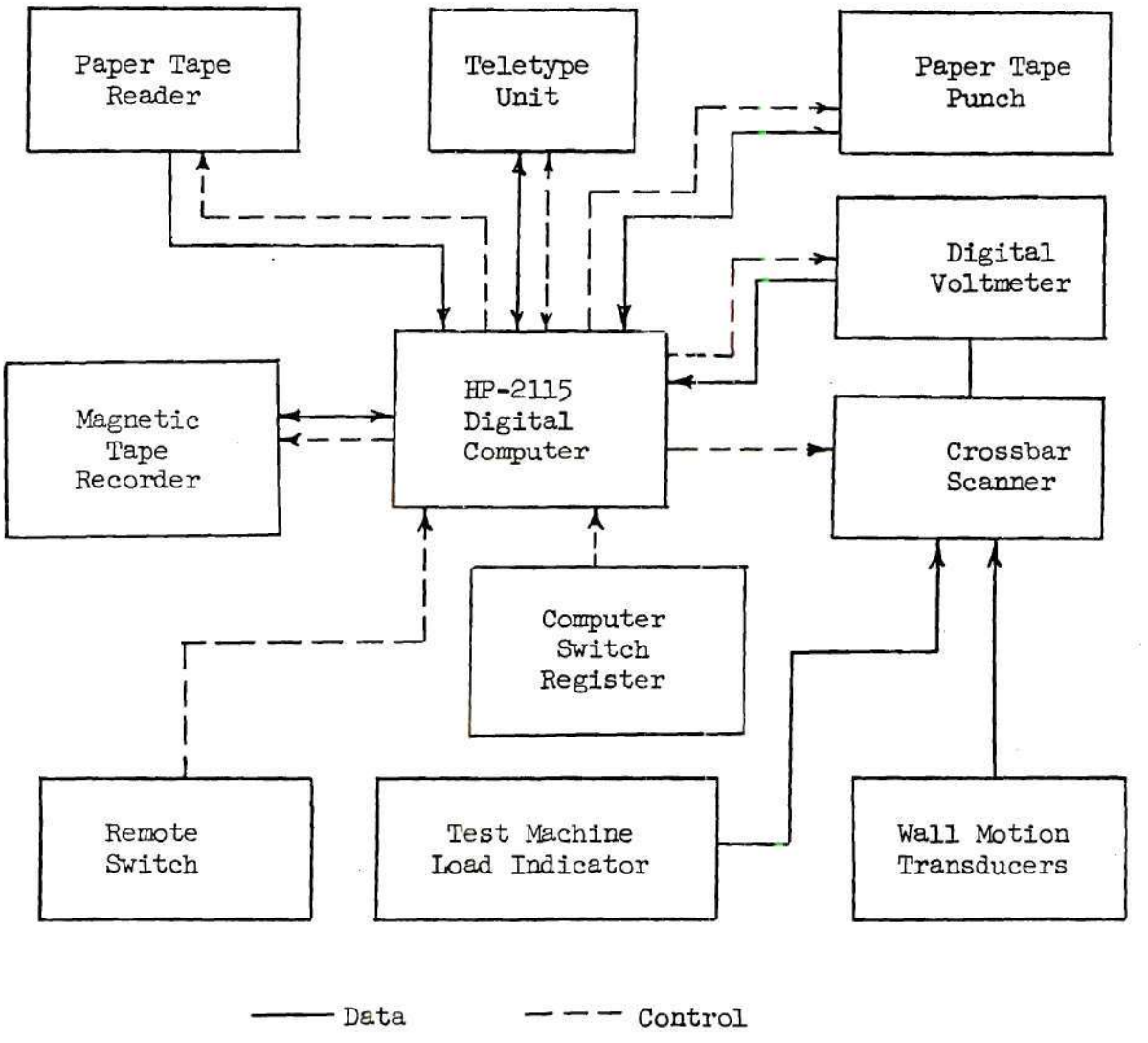

Figure 29. Data Acquisition System Flow Diagram.

APPENDIX B

ELLIPTICAL CYLINDER TEST DATA

Tables B1 through B22 present test data from axial compression tests on cylindrical shells of elliptical cross section as reported in Chapter III.

Symbols used in these tables are:

A	semi-major axis, inches
B	semi-minor axis, inches
L	length of cylinder between epoxy end-pottings, inches
P_1	axial load immediately preceeding buckling event, pounds
P_2	axial load immediately following buckling event, pounds
R	local radius of curvature at centerline of buckle
t	thickness, inches
Θ	angular location of buckle centerline, measured from end of semi-minor axis, degrees
Λ	width of buckle, inches

Table 23. Elliptical Cylinder Test Data

CYL 013

L/t = 1514 B/A = 0.862

t = 0.005 in.; A = 3.47 in.; B = 2.99 in.; L = 7.57 in.

P_1 (in)	P_2 (in)	Θ (deg)	Λ (in)	R (in)
1525	660	80	2.4	3.98
		60	1.45	3.64
		65	2.0	3.75
		45	2.0	3.27
		30	2.2	2.92
		15	1.6	2.67
		0	0.65	2.58
		0	1.55	2.58
		15	1.6	2.67
		25	1.6	3.82
		35	1.45	3.03
		55	1.6	3.53
		35	1.4	3.03
		25	1.45	2.82
		5	1.5	2.59
		5	1.8	2.59
		20	1.8	2.73
		40	2.1	3.15
		55	2.2	3.53
		35	1.25	3.03
		75	1.55	3.92
		75	1.75	3.92
835	620	85	1.35	4.02
		80	2.10	3.98
		45	2.0	3.27
		75	2.1	3.92
		55	2.15	3.53
		80	1.75	3.98

Table 24. Elliptical Cylinder Test Data

CYL 019

L/t = 1514 B/A = 0.855

t = 0.005 in.; A = 3.45 in.; B = 2.95 in.; L = 7.57 in.

P_1 (lb)	P_2 (lb)	Θ (deg)	Λ (in)	R (in)
1095	960	30	1.8	2.88
		55	1.35	3.51
		75	2.5	3.93
		80	2.0	3.99
		50	2.05	3.38
1090	570	0	1.25	2.52
		35	1.8	2.99
		55	1.65	3.51
		80	2.60	3.99
		75	2.25	3.93
		50	1.9	3.38
		35	1.5	2.99
		35	0.95	2.99
		25	1.25	2.78
		15	1.65	2.62
		5	0.95	2.53
		10	1.5	2.56
		15	1.6	2.62
		30	1.8	2.88
		35	1.1	2.99

Table 25. Elliptical Cylinder Test Data

CYL 015

L/t = 1514 B/A = 0.715

t = 0.005 in.; A = 3.46 in.; B = 2.48 in.; L = 7.57 in.

P_1 (lb)	P_2 (lb)	Θ (deg)	A (in)	R (in)
-	-	85	2.25	4.81
535	535	50	1.1	3.45
900	840	30	1.95	2.44
1140	700	15	1.35	1.94
		5	1.05	1.79
		5	1.1	1.79
		15	1.15	1.94
		25	1.5	2.24
		45	2.3	3.18
		90	1.85	4.84
		70	2.15	4.43
		45	1.95	3.18
		70	2.55	4.43
		30	1.6	2.44
		20	1.45	2.08
710	490	55	1.7	3.72
		35	1.85	2.67
		20	1.75	2.08
		10	1.35	1.85
		5	1.3	1.79

Table 26. Elliptical Cylinder Test Data

CYL 018

L/t = 1514 B/A = 0.580

t = 0.005 in.; A = 3.46 in.; B = 2.00 in.; L = 7.57 in.

P_1 (lb)	P_2 (lb)	Θ (deg)	Λ (in)	R (in)
725	715	65	2.05	4.95
820	760	40	2.05	2.85
		90	2.35	5.99
		35	1.55	2.46
1045	925	25	1.3	1.83
		35	1.1	2.46
		60	2.15	4.56
		90	2.15	5.99
		60	2.05	4.56
		35	1.85	2.46
		25	1.25	1.83
1000	960	15	1.0	1.40
975	940	50	1.95	3.69
		65	2.80	4.95
		35	1.3	2.46
		20	1.85	1.58
		5	0.9	1.18
		0	1.0	1.16
		5	0.65	1.18

Table 27. Elliptical Cylinder Test Data

CYL 016

L/t = 1514 B/A = 0.513

t = 0.005 in.; A = 3.48 in.; B = 1.78 in.; L = 7.57 in.

P_1 (lb)	P_2 (lb)	Θ (deg)	Λ (in)	R (in)
805	700	50	2.6	3.93
		85	2.2	6.71
		55	2.25	4.46
		3.35	2.15	2.44
965	850	40	2.4	2.90
		70	2.35	5.91
		30	1.5	2.03
		45	1.95	3.40
		70	1.6	5.91
		70	2.3	5.91
		25	1.65	1.68
1040	1005	20	1.35	1.40
1070	485	40	1.35	2.90
		10	0.55	1.04
		10	1.1	1.04
		0	1.1	0.92
		5	0.75	0.95
		10	1.05	1.04
		55	1.55	4.46
		50	0.95	3.93
		30	1.5	2.03

Table 28. Elliptical Cylinder Test Data

CYL 011

L/t = 2315 B/A = 0.851

t = 0.005 in.; A = 3.495 in.; B = 2.975 in.; L = 11.57 in.

P_1 (lb)	P_2 (lb)	Θ (deg)	Λ (in)	R (in)
1630	610	90	2.8	4.11
		60	2.0	3.69
		45	1.15	3.29
		40	2.25	3.15
		25	2.1	2.79
		5	1.65	2.54
		5	1.7	2.54
		20	1.9	2.70
		35	1.7	3.02
		60	2.15	3.69
		15	1.45	2.63
		0	1.5	2.53
		15	1.45	5.63
		25	1.25	2.79
		35	2.45	3.02
		50	1.85	3.43
		70	1.8	3.91

Table 29. Elliptical Cylinder Test Data

CYL 014

L/t = 2315 B/A = 0.720

t = 0.005 in.; A = 3.42 in.; B = 2.46 in.; L = 11.57 in.

P_1 (lb)	P_2 (lb)	Θ (deg)	Λ (in)	R (in)
650	610	80	2.05	4.65
1090	945	90	2.5	4.75
		60	2.45	3.92
		35	1.25	2.64
		65	2.15	4.15
		40	1.9	2.89
945	870	45	1.4	3.14
1040	720	70	1.5	4.36
		85	1.3	4.73
		80	1.45	4.65
		65	1.6	4.15
		45	1.7	3.14
		30	2.0	2.42
845	540	40	2.1	2.89
		65	2.45	4.15
		25	1.95	2.23
		5	1.4	1.79
		10	1.65	1.84
		20	1.9	2.07

Table 30. Elliptical Cylinder Test Data

CYL 012

L/t = 2315 B/A = 0.713

t = 0.005 in.; A = 3.45 in.; B = 2.46 in.; L = 11.57 in.

P_1 (lb)	P_2 (lb)	Θ (deg)	Λ (in)	R (in)
950	930	90	2.45	4.84
1000	970	50	2.1	3.44
1120	1060	50	2.3	3.44
1195	910	45	2.1	3.17
		70	1.95	4.43
		90	1.9	4.84
		65	2.05	4.22
		45	1.9	3.17
		30	1.45	2.43
		15	1.55	1.93
1070	650	45	2.45	3.17
		30	2.45	2.43
		10	1.20	1.83
		70	1.7	4.43
		70	2.75	4.43
		30	1.55	1.77
700	630	15	1.3	1.93
		0	0.85	1.75

Table 31. Elliptical Cylinder Test Data

CYL 009

L/t = 2315 B/A = 0.704

t = 0.005 in.; A = 3.47 in.; B = 2.44 in.; L = 11.57 in.

P_1 (lb)	P_2 (lb)	Θ (deg)	Λ (in)	R (in)
663	655	70	1.90	4.50
780	750	85	2.3	4.91
970	730	15	1.45	1.89
		30	2.1	2.41
		55	1.9	3.76
		35	1.75	2.65
		45	1.55	3.19
862	670	5	1.4	1.74
		5	1.4	1.74
		20	1.2	2.03
		15	1.45	1.89
		25	1.05	2.21
		45	2.35	3.19
		70	1.2	4.5
		85	2.0	4.91

Table 32. Elliptical Cylinder Test Data

CYL 008

L/t = 2315 B/A = 0.578

t = 0.005 in.; A = 3.43 in.; B = 1.99 in.; L = 11.57 in.

P_1 (lb)	P_2 (lb)	Θ (deg)	Λ (in)	R (in)
811	649	40	1.25	2.82
		50	1.25	3.66
		80	2.65	5.75
		40	1.85	2.82
		65	2.2	4.90
		25	1.15	1.82
		40	1.25	2.82
		60	1.85	4.51
		85	1.95	5.88
		65	2.4	4.90
		40	1.75	2.82
871	812	20	1.5	1.58
879	495	20	1.2	1.58
		0	1.3	1.15
		30	2.0	2.11
		15	1.7	1.39
524	470	10	0.75	1.26

Table 33. Elliptical Cylinder Test Data

CYL 010

L/t = 2315 B/A = 0.527

t = 0.005 in.; A = 3.42 in.; B = 1.80 in.; L = 11.57 in.

P_1 (lb)	P_2 (lb)	Θ (deg)	Λ (in)	R (in)
700	540	85	3.25	6.44
		55	2.5	4.32
		50	2.4	3.82
		30	1.2	2.01
		25	1.3	1.68
770	760	15	0.65	1.21
855	835	10	0.65	1.06
985	965	5	0.5	0.98
965	870	10	0.95	1.06
		0	0.80	0.95
900	600	65	2.65	5.28
		40	2.1	2.84
		20	1.4	1.41
		10	0.6	1.06

Table 34. Elliptical Cylinder Test Data

CYL 022

L/t = 2315 B/A = 0.855

t = 0.004 in.; A = 3.48 in.; B L 2.98 in.; L = 9.27 in.

P_1 (lb)	P_2 (lb)	Θ (deg)	Λ (in)	R (in)
750	292	15	1.75	2.65
		25	1.9	2.81
		45	1.65	3.28
		40	2.0	3.15
		65	2.35	3.77
		90	2.65	4.06
		75	2.3	3.95
		45	2.3	3.28
		30	1.95	2.91
		10	1.2	2.60
		60	1.5	3.66
		75	1.75	3.95
		85	2.1	4.04
		70	2.0	3.87
		60	1.2	3.66
		45	2.0	3.28
		30	2.05	2.91
		15	1.9	2.65
		0	1.7	2.56
366	278	0	1.8	2.56
		20	1.75	2.72
		15	1.1	2.65
		35	2.1	3.03

Table 35. Elliptical Cylinder Test Data

CYL 021

L/t = 2315 B/A = 0.717

t = 0.004 in.; A = 3.44 in.; B = 2.46 in.; L = 9.27 in.

P_1 (lb)	P_2 (lb)	Θ (deg)	Λ (in)	R (in)
498	490	80	1.9	4.70
		75	1.8	4.57
715	320	50	1.55	3.43
		60	1.65	3.95
		35	1.8	2.65
		25	1.5	2.23
		50	1.9	3.43
		25	1.8	2.23
		20	1.7	2.07
		10	1.25	1.84
		5	1.3	1.79
		10	1.5	1.84
		20	1.5	2.07
		35	1.6	2.65
		50	2.05	3.43
		80	2.15	4.70
		80	1.45	4.70
		70	1.85	4.40
		55	2.0	3.70

Table 36. Elliptical Cylinder Test Data

CYL 024

L/t = 2315 B/A = 0.701

t = 0.004 in.; A = 3.49 in.; B = 2.45 in.; L = 9.27 in.

P_1 (lb)	P_2 (lb)	Θ (deg)	Λ (in)	R (in)
398	295	80	1.3	4.86
586	482	80	2.4	4.86
		55	2.0	3.78
		35	1.75	2.66
		20	1.5	2.04
		50	2.05	3.49
		35	1.9	2.66
687	252	20	1.45	2.04
		10	1.25	1.80
		0	1.25	1.72
		10	1.5	1.80
		25	1.6	2.22
		40	1.8	2.93
		60	2.55	4.06
		90	2.55	4.97
		65	2.1	4.31
		60	2.15	4.06
		45	2.1	3.21
		25	1.65	2.22
		10	1.55	1.80
		5	1.3	1.74

Table 37. Elliptical Cylinder Test Data

CYL 023

L/t = 2315 B/A = 0.570

t = 0.004 in.; A = 3.46 in.; B = 1.97 in.; L = 9.27 in.

P_1 (lb)	P_2 (lb)	Θ (deg)	Λ (in)	R (in)
425	423	80	2.15	5.89
		65	1.85	5.01
450	410	40	1.80	2.85
		90	2.20	6.80
		40	1.80	2.85
		60	2.10	4.60
		60	2.15	4.60
558	515	45	1.7	3.27
		30	1.85	2.10
		40	1.15	2.85
		30	1.25	2.10
643	640	90	1.55	6.08
641	321	40	1.6	2.85
		30	1.45	2.10
		20	1.45	1.56
		10	1.60	1.23
		0	0.9	1.21
		5	0.8	1.15

Table 38. Elliptical Cylinder Test Data

CYL 020

L/t = 2315 B/A = 0.51

t = 0.004 in.; A = 3.49 in.; B = 1.73 in.; L = 9.27 in.

P_1 (lb)	P_2 (lb)	Θ (deg)	Λ (in)	R (in)
385	375	65	2.65	5.53
		45	2.35	3.42
		70	1.4	5.97
495	435	30	1.7	2.03
		45	2.25	3.42
		80	2.25	6.62
		70	2.35	5.97
		40	2.25	2.91
		20	1.25	1.40
643	265	50	1.8	3.96
		35	1.5	2.45
		20	1.65	1.40
		10	1.25	1.03
		5	0.95	0.94
		0	0.5	0.91
		10	0.9	1.03
		30	2.95	2.03
		60	1.7	5.03
		75	2.95	6.34
		40	1.25	2.91
		15	1.15	1.18

Table 39. Elliptical Cylinder Test Data

CYL 006

L/t = 2893 B/A = 0.718

t = 0.004 in.; A = 3.44 in.; B = 2.47 in.; L = 11.57 in.

P_1 (lb)	P_2 (lb)	Θ (deg)	Λ (in)	R (in)
442	430	70	1.85	4.39
571	556	85	1.73	4.76
683	664	25	1.3	2.24
		50	1.4	3.42
		55	1.35	3.69
720	2.97	85	0.70	4.76
		5	1.20	1.79
		5	0.95	1.79
		15	1.5	1.94
		15	1.3	1.94
		40	1.8	2.90
		50	2.2	3.42
		25	1.3	2.24
		55	1.45	3.69
		45	1.25	3.16
		45	1.5	3.16
		30	1.5	2.43
		20	1.3	2.07
		10	1.15	1.85
		5	1.05	1.79
		10	1.1	1.85
		25	1.35	2.25
		45	2.0	3.16
		60	1.85	3.94
		80	1.55	4.68
		70	1.75	4.39
		50	2.2	3.42
		30	1.65	2.43

Table 40. Elliptical Cylinder Test Data

CYL 004

L/t = 2893 B/A = 0.706

t = 0.004 in.; A = 3.40 in.; B = 2.40 in.; L = 11.57 in.

P_1 (lb)	P_2 (lb)	Θ (deg)	Λ (in)	R (in)
334	330	85	1.4	4.79
		75	1.2	4.58
425	413	55	1.8	3.67
		40	1.1	2.85
		55	1.3	3.67
491	460	35	1.8	2.60
511	455	80	3.0	4.71
		10	1.7	1.77
		20	1.6	2.00
		40	2.3	2.85
		65	2.5	4.18
562	540	90	2.1	4.81
		75	2.5	4.58
		60	2.3	3.94
567	290	45	1.9	3.12
		35	1.3	2.60

Table 41. Elliptical Cylinder Test Data

CYL 005

L/t = 2893 B/A = 0.567

t = 0.004 in.; A = 3.47 in.; B = 1.97 in.; L = 11.57 in.

P_1 (lb)	P_2 (lb)	Θ (deg)	Λ (in)	R (in)
300	300	80	1.3	5.92
408	400	65	1.75	5.04
		75	1.75	5.04
510	473	40	2.3	2.86
		65	1.5	5.04
640	385	65	1.55	5.04
		40	1.1	2.85
		40	1.8	2.85
		35	1.7	2.46
		15	1.15	1.36
		5	1.0	1.14
		15	1.1	1.36
		25	1.15	1.80
		50	2.7	3.73
		75	2.25	5.70
		15	1.5	1.36
		50	1.6	3.73
		35	1.6	2.46
		25	1.15	1.80
		20	1.9	1.55
429	400	5	0.7	1.14
405	282	5	1.0	1.14
		0	1.1	1.12
		5	0.85	1.14
		10	1.15	1.22
		20	1.15	1.55
		40	2.05	2.86
		70	3.0	5.40
		55	1.35	4.17
		65	2.3	5.04
		85	1.5	6.06

Table 42. Elliptical Cylinder Test Data

CYL 003

L/t = 2893 B/A = 0.515

t = 0.004 in.; A = 3.50 in.; B = 1.80 in.; L = 11.57 in.

P_1 (lb)	P_2 (lb)	Θ (deg)	Λ (in)	R (in)
430	395	15	0.75	1.196
450	402	35	1.7	2.45
630	520	60	2.2	5.02
615	210	90	2.4	6.80
		60	2.0	5.02
		80	2.1	6.58
		60	2.3	5.02
		60	2.5	5.02

Note: Load behavior data does not correspond to buckle data for this test.

Table 43. Elliptical Cylinder Test Data

CYL 017

L/t = 3855 B A = C.856

t = 0.003 in.; A = 3.48 in.; B = 2.98 in.; L = 11.57 in.

P_1 (lb)	P_2 (lb)	Θ (deg)	Λ (in)	R (in)
380	155	70	2.4	3.88
		85	2.95	4.05
		75	1.75	3.96
		70	1.70	3.88
		60	1.55	3.66
		50	2.25	3.41
		40	2.0	3.15
		30	1.40	2.91
		20	1.65	2.72
		10	1.25	2.59
		5	1.60	2.56
		10	1.65	2.59
		25	1.4	2.80
		35	1.45	3.02
		50	1.65	3.41
		65	1.4	3.78
		50	1.4	3.41
		35	1.3	3.02
		25	1.55	2.80
		10	1.65	2.59
		0	1.4	2.55
		10	1.6	2.59
		30	2.05	2.91
		45	1.9	3.28
		45	1.65	3.28
		50	1.45	3.41
170	135	70	2.05	3.88
		80	1.15	4.01
		85	2.05	4.05

LITERATURE CITED

1. Nash, W. A., "Bibliography on Shells and Shell-like Structures," TMB Report 863, David Taylor Model Basin, U. S. Navy Department, Washington, D. C., 1954.

2. Nash, W. A., "Bibliography on Shells and Shell-like Structures (1954-1956)," University of Florida, Contract DA-01009-ORD-404, Office of Ordnance Research, U. S. Army, Washington, D. C., 1957.

3. Hutchinson, J. W., "Buckling and Initial Postbuckling Behavior of Oval Cylindrical Shells Under Axial Compression," Transactions of the American Society of Mechanical Engineers, Journal of Applied Mechanics, March 1968.

4. Tennyson, R. C., Booton, M., and Caswell, R. D., "Buckling of Imperfect Elliptical Cylindrical Shells under Axial Compression," AIAA Journal, February 1971.

5. Feinstein, G., Erickson, B., and Kempner, J., "Experimental Investigation of the Buckling of Clamped Oval Cylindrical Shells Under Axial Compression," PIBAL Report 70-27, Polytechnic Institute of Brooklyn, 1970.

6. Kempner, J., and Chen, Y. N., "Large Deflections of an Axially Compressed Oval Cylindrical Shell," Proceedings of the 11th International Congress of Applied Mechanics, Munich, Springer-Verlag, Berlin, 1964.

7. Kempner, J., and Chen, Y. N., "Buckling and Postbuckling of an Axially Compressed Oval Cylindrical Shell," Proceedings of a Symposium on the Theory of Shells to Honor Lloyd H. Donnell (70th Anniversary Volume), University of Houston Press, 1967.

8. Kempner, J., and Chen, Y. N., "Postbuckling of an Axially Compressed Oval Cylindrical Shell," Proceedings of the 12th International Congress of Applied Mechanics, Stanford University, Stanford, California, 1968.

9. Zahorski, A. T., "Segmental Buckling of Monocoque in Compression and Bending," LSMC-A748486, Lockheed Missiles and Space Company, Sunnyvale, California, July 1965.

10. Bijlaard, P. P., "Stresses from Local Loadings in Cylindrical Pressure Vessels," Transactions of the American Society of Mechanical Engineers, Vol. 77 Part 1, p. 805, August 1955.

11. Komp, R. L., "The Influence of Geometry on the Buckling of Thin-Walled Circular Cylindrical Shells," Engineer's Thesis, Stanford University, Stanford, California, July 1965.

12. Hoff, N. J., "Buckling of Thin Shells," Proceedings of an Aerospace Scientific Symposium of Distinguished Lecturers in Honor of Dr. Theodore von Kármán on his 80th Anniversary, May 11, 1961, The Institute of the Aerospace Sciences, New York, 1962.

13. Horton, W. H., and Cox, J. W., "The Stability of Thin-Walled Unstiffened Circular Cylindrical Shells under Nonuniformly Distributed Axial Load," SUDAER No. 220, Stanford University, Presented at the 1965 ASME Aviation and Space Conference, Los Angeles, California, 1965.

14. Baker, E. H., Cappelli, A. P., Kovalevsky, L., Rish, R. L., and Verette, R. M., Shell Analysis Manual, NASA SID 66-398, Manned Spacecraft Center, Houston, Texas, Section 3.40, June 1966.

15. Hodgkinson, Eaton, "Experimental Researches on the Strength of Pillars of Cast Iron and Other Materials," Philosophical Transactions, 1840, Part II, pp. 385-456.

16. Horton, W. H., and Struble, D. E., "End Fixity of Columns," USAAVLABS Technical Report 70-10, August, 1970.

17. Salmon, E. H., Columns, A Treatise on the Strength and Design of Compression Members, Henry Frowde and Hodder and Stoughton, London, 1921.

18. Newmark, N. M., "A Simple Approximate Formula for Effective End-Fixity of Columns," Journal of the Aeronautical Sciences, Vol. 16, p. 116, 1949.

19. Hoff, N. J., "Elastically Restrained Struts," Journal of the Royal Aeronautical Society, Vol. 40, No. 309, p. 663, September 1936.

20. Hoff, N. J., The Analysis of Structures, John Wiley and Sons, Inc., New York, 1956.

21. Stephens, B. C., "Natural Frequencies of Structural Members as an Indication of End Fixity and Magnitude of Stress," Journal of the Aeronautical Sciences, Vol. 4, p. 54, 1936.

22. Massonet, C., Les Relations entre les Modes Normaux de Vibration et la Stabilité des Systemes Élastiques, Goemaere, Bruxelles, 1940.

23. Horton, W. H., Craig, J. I., and Struble, D. E., "A Simple, Practical Method for the Experimental Determination of the End

Fixity of a Column," Proceedings of the 8th International Symposium on Space Technology and Science, Tokyo, Japan, August 1969.

24. Struble, D. E., "Boundary Effects in Structural Stability: A New Approach," Ph.D. Thesis, Georgia Institute of Technology, Atlanta, Georgia, in preparation.

25. Horton, W. H., Iwamoto, T., and Rehfield, L. W., "Evaluation of Boundary Restraint Effects in Structural Stability," Proceedings of the XIV South American Conference of Structural Engineering and the IV Pan American Symposium of Structures, October 1970.

26. Iwamoto, T., "The Effect of End Fixity on the Stability of Structures," Ph.D. Thesis, Georgia Institute of Technology, Atlanta, Georgia, in preparation.

27. Baruch, M., "On Undestructive Determination of the Buckling Load of an Elastic Bar," GITAER 70-1, March 1970, Georgia Institute of Technology, Atlanta, Georgia; also, AIAA Journal, Vol. 8, No. 12, p. 2274, 1970.

28. Pierce, G. A., "Structural Stability of Columns and its Relationship to Normal Mode Characteristics," unpublished, Georgia Institute of Technology, Atlanta, Georgia, 1969.

29. Horton, W. H., "The Use of Rational Functions in Approximating Relationships of Significance in the Buckling and Vibration of Partially Restrained Beams," paper in preparation, Georgia Institute of Technology, Atlanta, Georgia.

30. Hanagud, S., Chaudhari, S. N., and Horton, W. H., "Approximate Relationships Between the Behavior of Plates Under Destabilising and Nondestabilising Loads," paper presented at the 9th International Symposium on Space Technology and Science, Tokyo, Japan, 1971.

31. Horton, W. H., and Singhal, M. K., "Approximation Formulae for the Instability of Partially Restrained Beams," paper in preparation, Georgia Institute of Technology, Atlanta, Georgia.

32. Horton, W. H., and Durham, S. C., "Repeated Buckling of Circular Cylindrical Shells and Conical Frusta by Axial Compressive Forces," SUDAER No. 175, Stanford University, November 1963.

33. Cox, J. W., "An Experimental Study of the Buckling of Thin Cylindrical Shells," Ph.D. Thesis, Stanford University, Stanford, California, 1965.

34. Bailey, S. C., "Experimental Studies on the Instability of Circular Cylindrical Shells," Ph.D. Thesis, Stanford University, Stanford, California, March 1967.

35. Tennerelli, D. J., and Horton, W. H., "An Experimental Study of the Local Buckling of Ring-Stiffened Cylinders Subject to Axial Compression," Israel Journal of Technology, Vol. 7, No. 1-2, 1964.

36. Horton, W. H., Cundari, F. L., and Johnson, R. W., "A Review of the Applicability of the "Southwell Plot" to the Interpretation of Test Data Obtained from Stability Studies of Elastic Column and Plate Structures," SUDAAR No. 296, Stanford University, Stanford, California, December 1967.

37. Flügge, W., Stresses in Shells, Springer-Verlag, Berlin, Germany, 1960.

38. Horton, W. H., and Cundari, F. L., "On the Applicability of the Southwell Plot to the Interpretation of Test Data from Instability Studies of Shell Bodies," Proceedings of AIAA/ASME 8th Structures, Structural Dynamics and Materials Conference, Palm Springs, California, March 1967.

39. Singer, J., "The Influence of Stiffner Geometry and Spacing on the Buckling of Axially Compressed Cylindrical Shells," IUTAM Symposium, Copenhagen, Theory of Thin Shells, Editor, F. I. Niordson, 1967.

40. Ford, J. S., "Parametric Studies on the Stability of Stringer and Ring Reinforced Circular Shells," Ph.D. Thesis, Georgia Institute of Technology, Atlanta, Georgia, November 1970.

41. Bank, M. H., "The Effect of Fiber Direction on the Instability of Single-Layer Glass-Cloth Cylinders under Torsion," Engineer's Thesis, Stanford University, Stanford, California, September 1966.

42. Craig, J. I., "An Experimental Study of Wall Motions in Circular Cylindrical Shells under Combined Loading," Ph.D. Thesis, Stanford University, Stanford, California, August 1968.

43. Galletly, G. D., and Reynolds, T. C., "A Simple Extension of Southwell's Method for Determining the Elastic General Instability Pressure," Proceedings of the Society for Experimental Stress Analysis, Vol. 13, No. 2, p. 141, 1956.

44. Donnell, L. H., "On the Application of Southwell's Method for the Analysis of Buckling Tests," Stephen Timoshenko 60th Anniversary Volume, McGraw Hill, New York, 1938.

45. Tuckerman, L. B., "Hetrostatic Loading and Critical Astatic Loads," National Bureau of Standards Research Paper RP 1163, Journal of Research, N. B. S., Vol. 22, p. 27, 1939.

46. Salmon, E. H., Materials and Structures, Longmans, Green and Co., London, 1941.

47. Fisher, H. R., "An Extension of Southwell's Method of Analyzing Experimental Observations in Problems of Elastic Stability," Proceedings of the Royal Society, Series A, Vol. 144, 1934.

48. Wang, C-T., "Inelastic Column Theories and an Analysis of Experimental Observations," Journal of the Aeronautical Sciences, p. 283, May 1948.

49. Braathen, B., and Noton, B. R., "Comparison of Theoretical and Experimental Results for 24 S-T and 75S-T Aluminum Ranges," Report No. 66, The Aeronautical Research Institute of Sweden, 1956.

50. Stapp, J. P., "Human Exposure to Linear Deceleration," WACD TR-5915, Wright Air Development Center, Wright-Patterson AFB, 1951.

51. Ewing, C. L., Thomas, D. J., Beeler, G. W., Jr., Patrick, L. M., and Gillis, D. B., "Dynamic Response of the Head and Neck of the Living Human to $-G_x$ Impact Acceleration," 12th Stapp Car Crash Conference, Society of Automotive Engineers, 1968.

52. Joyner, U. T., and Horne, W. B., "Considerations on a Large Hydraulic Jet Catapult," NACA TN 3203, National Advisory Committee for Aeronautics, 1951.

53. "A Wound Rotor Motor 1400 Feet Long," Westinghouse Engineer, Vol. 6, p. 160, September 1946.

54. Brosterhous, C. A. and Thompson, H. B., "Recent Developments in Braking of High Speed Test Vehicles," Aeronautical Engineering Review, Vol. 15, No. 12, p. 26, December 1956.

55. Lassiter, D., and Krupp, W., "Photographic Instrumentation at Project SMART," Journal of the Society of Motion Picture and Television Engineers, Vol. 66, February 1957.

56. Egbert, B. R., and Ankeney, D. P., "Supersonic Track Facilities at the Naval Ordnance Test Station," Jet Propulsion, Vol. 27, No. 9, September 1957.

57. Hewlett-Packard HP-2116B Specifications, Hewlett-Packard Company, Palo Alto, California, 1970.

58. Laithwaite, E. R., "Linear Induction Motors," Proceedings of the Institution of Electrical Engineers, Vol. 104A, p. 461, December 1957.

59. Adams, W. J., and White, B. A., "Applying Linear Induction Motors," Automation, p. 74, June 1967.

60. "Rocket Sled Design Handbook," INSTRACON REPORT No. 60-1, Intra-station Track Conference, Structures Working Group, Air Research and Development Command, January 1960.

61. Chandler, R. F., "The Daisy Decelerator," ARL-TR-67-3, 6571st Aeromedical Research Laboratory, Aerospace Medical Division, Air Force System Command, Holloman Air Force Base, New Mexico, May 1967.

VITA

Milton Harold Bank II was born August 11, 1935 in Brockton, Massachusetts, the son of Milton Harold Bank and Fern Elaine (Richey) Bank. His father being a minister of the Detroit Conference of the Methodist Church, he attended various schools in Michigan, graduating from Pontiac (Michigan) Senior High School in 1953. He entered the United States Naval Academy in June 1953, and graduated with the degree of Bachelor of Science in 1957.

Following graduation he entered flight training, and in June, 1959, was designated a Naval Aviator. He was assigned to duty as a carrier-based jet fighter pilot, and made two western Pacific deployments in that capacity.

In 1963 he was assigned to the Naval Postgraduate School, Monterey, California as an Aeronautical Engineering student. He received the degree of Bachelor of Science in Aeronautical Engineering in December, 1964. In September, 1965, he entered Stanford University under Navy sponsorship and completed the requirements for the degree of Engineer in Aeronautics and Astronautics in 1966.

He returned to duty as a carrier-based jet fighter pilot, flying in combat over North Viet Nam. In 1968 he was found to be diabetic, and was retired from the Navy for that reason in August of that year.

He entered the Georgia Institute of Technology in September 1968, under the Vocational Rehabilitation Program of the Veterans Administration.

LCDR Bank is married to the former Linda Hall of Falls Church,

Virginia, and they have two sons, Baynes Wesley, and Milton Harold III.